Dipl.-Ing. Alois DANNINGER

Online Calculation of Diesel Engine Torque

Dissertation

to achieve the university degree of

Doktor der technischen Wissenschaften

submitted to

Graz University of Technology

Supervisor

Univ.-Prof. Dipl-Ing. Dr.techn. Martin Horn

Institute of Automation and Control

Kapfenberg, March 2017

.

Acknowledgments

Statutory Declaration

I declare that I have authored this thesis independently, that I have not used other than the declared sources/resources, and that I have explicitly marked all material which has been quoted either literally or by content from the used sources.

Graz, _____   _____

           Date   Signature

Eidesstattliche Erklärung[1]

Ich erkläre an Eides statt, dass ich die vorliegende Arbeit selbstständig verfasst, andere als die angegebenen Quellen/Hilfsmittel nicht benutzt und die den benutzten Quellen wörtlich und inhaltlich entnommenen Stellen als solche kenntlich gemacht habe.

Graz, am _____   _____

           Datum   Unterschrift

---

[1]Beschluss der Curricula-Kommission für Bachelor-, Master- und Diplomstudien vom 10.11.2008; Genehmigung des Senates am 1.12.2008

Abstract

Aim of existing diesel engine control units is the fulfillment of performance and emission targets with best fuel consumption on a given hardware. Cross linking of functions across different control units e.g. for hybridization or automated transmission requires information about other powertrain elements.

This thesis proposes a solution to calculate diesel engine torque based on methods from traditional thermodynamic work process calculation. Simplifications enable online computation in embedded control units. The developed algorithm contains combustion modeling, simplified work cycle -, wall heat loss - and gas exchange calculation. Inner work is evaluated by the use of energy balance and leads to indicated mean effective pressure. Introduction of friction and auxiliaries enables engine torque calculation. Consideration of the air fuel equivalence ratio for current operation and smoke limitation enables the calculation of maximum instantaneously available torque and the torque reserve. A nonlinear state space model for air path dynamics predicts time to provide demand torque.

Validation is executed on desktop computer by simulation using step response measurements from engine testbed measurement. Current and future passenger car certification cycles are described, simulated and analyzed to validate the method. For online execution the proposed algorithm is compiled into a rapid prototype control unit. Results from stationary and transient tests are presented.

The method will be applied as combustion model for predictive powertrain optimization in realtime applications. Further on it provides key information for transmission control during gear shift.

Keywords: Diesel engine; torque calculation; energy balance; air path dynamics; combustion model; embedded model based control; online work cycle calculation

Kurzfassung

Motorsteuerungen haben die Aufgabe, die Fahrbarkeits- und Emissionsziele mit geringstem Verbrauch zu erreichen. Dabei stellen steuergeräteübergreifende Funktionen, insbesondere bei Hybridantrieben oder automatisierten Getrieben, eine Herausforderung dar. Im Rahmen dieser Arbeit wird eine Methode zur Drehmomentberechnung vorgestellt. Diese beruht auf der traditionellen Motorprozessrechnung. Der Algorithmus beinhaltet eine Modellierung zur Ermittlung des Verbrennungsverlaufs. Basierend auf einem vereinfachten Motorprozess und der Berechnung von Ladungswechsel- und Wandwärmeverlusten wird die innere Arbeit anhand der Energiebilanz ermittelt. Daraus ergibt sich der indizierte Mitteldruck, der mit Messergebnissen vom Motorprüfstand abgeglichen werden kann. Mit Hilfe der Reibungsverluste und dem Antrieb von Nebenaggregaten kann das abgegebene Drehmoment am Motorausgang berechnet werden. Durch Vereinfachungen wird eine Umsetzung in Steuergeräten realisiert. Das Verhältnis des aktuellen Luftverhältnisses mit der Rauchgrenze ermöglicht eine Berechnung der Drehmomentreserve, die unmittelbar bereitgestellt werden kann. Die Dynamik des Luftpfads ist durch ein nichtlineares Zustandsraummodell repräsentiert. Für Anforderungen über der Drehmomentreserve muss mehr Luft für die Verbrennung bereitgestellt werden. Die Zeit zur Umsetzung dieser benötigten Zustandsänderung wird durch das Modell des Luftpfads prädiktiert. Simulationen von Sprungantworten unter Verwendung von Messdaten wurden offline am Computer durchgeführt und die Abdeckung der Haupteinflussgrößen bestätigt. Die Berechnung wurde auf aktuelle und künftige PKW-Zertifizierungszyklen erweitert. Die Umsetzung im Prototyp-Entwicklungssteuergerät wird schrittweise erklärt. Ergebnisse vom Motorprüfstand, sowohl von stationärer Kennfeldvermessung als auch von transienten Prüfzyklen, vervollständigen die Gültigkeitsüberprüfung. Der vorgeschlagene Algorithmus wird als Motormodell für online Systeme zur prädiktiven Antriebsstrangoptimierung angewendet. Darüber hinaus stellt er benötigte Informationen zur Verbesserung von Getriebeschaltvorgängen bereit.

Schlagwörter: Dieselmotor; Drehmomentberechnung; Energiebilanz; Luftpfaddynamik; Motormodell; modellbasierte Motorsteuerung; online Motorprozessrechnung

Contents

1 Introduction

1.1 Quickstart

Introduction
- Motivation
- State of the art
- Challenges
- Approach and applications

Diesel engine combustion
- Diesel engine working principle: four strokes, cylinder pressure curve, injection, ignition, main combustion parameters, rail pressure, EGR - rate
- First & second theorem of thermodynamics
- System parameters: power, torque, IMEP, BMEP, relation to emission, MFB50
- Fuel related properties: air fuel ratio, heat value,...
- Standard cycle process:
  equivalent volume -, equivalent room – and combined process

Online torque calculation
- Calculation overview
- MFB50 estimation from main injection, ignition delay
- Equivalent room ratio function, separation to isochoric and isobaric combustion
- Cycle calculation, Intake and exhaust enthalpy
- Gas exchange, wall heat losses
- Energy conservation
- Auxiliaries, friction, calculation of brake specific torque

Engine dynamics
- Torque reserve
- Prediction of dynamic behavior
- Dependency on engine speed and EGR rate
- State space model on air path dynamics

Implementation and simulation results
- Model structure
- System and calibration parameters
- Step response test
- Variation of engine speed and EGR rate
- Transient test cycles

Experimental validation
- Implementation in rapid prototyping ECU
- Stationary operation
- Transient test results

Summary and conclusions
- Summary
- Conclusions and contributions
- Limitations and constraints
- Outlook

Appendix
- Symbols
- Acronyms
- Interfaces and labels
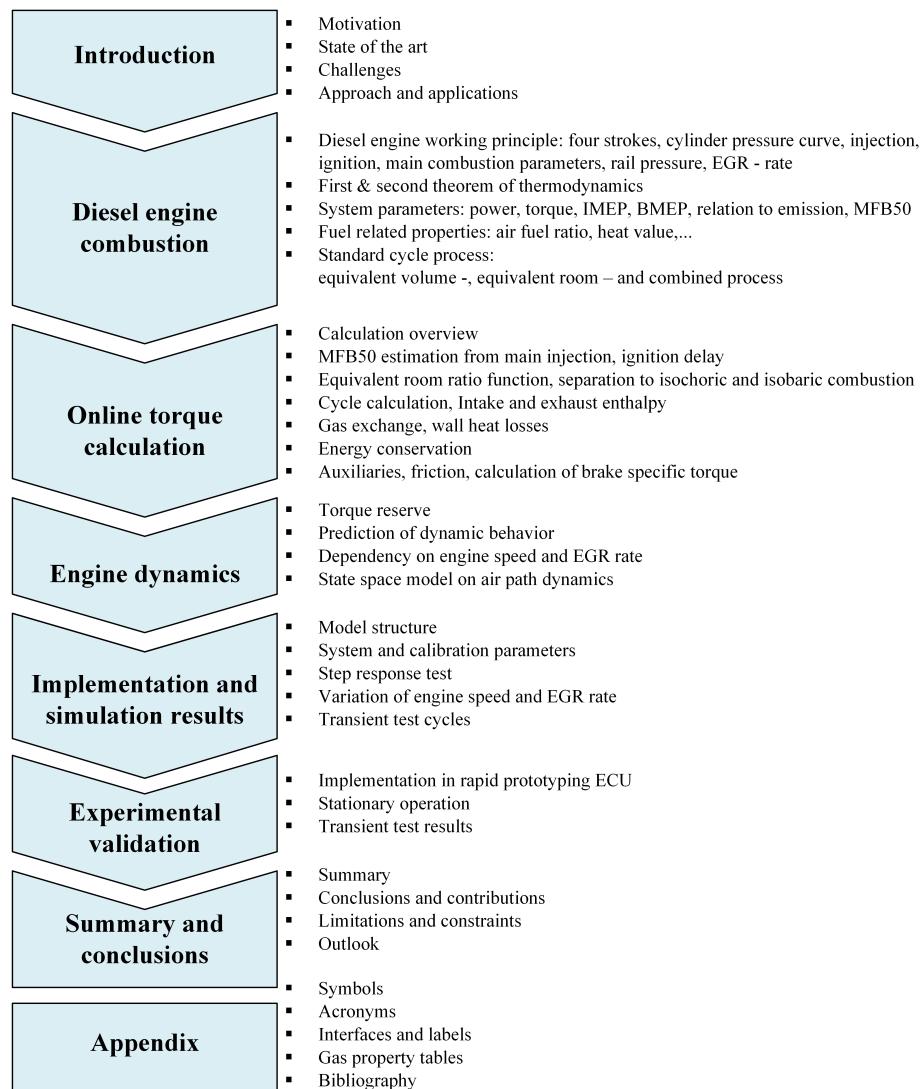- Gas property tables
- Bibliography

Figure 1.1: Overview on the entire work

1.2 Main overview of the work

The speed and torque request signals of an internal combustion engine are the main scheduling signals in the ECU, see Guzzella [9]. In contrast to engine speed the engine torque

- is not measured in standard applications,
- can change rapidly and
- is directly related to the driving comfort.

The standard online torque-estimation in an ECU starts from a base torque derived from the injected fuel mass flow at the current engine speed. The real physical state of the combustion engine is partly captured by correction functions: injection parameters such as fuel pressure and timing as well as temperatures from different sensors are used to introduce factors and/or offsets to the base torque value. As torque control is provided by the driver or cruise control, the common state of practice - a (static) *map based* estimation of the engine torque - is sufficient for the ECU.

Though several control units require high quality torque information including prediction of dynamic behavior, the ECU has direct access to the relevant information. Approaches for sensor based torque calculation have already been shown, see Andersson [1]. Analysis on torque estimation methods based on rotational dynamics with the energy level method is described in Koegeler [15]. Feedback estimation methods as well as torque estimation based on neuronal networks are presented in Huang [12]. Model-based approaches which are currently used e.g. within the air path or exhaust gas aftertreatment control offer reduced calibration effort compared to map based solutions, see Schopp [22].

Main contribution of this thesis is the model-based engine torque calculation using available maps in the ECU as well as providing characteristic parameters for the expectation of the dynamic torque behavior. This enables reduction of the calibration effort in interfacing control units e.g. the transmission control unit (TCU) or hybrid control unit (HCU). A detailed physics-based calculation scheme taking into account available information is presented in chapter 3 and 4.

1.3 State of the art

Modeling of the thermodynamic system in internal combustion engines has been an intensive field of research in engineering in the past decades and many technologies have been investigated as summarized by Tschöke [26]. Several research and development programs led to a physical respectively phenomenological representation shown in example by Stiesch and Merker [24]. Simulation and calculation software has been developed in diverse detailing depth as described by Pischinger [20] and Merker[18]. Physical approaches replaced simple empirical models due to increasing calculation power.

Main application is the 0, 1 and 3-dimensional simulation for design of combustion engines with respect to performance, emission and fuel consumption. These calculations use time and crank angle dependent simulations for air path and cylinder processes as outlined by Wurzenberger [33].

State space models of the torque response have already been used for diagnosis issues whereas models of the air path are used for control tasks.

1.4 Challenges

Identification of the most relevant influences is the basis for creating a nonlinear model to represent the real behavior of the engine. Separation of linear and nonlinear parts enable a useful mathematical representation. The main challenge of this work is to create a simple nonlinear model representing the main physical effects in a straight forward mathematical form that still enables a physical interpretation of the model values.

1.5 Approach

Existing models in combustion engine research as used for simulation software in combination with idealized principles known from literature, see Dubbel [10]. Implementations in modern control units used for internal combustion engines provide the physical basis for this work. It describes the method of model-based torque calculation and an extension to characterize the dynamic behavior of the combustion engine torque.

As depicted in figure 1.2 the calculation is split into three parts. The upper two blocks

represent the computation of the engine actual torque (*act. torque*) and of the maximum instantaneously available torque (*avail. torque*).
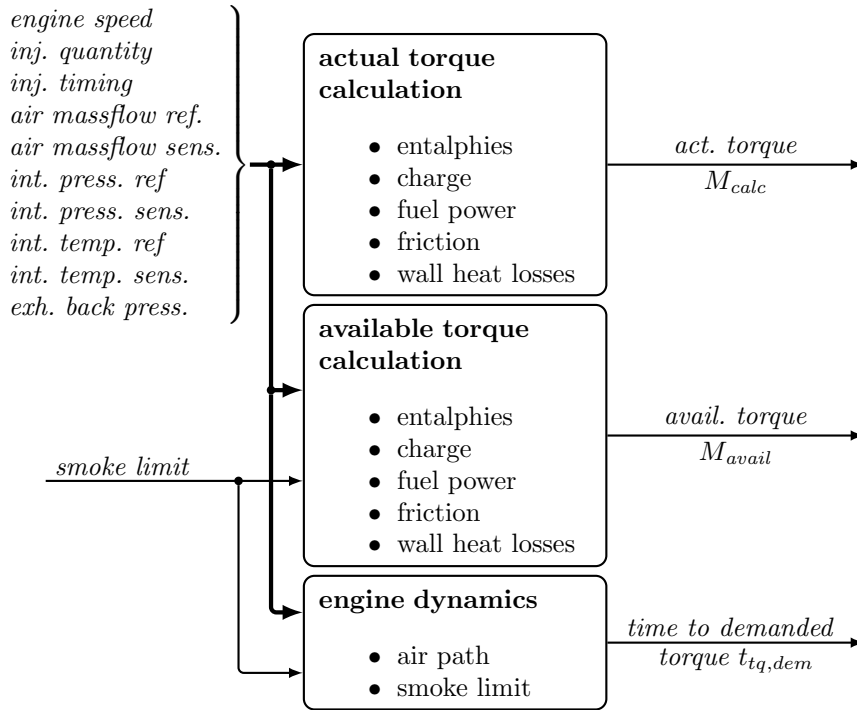
Figure 1.2: Overview of the main calculation components, their inputs and outputs.

The latter is based on the currently available charge and ambient conditions, calibration of smoke limitation and thereby takes the current engine status and configuration (ambient conditions, manufacturing tolerance, aging, etc.) into account. As an outcome the immediately available torque reserve can be derived. Torque requests up to the available torque can be provided within negligible time delay and therefore can be seen as directly accessible. Any torque request above this torque level up to full load is dominated by the air path dynamics. Both torque calculations base upon the same physical model described in detail in chapter 3.

The third block in figure 1.2 labeled *engine dynamics* delivers a straight forward estimation of the time until a specified *demanded torque* can be provided $t_{tq,dem}$. Details are given in chapter 4.

The proposed solution is designed to work online within the ECU as further described in chapter 5. The results from engine testbed validation are presented in chapter 6.

1.6 Target applications

The outcome of this work is intended to be used in industrial implementations of engine management systems. Beneficiaries of the resulting information are on one hand future algorithms in the ECU as well as the coordination with transmission and hybrid powertrains.

2 Diesel engine combustion

This chapter summarizes the basis for this thesis and provides the principles of internal combustion engines with specific view on the diesel engine combustion process and thermodynamics.

2.1 Working principle of a four stroke engine

The propulsion in conventional and hybrid vehicles is using the principle of an internal combustion engine (ICE). Passenger cars as well as on- and off-road commercial vehicles mainly use engines working on the 4-stroke principle. Although the principle is well known and described in detail e.g. in [19] or [20] a short explanation is given.

Fresh air from ambient is filtered and compressed by a turbocharger to increase the amount of oxygen that is available for the combustion process. For emission reduction some burned gas with very low oxygen content is mixed with fresh air to reduce peak temperature during combustion. This gas mixture in the intake manifold is called *charge*.

Due to the fact that the cylinder needs to be emptied and refilled at each working cycle the system can be seen as volatile. This discontinuous operation is split into 4 separate steps that are executed in sequential order:

1. Induction
2. Compression
3. Power
4. Exhaust

The piston is mainly operated by the processes in the cylinder and is moving up and down in a reciprocating way. Each stroke is a movement from the position nearest to the valves -

the top dead center (TDC) to the opposite position furthest from them - bottom dead center (BDC) or vice versa, see figure 2.1. The crankshaft moves half a revolution per stroke and a total of 2 revolutions per working cycle. The conrod connects the piston to crankshaft that finally provides the resulting energy to the power-train.
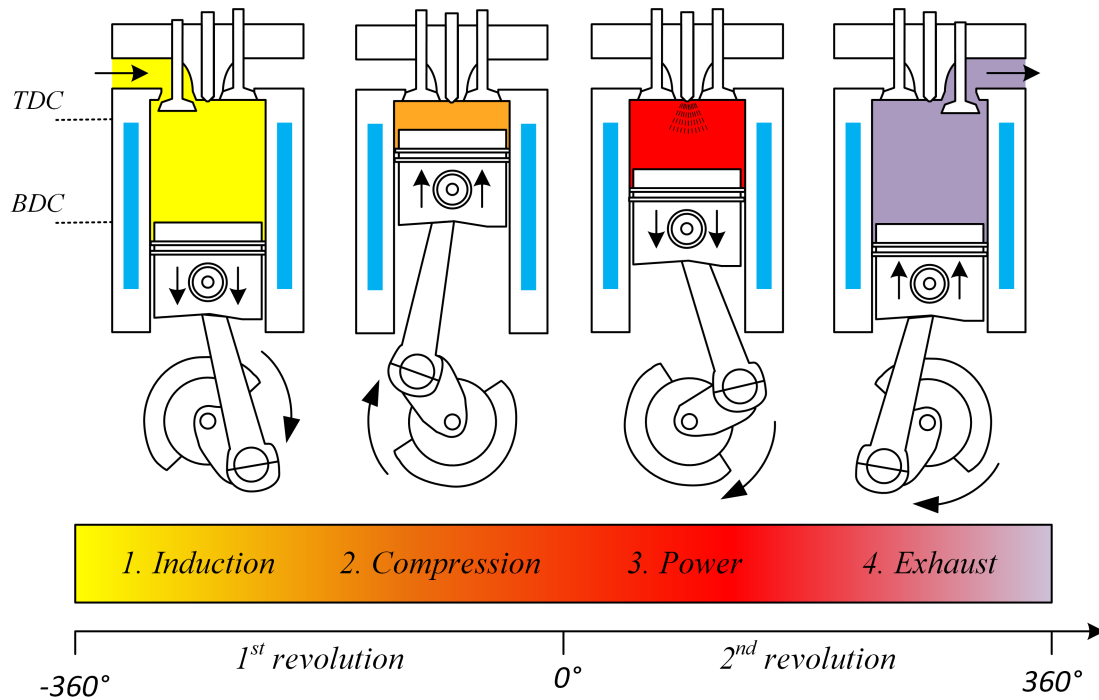
Figure 2.1: Operation principle of a 4-stroke diesel engine.

1. Induction

At start of the induction stroke the piston is at the top dead center, exhaust valves are closing and the intake valves are opening. The piston moves downwards and increases the available volume. Gas mixture is aspirated into the combustion chamber and replaces the burned gas.

2. Compression

Around the bottom dead center the inlet valves close and the combustion chamber becomes almost gas-tight. Rotating masses provide energy to compresses the charge, gas density and pressure raises. The temperature exceeds the ignition temperature and reaches up to approx. 650° C.

3. Power

State of the Art diesel injection systems allow multiple injections with different injection duration and quantity. Fluid diesel is injected directly into the combustion chamber. To reach best atomization the spray injects diesel with very high pressure of 1600 - 2000 bar into the combustion chamber. The resulting very small droplets ignite due to the high temperature. Local gas temperature reaches up to 2500°C with many different zones that influence resulting emissions. More detailed explanation is given in section 2.3. The piston is pushed downwards and provides mechanical work. Expansion leads to decreasing gas temperature and therefore a decrease of reaction rates.

4. Exhaust

After reaching BDC the exhaust valves open and the moving piston pushes the burned gas into the exhaust manifold. At the end of this phase both, intake and exhaust valves, are open simultaneously.

2.2 Thermodynamic principles

The working process of an ICE contains multiple state-changes including chemical processes before, during and after the combustion. This leads to instationary events including flows and heat transfer in a wide temperature and pressure range as well as evaporation, gas exchange and so on. This section summarizes the main principles for diesel combustion processes as they are relevant for the content of online modeling of the engine torque. An overview is given in Pischinger [20], more detailed physical and thermodynamic explanations can be found in in Bähr [4], Mollenhauer [19] and Merker [18].

The two theorems of thermodynamics define the main information about energy balance and process direction as well as on the equilibrium condition. State properties are a key element for using these theorems and are usually defined by their pressure and temperature state. Chemical pure units are fully described by these two states and all further representations e.g. inner energy, enthalpy, ... can be derived [10].

2.2.1 System definition

For calculation of thermodynamic processes a clear boundary definition is required. Figure 2.2 shows the system of the ICE and the fed and led away mass or energy. During induction the intake valve is open and the fresh air mass $\dot{m}_{in}$ flows from the intake manifold into the system. For compression the intake valve closes and the system becomes gas-tight. As long as both valves are closed the mass in the combustion chamber m_c only changes by the injected fuel mass that also adds chemical energy dQ_{fuel} to the system. This energy is converted into mechanical energy dW and heat. During the combustion process the internal state of the gas mixture in the combustion chamber p_c and T_c massively changes. Some of the heat is transmitted through the system border as wall heat losses dQ_{wall}. After the combustion the exhaust valves open and led away the hot gas $\dot{m}_{exh}$ into the exhaust manifold.
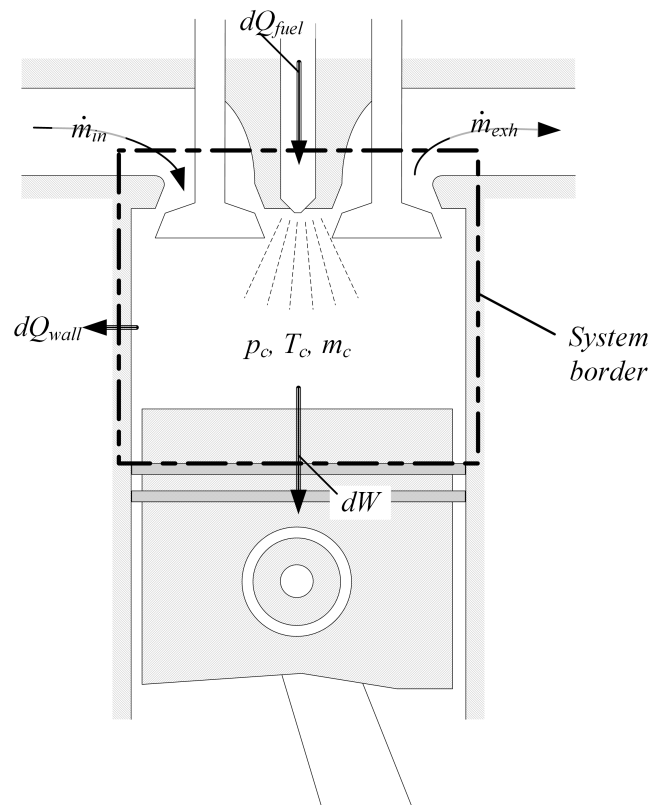

Figure 2.2: Overview of the main calculation components, their inputs and outputs.

During the working cycle the piston moves two times up and down. Therefore the volume change need to be considered in the system boundary definition.

In stationary operation of the entire ICE represents a *stationary open system*. The cylinder with closed valves during the high pressure phase is a *closed system* and with open valves the system is called an *instationary open system*.

The system can be described by the state variables pressure p and temperature T that are independent from the mass of the system. Therefore these are called *intensive states*. The volume V and the inner Energy U are related to the mass. They are called *external states* and are denoted by capital letters.

For calculation of the combustion process the system definition can be set to the combustion chamber boundaries by closing the intake and exhaust valves as shown in figure 2.2. First step of calculation is a representation of the physical and thermodynamic effects by a phenomenological approximation. This enables calculation of the resulting working power respectively the engine torque. For further calculation following input information is required:

- engine speed n;
- fuel mass $\dot{m}_{fuel}$;
- position of fuel injection(s) φ;
- air mass flow $\dot{m}$;
- pressure in intake - p_{in} and exhaust manifold p_{exh};
- temperature in intake manifold T_{in},

2.2.2 Energy conservation law

The law of energy conservation is known as the 1st law of thermodynamics. It states that the sum of transported energy (by work, heat of mass exchange) is equal the stored inner and outer energies. For the instationary open systems with gas exchange the energy conservation equation is written as

$$\underbrace{dW_t + dQ + \Sigma dm_i(h_i + e_{oi})}_{transported\ energy} = \underbrace{dU + dE_o}_{stored\ energy} . \tag{2.1}$$

The transported energies contain the technical work W_t and the heat dQ (outer heat) transferred across the system boundaries and the sum of the transferred mass m_i multiplied

by specific enthalpy h_i and the specific outer energy e_{oi} (e.g. potential or kinetic energy). The right hand side represents the inner energy U of the system and the outer energy E_o i.e. potential or kinetic energy of the system. The stored inner energy shall be equal to the energy transported by mass. The enthalpy is defined therefore as

$$h = u + p \cdot v. \tag{2.2}$$

that contains beyond the inner energy also the displacement energy $p \cdot v$.

The energies are considered with positive sign, if the energy flows into the system.

If there is no energy transport e.g. during compression and expansion the equation (2.1) is simplified to

$$dW_t + dQ_o = dU + dE_o. \tag{2.3}$$

For gases potential and kinetic energy is very small with respect to the inner energy, therefore the outer energy can be neglected. The process work without consideration of friction is equal to the volumetric work W_V with the pressure p at the system boundary and volume V:

$$dW_V = -p \; dV. \tag{2.4}$$

Figure 2.3 shows the pressure curve of a real engine. On top the intake and exhaust valves are visible. The piston is displayed in both extreme points. Left border of the piston represents the lowest possible volume defined as *compression volume V_c* and is named *TDC*. Right border gives the maximum volume at *BDC* that is also defined as the *displacement volume V_d*. The lower part of Figure 2.3 shows the change in the pressure and volume domain. The high pressure part of the combustion cycle starts with intake valve closing with the intake manifold pressure p_{in}. Compression leads to a pressure raise and around the TDC fuel is injected and combustion takes place that leads to further pressure raise. Following the pressure curve clockwise the expansion decreases the pressure. At exhaust value opening the pressure drops to p_{exh}. The enclosed area of the high pressure curve defines the available work provided by the combustion cycle.

Low pressure part of the curve defines the gas exchange work that is necessary to emit the burned gas to the exhaust manifold and fill the combustion chamber with fresh charge. It

is counted with negative sign. In a balanced state the input and output of energy- and mass-flow does not lead to a change of the stored energy. This is called a *stationary flow process*.
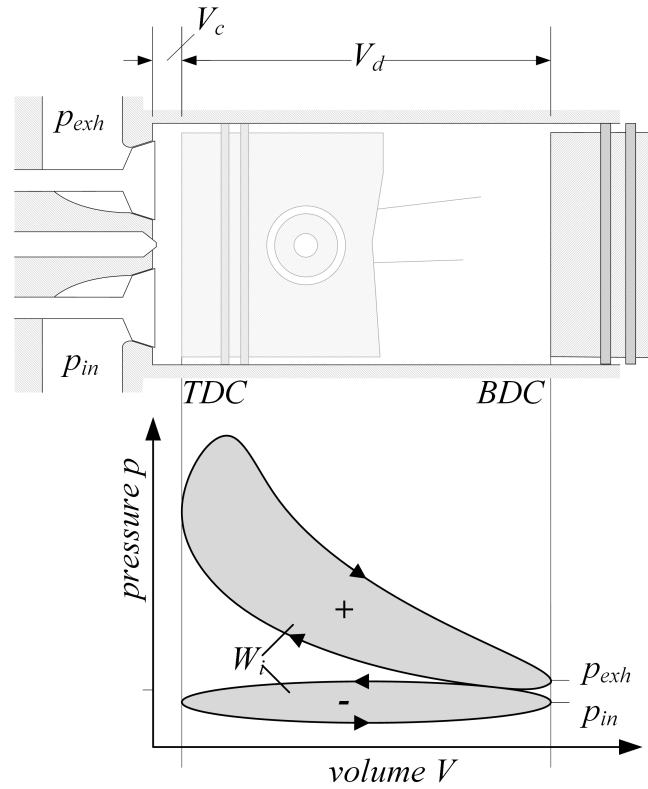
Figure 2.3: Pressure curve and resulting work of a real engine.

An internal combustion engine as a whole can be treated like this in stationary operation. For this state equation (2.1) can be converted to

$$W_t + Q_o + \sum_{i=1}^{n} m_i(h_i + e_{oi}) = 0. \tag{2.5}$$

Considering state 1 with a constant mass input and state 2 with an output the equation can be rewritten as

$$W_t + Q_o = m(h_2 - h_1 + e_{o2} - e_{o1}). \tag{2.6}$$

The outer energy of gases can be neglected as it mainly consists of potential and kinetic energy. Therefore equation 2.6 simplifies to

$$W_t + Q_o = m(h_2 - h_1). \tag{2.7}$$

From the transported work the inner work W_i can be calculated as it will be described in chapter 3.

Further details to the given equations and figures are described in Pischinger [20].

2.2.3 Principle of irreversibility

The second law of thermodynamics states, that the sum of the entropies S of the participating bodies always increases. It defines the direction of the processes and shows the balance of a system:

$$dS_i \geq 0. \tag{2.8}$$

Considering the entropy change of the irreversible process of an adiabatic system (no heat exchange with the environment) the entropy can only increase [10]. For the balance point of an adiabatic system the entropy must maximize to reach

$$\sum dS = 0 \tag{2.9}$$

Usually a fully reversible process cannot be established but only the balance of some state variables. Reversible heat equals to the surface below the state change in the TS-diagram [20].

The main outcome of this definition is that every heat is always transferred from higher to lower states. Impact on combustion engines is that efficiency cannot exceed the maximum level for the ideal working process defined by Carnot in 1824 [10].
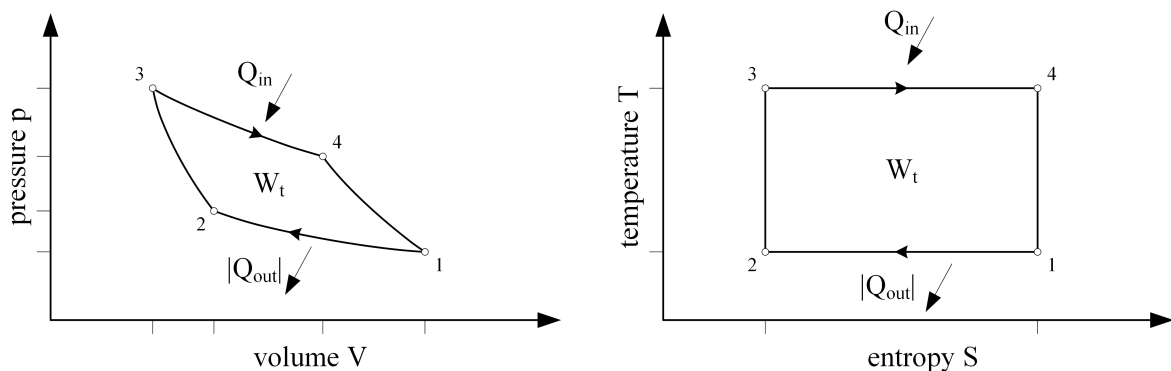

Figure 2.4: pV and TS diagram of the Carnot process.

This process presents the following state changes as shown in figure 2.4 based on [10]:

1-2: Isotherm compression at T_1 with decreasing heat energy Q_{out}

2-3: Reversible adiabatic compression from p_2 to p_3

3-4: Isotherm expansion at T_3 with introduction of heat Q_{in}

4-1: Reversible adiabatic expansion from p_4 to p_1

The introduced heat Q_{in} is calculated as

$$Q_{in} = m \ R \ T_3 \ ln\frac{V_4}{V_3} = T(S_4 - S_3) \tag{2.10}$$

and the decreasing heat $|Q_{out}|$ as

$$|Q_{out}| = m \ R \ T_1 \ ln\frac{V_2}{V_1} = T(S_2 - S_1). \tag{2.11}$$

The Carnot process is the basis for all thermal engines. Internal combustion engines cannot fully follow the ideal process as defined by Carnot. Figure 2.5 shows the TS diagram of an ICE. The dash-dotted area between the x-axis and the points 2 and 3 define the complete introduced energy Q_{in}. It consists on one hand of the enthalpy of the inducted gas and on the other hand of the energy stored in the injected fuel.
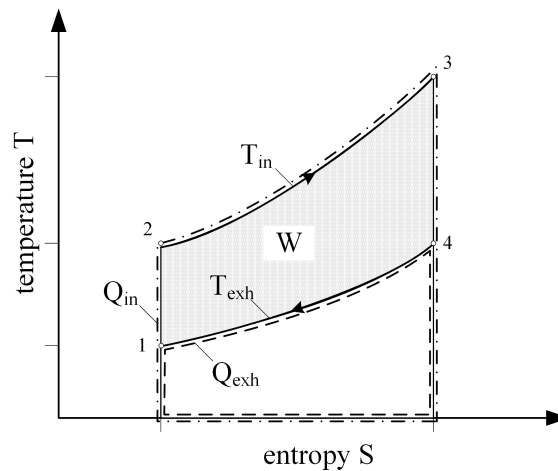

Figure 2.5: TS diagram of a cycle process (own graphic based on [20]).

Decreasing heat Q_{out} is defined by the area below the points 1 and 3 and physically consists of the exhaust gas enthalpy as well as heat losses.

The remaining area enclosed from the points 1 as starting and end point via 2, 3 and 4

defines the thermal work that is provided by the cycle process. For increasing efficiency it is always the target to maximize this area.

The impact on combustion engines is that efficiency cannot exceed the maximum level defined by Carnot for the ideal working process [10].

2.2.4 Ideal gas

Although real gases are not in the ideal state, the calculation leads to good estimation [4]. Thermodynamic behavior of ideal gases is defined by simple laws as provided in [10] and [20]. The thermodynamic state equation provides a relation between pressure p, specific volume V_m and the temperature T. The equation for reference quantity of 1 kmol is written together with the general gas constant $R_m = 8313.3$ J/kmol K as

$$pV_m = R_m \, T. \tag{2.12}$$

The specific gas constant R can be calculated by using the molar mass M as $R = R_m/M$. For a defined gas mass m, the ideal gas equation is written as

$$pV = m \, R \, T. \tag{2.13}$$

The specific heat constant can be defined for a constant volume c_v or for a constant pressure c_p; in both cases it depends on the temperature.

With the gas constant R or with the isentropic coefficient κ the equations are defined as

$$\begin{aligned}
R &= c_p - c_v \\
\kappa &= \frac{c_p}{c_v} \\
c_v &= \frac{1}{\kappa-1} R \\
c_p &= \frac{\kappa}{\kappa-1} R.
\end{aligned} \tag{2.14}$$

It is obvious that only one of the values c_v, c_p and κ needs to be known beside the specific gas constant R to calculate the other ones. Due to big changes of the operation conditions in ICE the calculation needs to consider different values. The values of the used specific gas properties are attached in appendix D.

2.3 System parameters

This section defines the main parameters in the combustion cycle and their relations to each other.

Compression ratio

The reciprocating working process leads to a changing volume. The ratio between the displacement volume V_d and the compression volume V_c is called the compression ratio and represents one of the main design parameters:

$$\epsilon = \frac{V_d + V_c}{V_c}. \tag{2.15}$$

Mean effective pressure

To compare power between different engines, commonly the provided work W is correlated to the displacement volume. It is called the *mean effective pressure p_m*.
If the *inner work W_i* provided by the gas pressure on the piston is used, the *indicated mean effective pressure (IMEP)* or p_i results in:

$$p_i = \frac{W_i}{V_d}. \tag{2.16}$$

The indicated work is represented by the area of the pV-diagram and will be one of the main calculation variables of this work, see chapter 3. It can be determined from indication or via a torque measurement system at an engine testbed. Therefore a comparison between calculation and measurement can be done based on the mean pressure.
The difference between the inner work and the effectively provided work is caused by friction losses calculated by the friction work W_f respectively the *friction mean effective pressure (FMEP) p_f*:

$$p_f = \frac{W_f}{V_d} = \frac{W_i - W_e}{V_d}. \tag{2.17}$$

When using the effectively provided work W_e one can calculate the *brake mean effective pressure (BMEP)* or p_e:

$$p_e = \frac{W_e}{V_d}. \tag{2.18}$$

Power

The power of the four stroke engine additionally to effective pressure depends on rotational speed ω in rad/s

$$P = \frac{\omega}{2} V_d \, p_e. \tag{2.19}$$

Torque

Engine torque is the turning force which rotates the crankshaft. It is mainly responsible for the performance of a vehicle and therefore represents an outstanding value for automotive applications.

From the second definition of the power $P = 2\pi \, N \, M$ the engine torque can be calculated by using the calculation from equation 2.19.

Based on the mean effective pressure as described above one can calculate the torque of a four stroke engine follows this method [10]:

$$M = \frac{V_d \, p_m}{4\pi}. \tag{2.20}$$

Together with the speed the torque defines the engine operating point.

Gas mixture and air – fuel equivalence ratio

The amount of carbon and oxygen must be in a defined ratio for a complete combustion with carbon dioxide and water as products.

In stoichiometric combustion conditions the chemically bound energy is transferred into heat and non-toxic emissions. Further details are given in Pischinger [20].

$$C_x H_y O_z + (x + \frac{y}{4} - \frac{z}{2}) \longrightarrow xCO_2 + \frac{y}{2}H_2O \tag{2.21}$$
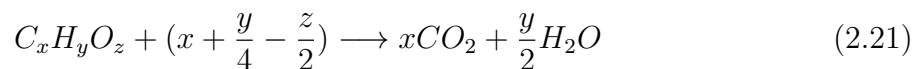
This leads to the stoichiometric oxygen requirement of

$$O_{2st} = (x + \frac{y}{4} - \frac{z}{2}). \tag{2.22}$$

This stoichiometric value can be identified by an elementary analysis of carbon, hydrogen,
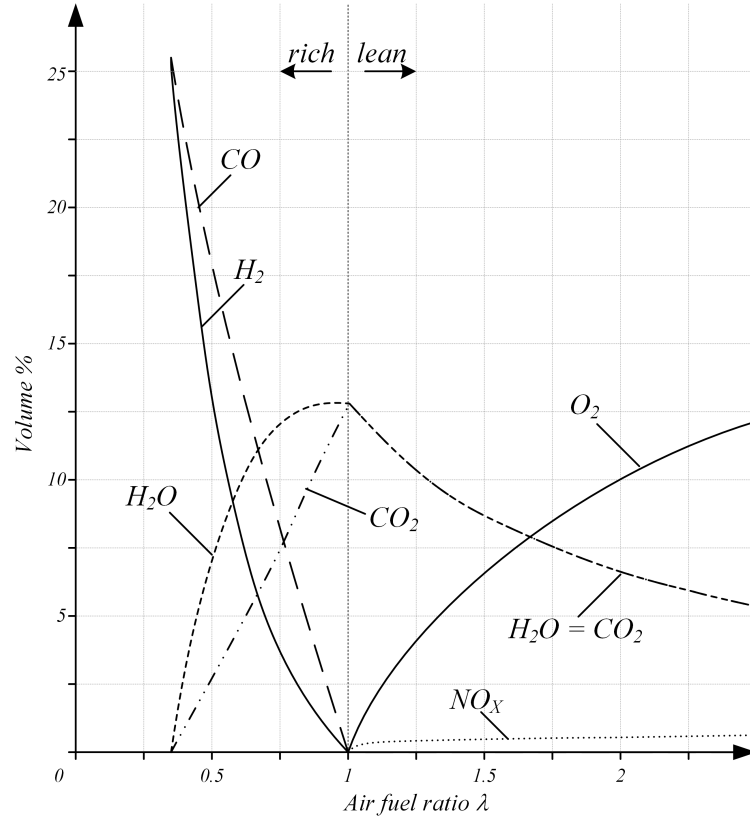
Figure 2.6: Composition of exhaust gas for C:N = 1:2 at 1000K depending on air fuel ratio (own figure based on [20]).

sulfur and oxygen.

The air fuel ratio (AFR) brings the mixture of fuel and air into a unit-less relation:

$$AFR = \frac{\dot{m}_{\text{air}}}{\dot{m}_{\text{fuel}}}. \tag{2.23}$$

By a consideration of the stoichiometric oxygen requirement the given mixture is defined as:

$$\lambda = \frac{AFR}{AFR_{\text{stoich}}}. \tag{2.24}$$

Stoichiometric air fuel ratio of $AFR_{st} = 14.5$ is applied on diesel combustion.

In combustion processes usually the amount of air differs from the ideal value, the deviation is defined by the *air fuel equivalence ratio* λ as

$$\lambda = \frac{\dot{m}_{air}}{AFR_{st} \ \dot{m}_{fuel}}. \tag{2.25}$$

A mixture has a value of $\lambda = 1.0$ at stoichiometry, rich mixtures $\lambda < 1$ have fuel excess and lean mixtures $\lambda > 1$ have an excess of air. Diesel combustion usually takes place in the range of $\lambda = 1.2 \ldots 5.0$ or higher. Lower values lead to extensive rise of soot formation and shall be avoided.

Figure 2.6 shows the dependency of the main exhaust gas components from the air fuel equivalence ratio. At stoichiometric combustion all carbon is oxidized to CO_2 and all hydrogen is oxidized to H_2O. In rich combustion the amount of oxygen is too low for complete combustion. This leads to an increasing share of CO and H_2 as chemical products. Below a value of about 0.3 the amount of oxygen gets too low for any combustion.

Looking on the right hand side of the figure one can see lean combustion with increasing share of oxygen and equivalence of CO_2 and H_2O. This combustion leads to increasing nitrogen oxides NO_x with the dominating effect of thermal NO as described by Zeldovich in 1948 [34]. The three principal reactions of the extended Zeldovich mechanism that takes place above 1600°C are:

$$
\begin{aligned}
N_2 + O &\rightarrow NO + N \\
N + O_2 &\rightarrow NO + O \\
N + OH &\rightarrow NO + H.
\end{aligned}
\tag{2.26}
$$
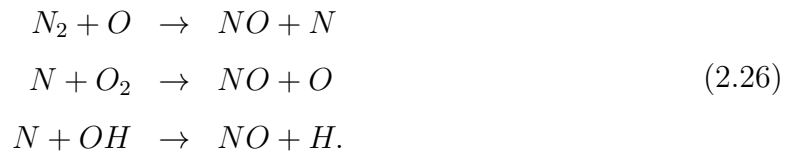
Although the NO_X emissions have a low total share it is a strong stimulus on human, fauna and flora. It disturbs the metabolism in very small concentration.

Therefore the calculation and reduction of NO_X emission is an important field in combustion engineering [10].

Exhaust gas recirculation

Lean combustion always goes along with nitrogen oxides (NO_X) as product. The most effective measure to reduce NO_X prevails exhaust gas recirculation (EGR). The fresh air is diluted with inert gas (CO_2 and H_2O) that leads to significant reduction of local gas temperature peaks. This leads to lower activation energy for the NO_X formation mechanism. Nowadays EGR is commonly used in most state of the art diesel engines [21] and [19].

One drawback is the reduced amount of oxygen in the combustion chamber by dilution of fresh air with incombustible inert gas. Increasing power request as a result of transient

operation condition results in increasing fuel quantity and therefore a drop of the air fuel equivalence ratio. This is the available torque reserve, detailed explanation will be given in chapter 4. Low λ values lead to extensive raise of soot formation due to locally rich combustion zones. To increase the amount of available oxygen for combustion in such conditions, the amount of EGR is reduced by the engine control.

Heat value

Diesel is getting gaseous at temperatures between 200 - 300 °C and is modified for specific climatic conditions. The cetane number (CN) is an inverse function of the ignition delay and defines the willingness for combustion. Diesel combustion works well with cetane numbers between 40 - 60, for best combustion properties a high CN is desirable.

The combustion converts chemical energy into heat. The zero point for internal energy or enthalpy of the fuel and air as well as the products of the complete combustion is defined at a common temperature e.g. at 0°C. The difference between this arbitrary zero and the absolute zero is called heat value. The value differs at constant volume H_v and at constant pressure H_p.

For adiabatic combustion the energy balance at constant volume can be written for an isochoric combustion process as

$$U' + H_v(T_0) = U'' \tag{2.27}$$

and for the isobar combustion

$$H' + H_p(T_0) = H''. \tag{2.28}$$

Inner energy of air and fuel U' respectively the enthalpy H' are converted to the inner energy of the combustion gas U'' and the enthalpy H'' in relation to the arbitrary zero T_0. The heat values of constant pressure and constant volume have the relation

$$H_v - H_p = p\Delta V \tag{2.29}$$

with the combustion pressure p and the volume increase at constant pressure after cooldown. For combustion cycle calculation in internal combustion engines usually the heat

value at constant volume is used, although the difference can commonly be neglected. For further calculation the lower heat value of diesel $H_l = 43\ MJ/kg$ is used.

Fuel energy

Q_{fuel} is calculated from injection mass flow $\dot{m}_{fuel}$, lower heat value H_u and the stoichiometric air fuel ratio AFR_{st}

$$Q_{fuel} = \frac{H_u}{AFR_{st}}\ \dot{m}_{fuel}. \tag{2.30}$$

Rate of heat release

The diesel combustion process is an exothermic reaction that starts as soon as thermal energy is high enough. The temperature increase accelerates the reactions. Typical the velocity coefficients have a very strong, nonlinear dependency from temperature.
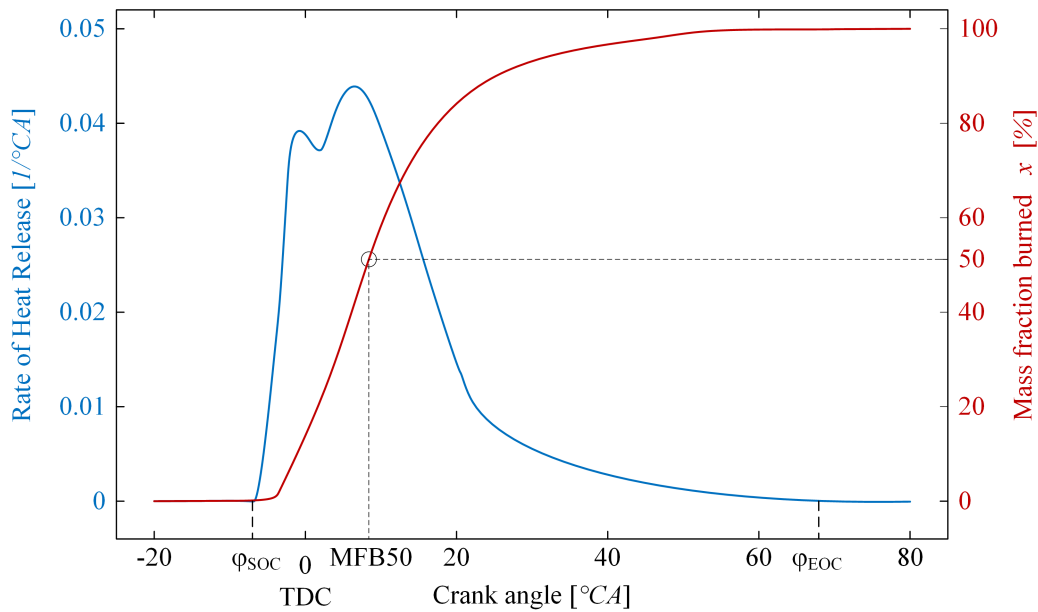
Figure 2.7: Rate of heat release and mass fraction burned of a real engine.

According to the approximation defined by S. Arrhenius in 1889 [10], heat release respectively the produced heat $\dot{Q}_c$ is simplified written as a single step reaction:

$$\dot{Q}_c = \dot{q}_{fuel}V[B]^a A\ e^{\frac{-E}{RT}}. \tag{2.31}$$

This equation uses the chemical heat release $\dot{q}_{fuel}$, the concentration of the fuel $[B]$ and the reaction order a in the volume V and reaction rate. The reaction shows that the system

gas/fuel mixture burns what leads to increase of temperature and reaction velocity up to the complete reaction. Further detailed explanation is given in Pischinger [20]. Figure 2.7 shows the combustion process of a real engine depending on the crank angle.

The axis on the left hand side shows the *rate of heat release (ROHR)*. Position of *start of combustion* φ_{SOC} significantly influences the combustion process and further on the engine efficiency. Mass fraction burned is the integral of the ROHR as described on the axis on the right hand side. One can see in the shape of *mass fraction burned (MFB)* that *end of combustion* φ_{EOC} has only few impact on the MFB.

The angle where 50% of the fuel is burned is called *mass fraction burned 50% (MFB50)*. It is an important indicator of the position of combustion in the working cycle and therefore also for the efficiency and the produced mechanical work on the crankshaft. This value can be determined by the heat release curve.

2.4 Standard cycle process

The real combustion process is too complex for mathematical formulation. Numerical simulation can be done with focus on flame front for deeper understanding of reaction kinetics and transport mechanism. Secondly numerical simulation can be done for technical reactive flow analysis for prediction of flame propagation and heat release. Due to massive computational effort these simulations are usually done in one-dimensional simulation.

To enable a calculation in a real time environment on an embedded system further simplification by the use of standard combustion cycle can be used. Following assumptions are considered in Pischinger [20]:

- charge consists of ideal gas with constant gas properties;
- combustion take place in a predefined shape;
- wall heat losses are not considered;
- no consideration of flow losses or leakages;
- friction-free compression and expansion.

Although combustion engines do not have a closed cycle process due to gas exchange, the methodology can be used by consideration of heat transfer. Then all laws of cycle processes can be used for calculation. The change of system states can be seen as closed

cycles in the pV- and TS-diagram that are passed through clockwise. Based on this, three different cases can be identified:

- constant volume process;
- constant pressure process;
- combined process is separated in a constant room - followed by a constant volume combustion.

As we remember from figure 2.5 the surface in the TS-diagram below the points 4 and 1 define the exhaust heat.
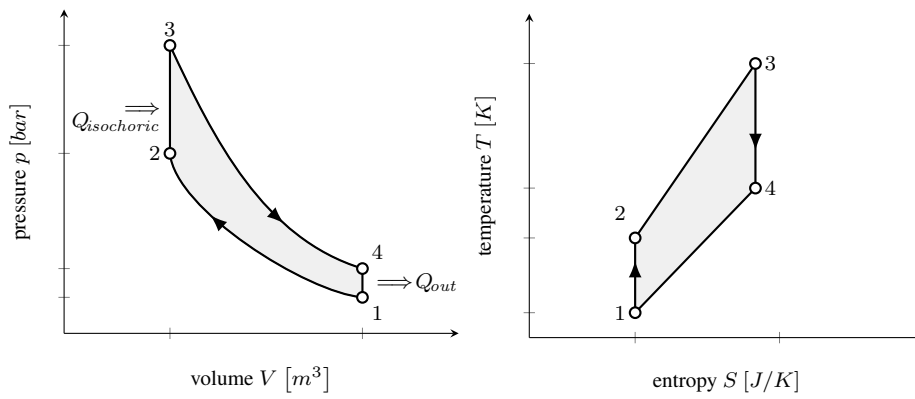
Figure 2.8: pV and TS-diagram of combustion at constant volume

Constant volume process has the smallest surface which leads to lowest thermal losses and highest efficiency.
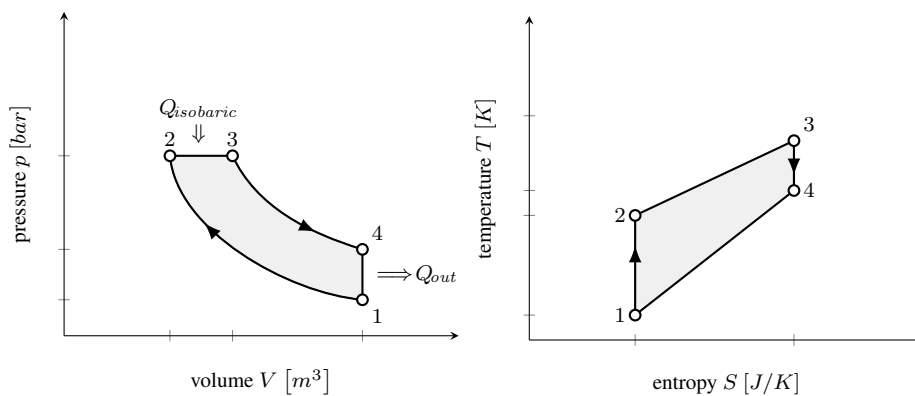
Figure 2.9: pV and TS-diagram of combustion at constant pressure

The assumption of a combustion with constant pressure leads to the shape in pV and TS-diagram as shown in figure 2.9. This process has the highest peak firing pressure and temperature which leads to increased thermal and mechanical stress.

This work further uses the combined working process of the internal combustion engine shown in figure 2.10.

Figure 2.10: pV and TS-diagram of combined standard cycle process.

The combined working process shows best comparability of idealized processes with the real combustion shape.

In standard conditions the enclosed surface and therefore the work is very well comparable. As this work does not consider crank-angle resolved calculations but uses the integral of the combustion cycle for further calculations the model deviation is acceptable.
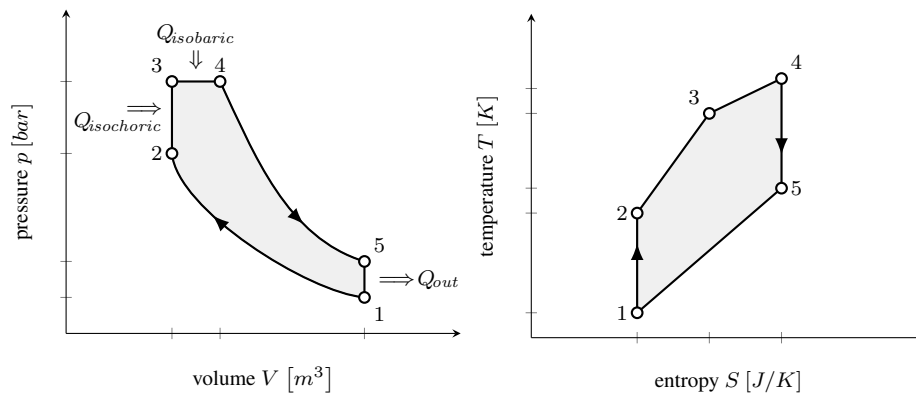
2.5 Conclusion

Chapter 2 provided the basis for the further work. Starting from the working principle of the 4 stroke engine the explanation came to the thermodynamic principles.

Further on the relevant system parameters were defined and explained. This includes the main influences, intermediate and target results like the mean effective pressure and the engine torque. These are massively effecting the performance of the ICE, they can be measured on engine testbed and are provided as calculation results in this work. Properties like the air-fuel equivalence ratio that are relevant for the combustion process in respect to resulting power but also for emission were given.

The chapter closes with the explanation of standard cycle processes. Different possibilities and the argumentation for using the combined standard cycle process for the calculation as given in chapter 3.

3 Online torque calculation

3.1 Calculation overview

This chapter presents the calculation of the engine torque using the principles of diesel engine combustion. Figure 3.1 illustrates the calculation steps and the proposed workflow.
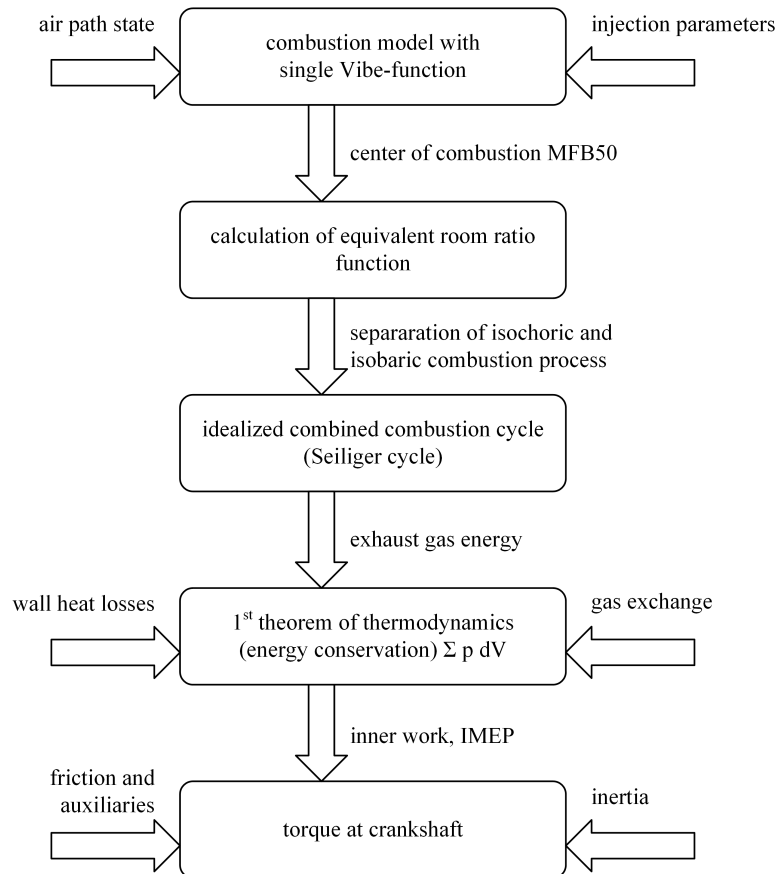

Figure 3.1: Workflow to calculate torque at crankshaft.

The phenomenological method presented by Danninger [6] directly uses signals already available in the ECU. These are control reference and sensor signals from air path as well as command signals e.g. injection quantities and soot limitation. Remaining parameters in

the calculation can be derived from simple tests at the engine testbed.

The presented combustion model provides the center of combustion that is used for several calculations. First use is the separation of injection energy for the combined standard cycle process that leads to intake- and exhaust enthalpy. Secondly it is used to evaluate geometric parameters that are required for wall heat loss calculation. This follows a phenomenological approach and can be used as a tuning parameter to fit the model to measurements. Simplified calculation of gas exchange finally provides all information to compute the energy balance equation and evaluation of inner work. Further on and indicated mean effective pressure can be computed. Based on this the final outcome is the resulting engine torque at the crankshaft considering inertia, friction and auxiliaries.

3.2 Combustion model

The calculation of the simplified work cycle requires a separation of the injected fuel for the isochoric and the isobaric combustion. This section illustrates the calculation steps from combustion model via the computation of combustion center to the evaluation of the equivalent room ratio function.

3.2.1 Approximation using a single Vibe function

This work uses a simple approach to model the combustion process by a direct specification of the ROHR to address the requirement for online calculation in an ECU. It represents the complex thermodynamic processes during combustion, the importance was outlined in previous chapter.

At first the rate of heat release is calculated by a single Vibe-function describing the heat release during combustion. Dubbel [10] provides possible procedures for implementation. Parameters of ROHR are determined from measured cylinder pressure data at specific engine operation points. The dimensionless heat input characteristic must be specified over crank angle. Based on this a calculation to estimate crank angle of MFB50 is presented. The use of a function, as introduced by Vibe [30], for the rate of heat release calculation is based on reaction-kinetic considerations. It is often used for approximation due to simple use[10], [2]. Figure 3.2 shows the approximation of the rate of heat release and mass

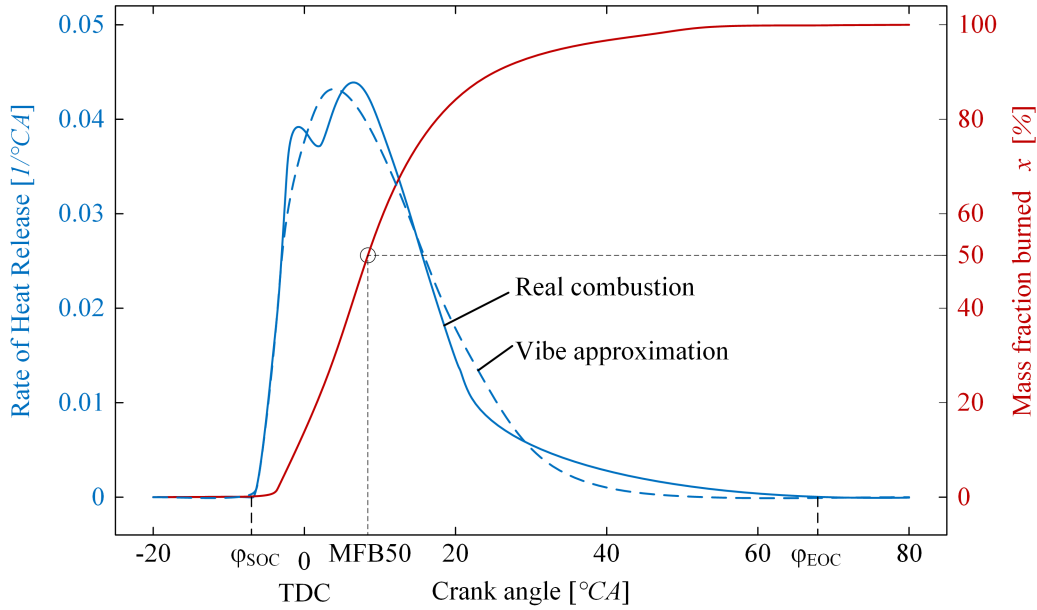fraction burned by a single vibe function as an extension to Figure 2.7.

Figure 3.2: Approximation of rate of heat release and mass fraction burned by a single Vibe function.

The simplified approach does not represent all effects like the typical two peaks in the rate of heat release. Although the mass fraction burned fits very well between real engine and Vibe approximation.

The approach uses the *shape factor* β and the *Vibe-constant* $a = -6.908$ for complete combustion. Angle information as the start of combustion φ_{SOC} and the *combustion duration* φ_d leads to the *mass fraction burned* x at this position. The relation to the total fuel mass Q_{fuel} leads to the rate of heat release:

$$\frac{dx}{d\varphi} = \frac{a}{\varphi_d}(\beta + 1)y^\beta e^{-ay^{(\beta+1)}} \ with \ y = \frac{\varphi - \varphi_{SOC}}{\varphi_d}. \tag{3.1}$$

Based on this equation the integral of the Vibe function leads to the rate of heat release function as it provides the fraction of fuel that is burned since start of combustion as

$$x = \int \frac{dx}{d\varphi} \cdot d\varphi = 1 - e^{-ay^{(\beta+1)}}. \tag{3.2}$$

These parameters can be identified based on measurements of the combustion curve with an indication system on engine testbed during the engine development phase. The reference values for stationary operation points are stored in maps depending on the engine speed
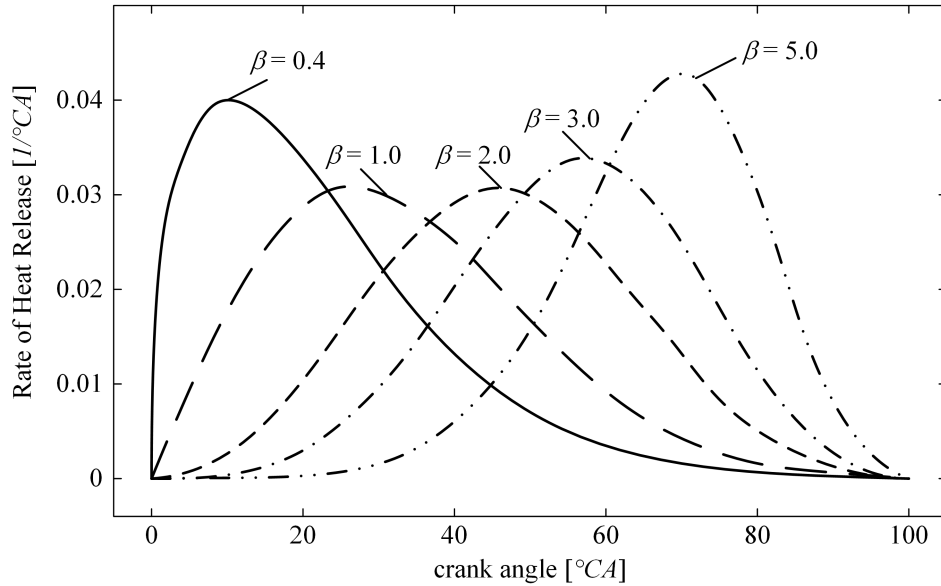
and injection quantity.

Figure 3.3: Influence of the shape factor β on the heat release.

The impact of the shape factor is given in figure 3.3. It has a significant impact on the combustion shape and is used as calibration parameter.

For adaptation of the Vibe-function to conditions that differ from the steady state operation point the approach of Woschni and Anisits [32] is used. Especially in transient operation significant deviations of the heat release have been observed compared to the reference point. At first it considers a deviation of combustion duration as function of the air fuel equivalence ratio λ, combustion efficiency η_c and engine speed N

$$\varphi_d = \varphi_{d,ref} \left(\frac{\lambda}{\lambda_{ref}} \right)^{-0,6} \left(\frac{N}{N_{ref}} \right)^{0.5} \eta_c^{0.6}. \tag{3.3}$$

Secondly cylinder charge variables pressure p_{int}, T_{int} at closing intake valve and λ correct the reference shape factor to reflect the changed circumstances in transient operation. The calculation of the shape parameter β is defined as

$$\beta = \beta_{ref} \left(\frac{\lambda}{\lambda_{ref}} \right)^{-0.6} \frac{p_{int}}{p_{int,ref}} \frac{T_{int}}{T_{int,ref}}. \tag{3.4}$$

For intake pressure $p_{int,ref}$ and intake temperature $T_{int,ref}$, interpolated values are calculated from the lookup-tables corresponding to the current engine speed and injection quantity.

The influence of the exhaust gas recirculation (EGR) is covered by the air-fuel equivalence ratio λ.

By solving the Vibe-function from equation 3.2 at $x = 50\%$ fuel conversion, the angle of combustion center MFB50 can be derived in crank angle domain depending on the combustion duration $\varphi_{d,Ref}$ and start of combustion φ_{SOC}:

$$\varphi_{MFB50} = 0.10034^{\frac{1}{\beta+1}} \cdot \varphi_{d,ref} + \varphi_{SOC}. \tag{3.5}$$

The diesel combustion relies on the compression ignition of the injected fuel. The time between start of injection until the start of combustion is called ignition delay. It represents an important value for pollutant emission formation and combustion noise. For simplification reasons the value is identified using stationary testbed measurements.

The adaptation of combustion center MFB50 therefore is mainly influenced by a injection timing change and the calculated shape parameter from cylinder charge states.

3.2.2 Equivalent room ratio function

In general, the equivalent room combustion provides the combustion efficiency. The real combustion process differs from the ideal one, so that even in complete combustion thermodynamic losses need to be considered.

Main influence factors are the compression ratio at combustion center and gas property changes, represented by the isentropic coefficient κ.

The split ratio of the fuel energy is defined by the equivalent room ratio function η_{ERR} (see Pischinger [20]) that is used to separate the heat applied within both combustion processes

$$\eta_{ERR,MFB50} = \frac{1 - \varepsilon_{MFB50}^{\kappa-1}}{1 - \varepsilon_{nominal}^{\kappa-1}}. \tag{3.6}$$

The equivalent room ratio function provides the ratio of the work in respect to the equivalent room combustion as efficiency depending on crank angle. The upper part of figure 3.4 shows the dependency of the function from compression ratio ϵ. Although for most engines this is a design parameter that can be modified also in operation by variable valve timing as described by Schutting [23].

The lower part presents the influence of the equivalent room ratio function from the
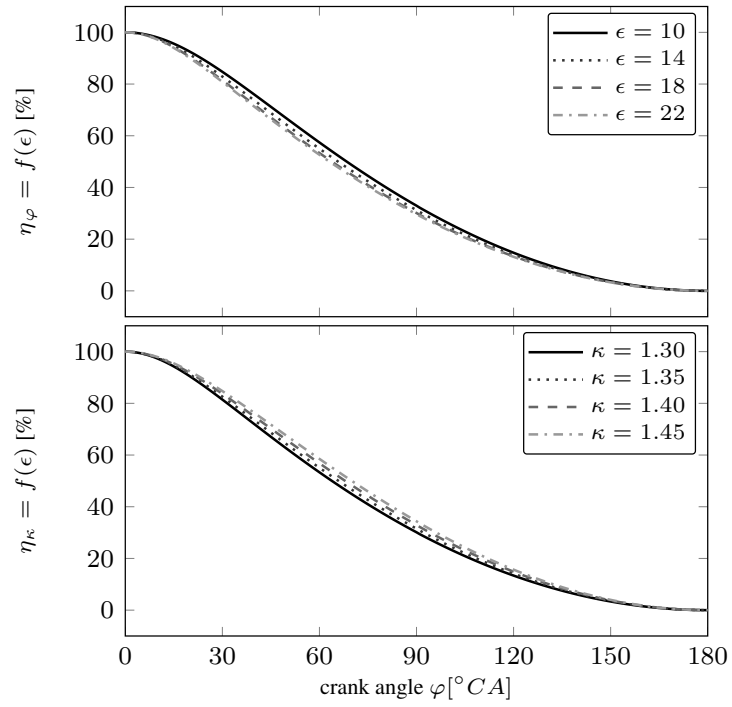
Figure 3.4: Equivalent room ratio function depending on compression ratio ϵ and isentropic coefficient κ.

isentropic exponent κ. As described in section 2.3 the isentropic exponent mainly depends on temperate, pressure, volume and gas composition.

For the relevant value η_{ERR} the compression ratio ε_{MFB50} is calculated at φ_{MFB50}.

3.3 Cycle calculation

The work cycle calculation covers the state changes starting at intake valve closing until the exhaust valve open. Main outcome for further use is the energy Q_{out} as the difference of intake- and exhaust enthalpy. These are main contributors to calculate the energy balance equation.

Changes of the system states of a cycle process can be seen as closed cycles as provided in section 2.4.

Continuous combustion process is defined by closed curves in clockwise direction in the p-V diagram. Thermodynamic efficiency η_{th} is the quotient of emitted and supplied power:

$$\eta_{th} = \frac{-W}{Q_{supplied}} = 1 - \frac{Q_{emitted}}{Q_{supplied}}. \tag{3.7}$$

The optimal process (Carnot-process, see 2.2.3) is characterized by supplying heat at highest possibly temperature and emitting it at lowest possible temperature [10]. This leads to a rectangle in the TS-Diagram and a maximum efficiency of

$$\eta_c = 1 - \frac{T_{emitted}}{T_{supplied}}. \tag{3.8}$$

Within this process significant changes of temperature, pressure and volume take place. The gas property values strongly depend on the temperature, pressure and gas mixture. Therefore it is required to determine the gas property values separately for each of the process steps. Specific gas constant R, specific heat capacity at constant pressure c_p respectively at constant volume c_v and their relation as the isentropic exponent $\kappa = \frac{c_p}{c_v}$ (see equation 2.14) are given in $\frac{J}{kgK}$. The values are taken from tables in literature, see Pischinger [20] and Bähr [4], and are provided in appendix D. For the calculation of the combined isobaric and isochoric combustion process following assumptions are required:

- combustion separated in isochoric and isobaric combustion;
- adiabatic process, separate treatment of heat losses;
- isentropic compression and expansion, friction treated separately;
- neglecting blow by and flow losses;
- valve opening and closing at top and bottom dead center.

The combined combustion process as shown in figure 3.5 presents the used calculation steps. Starting from intake valve closing (starting point 1) the compression leads to start of combustion (point 2). Combustion itself is separated into isochoric (point 3) and isobaric combustion (point 4). The expansion leads to the conditions at exhaust valves opening (point 5).
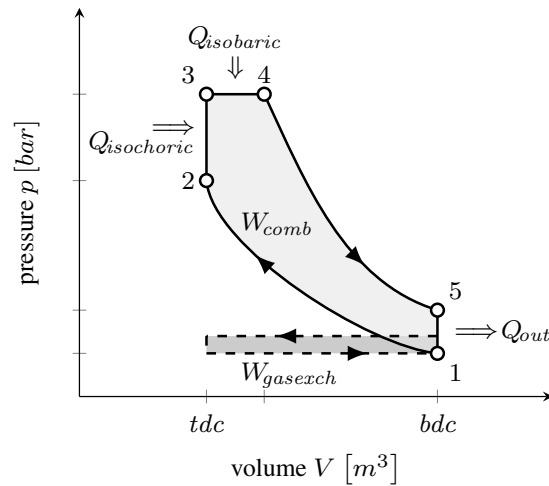
Figure 3.5: pV-diagram of the ideal internal combustion working cycle (Seilinger cycle) with transported heat flows replacing transported mass flows.

This work uses ideal gases but considers changing gas properties. In general, this is similar to the real engine with following assumptions

- gas charge without residual gas or scavenging;
- rate of heat release following a defined combustion shape until equivalence;
- air fuel ratio as on the real engine;
- no wall heat losses;
- no gas losses;
- ideal gas exchange process.

If valve opening times differ from top / bottom dead center by using e.g. Miller or Atkinson-cycle [23] the calculation needs to be adapted. In case of variable valve actuators the current scavenging profile shall be considered with respect to mixture and amount of the charge and gas exchange work.

Limited computation power and real time calculatino requirements enforce simplified approaches to analyze the combustion cycle. Reductions are done with respect to combustion

process, wall heat losses, gas exchange and gas properties.

For this working process as outlined in section 2.4 the main states can be calculated in a straight forward way.

The points, the calculation refers to, are numbered in figure 3.5. This section provides the calculation of input, output and each process between these points.

Injection power

The added heat of the diesel engine is a function of the lower heat value H_l, the air fuel equivalence ratio λ and the stoichiometric value L_{st} and results in

$$q_{in} = \frac{H_l}{\lambda\ L_{st}}. \tag{3.9}$$

Intake enthalpy

At closing the intake valve, the state before compression is calculated with the cylinder charge mass $\dot{m}_{cyl}$. Temperature from intake manifold $T_1 = T_{int}$ and the specific heat constant c_v at intake manifold conditions complete required information.

$$U_{h,1} = c_{v,1}\ T_1\ \dot{m}_{cyl}. \tag{3.10}$$

Starting point

Point 1 is used as a reference value for start and end of the combustion cycle. The state is defined by following equations with the general gas constant $R_{air} = 287\ J/kgK$:

$$p_1\ v_1 = R\ T_1,$$
$$h_1 = \int_{T_0}^{T_1} c_p dT, \tag{3.11}$$
$$u_1 = h_1 - R\ T_1.$$

This work defines the reference temperature T_0 at $20°C = 293,15\ K$. The value for the specific heat value at constant pressure c_p is taken from the table in the appendix D.

Compression

The isentropic compression from starting point to the begin of combustion leads to volume and temperature change and is calculated by

$$\frac{T_2}{T_1} = \left(\frac{v_1}{v_2}\right)^{\kappa-1} = \epsilon^{\kappa-1}. \tag{3.12}$$

Equivalent room combustion

To calculate point 3 the amount of fuel for this part needs to be defined. Introducing the fuel into the combustion chamber increases the total mass.

To estimate the amount of fuel related to equivalent room - and equivalent volume combustion, the calculated equivalent room ratio function as described in section 3.2.2 is used. The split of fuel power can now be calculated by using 3.6:

$$Q_{isochoric} = Q_{23} = Q_{fuel}\ \eta_{ERR,MFB50}$$
$$Q_{isobaric} = Q_{34} = Q_{fuel}\ (1 - \eta_{ERR,MFB50}). \tag{3.13}$$

Using equation (2.30) the enthalpy of the introduced and immediately burned fuel leads to

$$T_3 = \frac{Q_{23}}{c_{v,23}\ m_c} + T_2 = \frac{m_{f,23}\ H_l}{c_{v,23}\ m_c} + T_2$$
$$p_3 = \frac{m_{cyl} R\ T_3}{v_{MFB50}}. \tag{3.14}$$

Equivalent pressure combustion

With the heat referenced to the equivalent pressure $Q_{34} = Q_{isobaric}$, point 4 is calculated by:

$$T_4 = \frac{Q_{34}}{c_{p,34}} + T_3. \tag{3.15}$$

Expansion

Similar the isentropic expansion is given by

$$T_5 = T_4\ \epsilon^{1-\kappa},$$
$$p_5 = \frac{m\ R\ T_5}{V_d}. \tag{3.16}$$

Due to volume change and heat losses in the exhaust manifold the value of T_5 differs from mean exhaust manifold pressure measurement on engine testbed.

Exhaust enthalpy

Based on the temperature after expansion T_5, specific heat constant c_v, total mass consisting of the induced charge $\dot{m}_{cyl}$ and the injected fuel $\dot{m}_{fuel}$ the exhaust enthalpy is calculated by

$$U_{h,exh} = c_{v,5} \ T_5 \ (\dot{m}_{cyl} + \dot{m}_{fuel}). \tag{3.17}$$

3.4 Wall heat losses

For the estimation of wall heat losses, heat transfer and surface temperature have significant influence on the energy balance.

For reduction of calculation effort, the position of combustion center MFB50 is selected as the point to calculate a mean value of wall heat losses. The calculation of surface and volume of the combustion chamber at this position using geometric relations is presented in the upcoming section.

A comparison of several different methods as outlined by Ma [17]. To reduce calculation effort to its minimum this work basically follows the phenomenological approach introduced by Woschni [31].

Wall temperature can either be derived from a calibration map or can be estimated by calculation of thermal states.

3.4.1 Kinematics of the crank-rod system

Crank-angle resolved algorithms calculate the surface at each piston position and uses this in the calculation of wall heat losses. In contrast to this a single surface needs to be selected for the integral calculation as it is done in this work. The piston position at *50% fuel burned* is chosen to determine the combustion chamber surface A_{MFB50} and volume V_{MFB50}. At first the piston position at φ_{MFB50} need to be evaluated based on the kinematics of the crank-rod system. Basis for the calculation is given in section P of Dubbel [10]. Figure 3.6 shows the principle of the crank-rod system and its calculation.
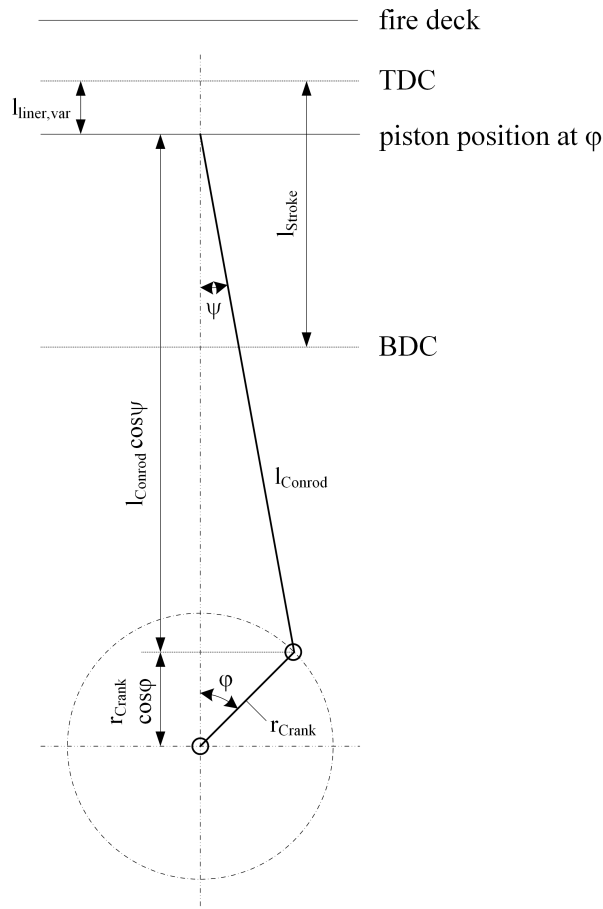
Figure 3.6: Crank-rod system of an internal combustion engine.

The distance $l_{liner,var}$ between the requested piston position and TDC is calculated with the conrod length l_{conrod} and crankshaft radius given by the stroke length $r_{crank} = \frac{l_{stroke}}{2}$ by

$$l_{liner,var} = r_{crank} + l_{conrod} - r_{crank} \; cos\varphi - l_{conrod} \; cos\psi. \tag{3.18}$$

Based on geometric relations the conrod angle is defined as

$$sin\psi = \frac{r_{crank}}{l_{conrod}} \; sin\varphi. \tag{3.19}$$

Using the geometric relation $sin^2\psi + cos^2\psi = 1$ the distance of the piston from TDC can be calculated via

$$l_{liner,var} = r_{crank} \; (1 - cos\varphi) + l_{conrod} \left(1 - \sqrt{1 - \left(\frac{r_{crank}}{l_{conrod}}\right)^2 sin^2\varphi} \right). \tag{3.20}$$

Together with the compression ratio ϵ the liner wall surface can be computed as

$$A_{liner} = l_{bore}\ \pi\ \left(\frac{l_{stroke}}{\epsilon} + l_{liner,var}\right). \tag{3.21}$$

Assuming the surface of the fire deck is equal to the piston surface A_p the relevant surface for wall heat losses results in

$$A_p = 2\ \pi\ \left(\frac{l_{bore}}{2}\right)^2. \tag{3.22}$$

From these values the surface can be calculated via

$$A_{MFB50} = 2A_p + A_{liner}. \tag{3.23}$$

Additionally the cylinder volume is calculated by

$$V_{MFB50} = A_p\left(\frac{l_{stroke}}{\epsilon} + l_{liner,var}\right). \tag{3.24}$$

3.4.2 Heat transfer coefficient

According to the method from Woschni [31] and his joint work with Huber [13] the gas-wall heat transfer coefficient α_{gw} can be determined via the mean piston velocity v_c.

Based on his work, Hohenberg [8] uses the characteristic volume to determine the heat transfer coefficient based on cylinder pressure and temperature.

All these approaches use crank-angle dependent calculation. This work uses a simplified approach by calculation of a single point at MFB50. The volume V_{MFB50} at this crank position and the indicated mean pressure p_i (IMEP) lead to the calculation of the relevant velocity as

$$v = v_c(1 + 2\ V_{MFB50}^2\ p_i^{-0.2}) = \frac{2\ l_{stroke}}{n}(1 + 2\ V_{MFB50}^2\ p_i^{-0.2}). \tag{3.25}$$

Based on the cylinder volume at combustion center $V_{cyl,MFB50}$, velocity v, indicated cylinder pressure p_{cyl} and temperature T_4, the gas-wall heat transfer coefficient is calculated as

$$\alpha_{gw} = 130\ V_{cyl,MFB50}^{-0.06}\ p_{cyl}^{0.8}\ T_4^{-0.4}\ (v + 1.4)^{0.8}. \tag{3.26}$$

3.4.3 Wall heat loss based on empirical wall temperature

Measurement of the cylinder liner temperature at the surface is very difficult as contact related measurement due to extremely high temperatures. Optical measurement is strongly influenced by luminousness effects during combustion.

Validation is done on special testbeds e.g. single cylinder research engines. Rough magnitude of wall temperature is known from experience.

As this is one of the main uncertainties within this calculation method, the wall temperature can be used as calibration parameter to adapt the calculation results to testbed measurements.

According to the method from Woschni and Huber [13] one can calculate the wall heat losses as follows:

$$Q_{wall} = \alpha_{gw} \ A_{MFB50} \ (T_{wall} - T_4). \tag{3.27}$$

3.4.4 Wall heat loss based on thermal state estimation of wall temperature

The approach of thermal state estimation of a diesel engine is described in detail by Traussnig [25] and Hage [11]. The transformation of energy is modeled by the thermal resistance concept. This allows calculation of thermodynamic systems with using Kirchhoff's laws that are well known from electrical networks.

For complexity reduction the real mass of the system elements is simplified by using lumped masses. In case of the research the model was designed with four equivalent masses. Figure 3.7 shows the distribution and the connections for heat flow between them. The representative cylinder was designed in case of the rough approach with the help of the following components:

- Gas mass m_{gas};
- Piston m_p;
- Structure including liner, cylinder head, inlet- and outlet valves m_s;
- Cylinder block m_b;
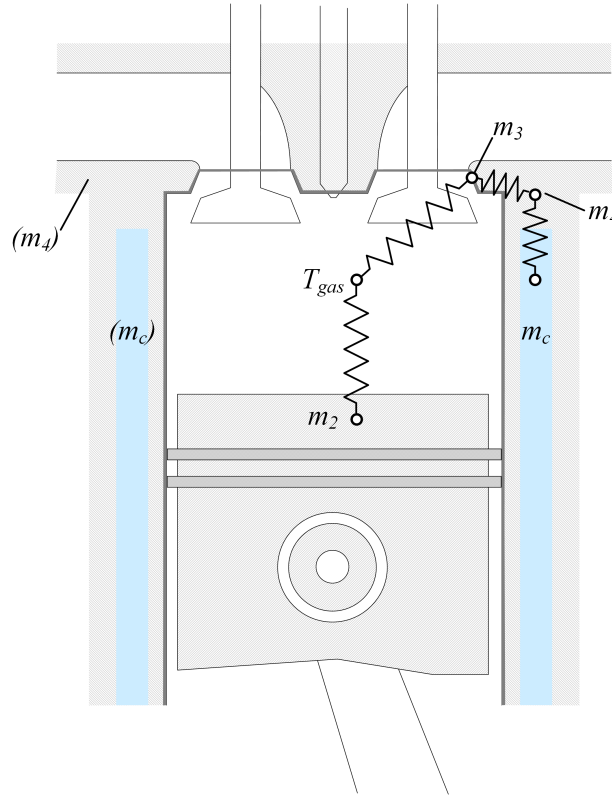- Coolant in the cylinder block water-jacket m_c.

Figure 3.7: Discretization of the combustion chamber to lumped masses.

Based on the energy conservation law as given in formula 2.1, the balance of thermal states using lumped masses can be written as Ordinary Differential Equation (ODE) for each node i.

$$m_i c_i \dot{T}_i = \dot{Q}_i + \sum_j \frac{T_j - T_i}{R_{i,j}} + \sum_j \dot{m}_{in} c_{in} T_j + \sum_i \dot{m}_{out} c_{out} T_i. \tag{3.28}$$

The left side represents the thermal inertia with the temperature T_i, the mass m_i and the specific heat capacity c_i. The directly induced heat flow Q_i and the heat transfer between the nodes as well as across the boundaries represent the right hand side.

Figure 3.7 shows the approach of discretization of the combustion chamber to lumped masses. The representative cylinder is replaced by the piston mass m_2, the mass with direct contact to the combustion m_3, the cylinder block m_4 and the coolant m_c.

When applying this approach to the system a set of ODEs and using the related thermal resistances, the physical behavior follows:

$$\text{piston}: m_p c_p \dot{T}_p = \frac{T_{gas} - T_p}{R_{gas,p}} + \frac{T_s - T_p}{R_{p,s}}$$

$$\text{structure}: m_s c_s \dot{T}_s = \frac{T_{gas,s} - T_s}{R_{gas,s}} + \frac{T_p - T_s}{R_{p,s}} + \frac{T_b - T_s}{R_{s,b}}$$

$$\text{cylinderblock}: m_b c_b \dot{T}_b = \frac{T_s - T_b}{R_{s,b}} + \frac{T_c - T_b}{R_{b,c}} \tag{3.29}$$

$$\text{coolantwater}: m_c c_c \dot{T}_c = \frac{T_b - T_c}{R_{b,c}} + \dot{m}_c (c_{c,in} T_{c,in} - c_{c,out} T_{c,out})$$

Based on the temperature of the gas T_4, piston T_p and structure T_s the wall heat losses can be calculated similar to equation 3.27. Overall combustion chamber surface A_{MFB50} is separated of the into the piston surface A_p and the surface of fire deck and liner as

$$Q_{wall} = \alpha_{gw} \left[A_p (T_p - T_4) + (A_{MFB50} - A_p)(T_s - T_4) \right]. \tag{3.30}$$

3.5 Gas exchange

At the end of the working cycle the exhaust gas is pressed through the exhaust valves and the cylinder is then filled with fresh charge. The calculation provided in section 3.3 defines the pressure and temperature state before and after exhaust valve opening.

While the pressure upstream turbine is measured in some production engines other ones rely on already existing models. Therefore the mean exhaust gas pressure is considered as given for this calculation procedure.

The gas exchange work is represented by the area in the p-V diagram in figure 3.5. As only integral values are considered the calculation is simplified by a rectangular shape with the displacement volume V_d and mean pressure difference between intake- and exhaust manifold.

$$W_{gasexch} = \frac{p_{exh} - p_{int}}{V_d} \tag{3.31}$$

3.6 Energy conservation to calculate inner work

The calculation scheme is based on the energy conservation law and considers the main process steps along the combustion cycle. These are

- fuel power;
- intake charge power;
- the exhaust power based on combustion calculation;
- the charge exchange work;
- wall heat losses.

Starting point for the model is the 1st theorem of thermodynamics (the energy conservation law) which is formulated for an open in-stationary system in differential form as

$$\underbrace{dU}_{stored\ energies} = \underbrace{dW + dQ + dm\,h}_{transported\ energies}. \tag{3.32}$$

W represents the work, Q the heat, dm the mass with corresponding specific enthalpy h transmitted over the system boundaries intake (in) and exhaust (exh) valves. U denotes the inner energy of the system.

The partial derivation with respect to crank angle $d\varphi$ leads to

$$\underbrace{\frac{d(m_c\,u)}{d\varphi}}_{dU} = \underbrace{-p_c\,\frac{dV}{d\varphi}}_{dW} + \underbrace{\frac{dQ_{fuel}}{d\varphi} - \sum \frac{dQ_{wall}}{d\varphi}}_{dQ} + \dots$$

$$\dots + \underbrace{h_{int}\,\frac{dm_{int}}{d\varphi} - h_{exh}\,\frac{dm_{exh}}{d\varphi}}_{dm\ h}. \tag{3.33}$$

Closed integration over the entire working cycle resolves the dependency on the crank angle and leads to an algebraic form. It states that the indicated work W_i is equal to the fuel power plus the intake charge inner energy $U_{h,int}$ minus exhaust gas inner energy $U_{h,exh}$, wall heat losses Q_{wall} and the gas exchange work $W_{gasexch}$. Due to the closed integration the change of inner energy dU is zero and the equation can be written as follows:

$$W_i = \underbrace{Q_{fuel} + U_{h,int} - U_{h,exh}}_{W_{comb}} - Q_{wall} - W_{gasexch}. \tag{3.34}$$

Note that by replacing transported mass flows by corresponding inner energies the open process is mapped to an equivalent closed process.

3.7 Torque calculation

Main calculation principle of the engine torque is given in section 2.3. The torque provided at the crankshaft is one of the main values to validate the calculation principle. This section provides the application of the calculation methodology for the actual torque at crankshaft.

3.7.1 Calculation of inner torque

The torque represents a rotational force. The inner work as outcome of the energy conservation law leads to following calculation:

$$M_i = \frac{W_i}{4\pi} = \frac{Q_{fuel} + U_{h,int} - U_{h,exh} - Q_{wall} - W_{gasexch}}{4\pi}. \tag{3.35}$$

The inner torque cannot be measured directly. For validation of the calculated signal the IMEP, directly derived from the inner work, is used.

3.7.2 Auxiliaries and friction

The most relevant information is the resulting engine torque at the crankshaft. This can be calculated starting from inner torque M_i, the torque that is generated within the engine. Subtracting the friction torque M_{fric} (depending on engine speed n) and torque of auxiliary components M_{aux} from the inner torque leads to a calculated torque at the crankshaft

$$M_{calc} = M_i - M_{fric}(n) - M_{aux}. \tag{3.36}$$

The difference between inner torque and measurement signal at the crankshaft are losses and torque used for auxiliaries $M_{fric,aux}$. Although friction represents a discipline by its own the friction torque used for this calculation is represented by a calibration map. Main influence factor is the engine speed. Due to torque dependence these two properties define

the x and y axis.

Additional required torque to cover losses and requested torque e.g. for auxiliaries like the compressor for air condition is added to the demand torque. The final torque is converted into a fuel injection quantity.

These signals are treated as known and accessible for the provided calculation as it is embedded in the ECU.

3.7.3 Torque at crankshaft

Final step in the calculation is a simple subtract of the losses and auxiliaries from the inner torque. The resulting signal provides the main physical outcome of the ICE.

$$M_{calc} = M_i - M_{fric,aux}. \tag{3.37}$$

Engine torque is a basic signal that is evaluated on engine testbed measurement. Development testbeds usually have an asynchronous machine that enables a four quadrant operation. The electric machine is set up as a pendulum and the stator braces on a load cell. Measured forces and the known lever length enables the calculation of the torque. This is the main reference signal to validate the outcome of the calculation.

3.8 Conclusion

The proposed algorithm applies the basic equations of an internal combustion engine and provides the main contributors of the energy balance equation. Outcome of this calculation is the inner work that a specific engine can provide with the given operation conditions. The energy of one cycle corresponds to the area within the working cycle in the pressure - volume diagram.

Conventional work process calculation involves calculation of many intermediate points e.g. every degree crank angle (°CA) from BDC to TDC for two full revolutions and integration along the resulting process curve. This leads to an enormous computational effort, exceeding the today's processing power of embedded control hardware used in ECUs.

The presented implementation shows a significant reduction of calculation effort by idealiz-

ing the combustion process. Splitting the process into separate parts that can be calculated independently from each other leads to a real-time algorithm that can be executed on standard ECUs.

4 Engine dynamics

In the past decades many different technologies have been introduced to improve power density, torque response and emissions, see Tschöke [26]. Some technologies significantly contribute to improvements and are seen as state of the art for applications in passenger cars and commercial vehicles.

Supercharging led to benefits like smaller packaging, better power to weight ratio and lower cost for the same power. Better engine efficiency by use of exhaust gas power, lower pollutant emissions and less noise are achievable, see Dubbel [10].
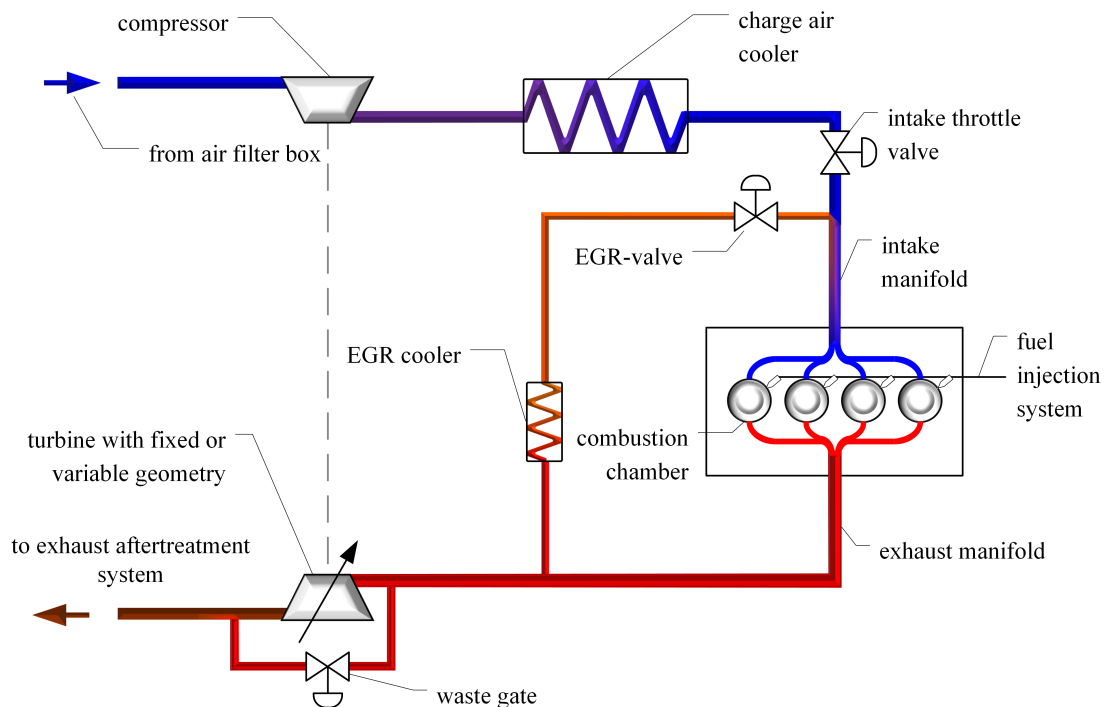

Figure 4.1: Diesel engine system including a typical air system.

As outlined in section 2.3, exhaust gas recirculation leads to a dilution of the air by inert gas. This leads to a decrease of the combustion velocity and therefore to lower local gas temperature and nitrogen oxide emission.

This work uses a common engine layout with a exhaust gas turbocharger, charge air cooler and EGR as shown in figure 4.1 on both engines used for validation.

Table 4.1 illustrates further details on the engine specifications. EGR valve position is defined as opened with 0% and closed with 100%.

Main task of the charging system is to provide sufficient amount of air for the combustion process. Energy for the compression is provided by the turbine. This element decompresses the exhaust gas and converts parts of the exhaust gas enthalpy into mechanical power to drive the compressor with a rotational speed of turbochargers of up to 160 000 rpm. To prevent overspeed, either a variable turbine geometry (VGT) - or wastegate actuator is used to bypass some exhaust gas energy and reduce the pressure drop.

	engine 1	engine 2
type	4 stroke diesel engine	4 stroke diesel engine
number of cylinders	5 cylinder inline	4 cylinder inline
displacement volume	2.5 dm^3	1.6 dm^3
maximum power	129 kW	96 kW
maximum torque	420 Nm	320 Nm
maximum speed	5000 rpm	5200 rpm
charging system	1 stage VGT	1 stage VGT
EGR System	cooled low & high pressure	cooled low pressure
compression ratio	16.5 : 1	15.4 : 1

Table 4.1: Specification of test engine 1 and 2.

The amount of available exhaust gas for the charging system is directly influenced by the EGR. The more exhaust gas is recirculated the less energy is available for the turbine.

Compression of the intake air leads to a temperature increase mainly depending on the pressure difference. A charge air cooler reduces the negative impact on the degree of supercharging and higher temperature for the combustion process. Further benefits are lower heat losses, nitrogen oxides and fuel consumption. The increased volume on the high pressure side has a negative impact on transient performance as some delay for pressure increase occurs.

4.1 Torque reserve

As discussed in section 2.3, low values of the air fuel equivalence ratio λ lead to extensive rise of soot emission. This can be prevented by limitation of the maximum injection quantity as well as by sufficient amount of air available.
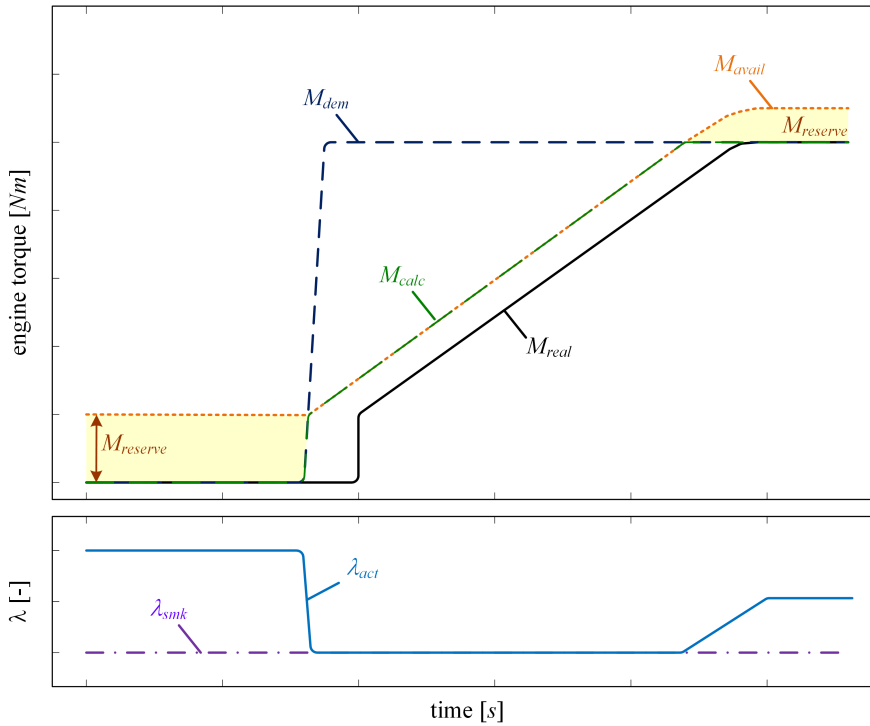

Figure 4.2: Schematic of torque response behavior of a diesel engine.

Figure 4.2 shows the relation of λ and torque in a demand step. The diesel engine is operated in lean combustion with an actual air fuel equivalence ratio λ_{act}.

In case of a torque request the injected fuel quantity is raised to provide the demand value. By this λ_{act} drops with the time constant of the injection system. If the demand torque cannot be covered by the torque reserve the air fuel equivalence ratio would drop to very low values. Therefore it is required to introduce a smoke limit λ_{smk} to avoid extensive pollutant emission.

Rewriting equation 2.25, $\lambda = \frac{\dot{m}_{air}}{AFR_{st}\ \dot{m}_{fuel}}$, to determine the injection quantity depending on available air mass flow $\dot{m}_{air,act}$ and the smoke limit leads to

$$\dot{m}_{fuel,smk,max} = \frac{\dot{m}_{air,act}}{AFR_{st}\ \lambda_{smk}}. \tag{4.1}$$

The maximum fuel quantity at the smoke limit can be converted into a maximum engine torque that can be provided by increase of injection quantity only. As the fuel quantity is limited the amount of air needs to be raised. This follows the time constant of the air path. During this phase the injection quantity remains limited by the smoke limitation. As soon as sufficient air is available to fulfill the demand torque with higher λ values, a torque reserve becomes accessible again.

The determination of torque reserve requires the calculation of the available torque under consideration of the maximum fuel injection quantity defined by the smoke limitation. This calculation follows the same procedure as defined within the calculation of the inner torque. The calculated maximum available inner engine torque $M_{i,avail}$ that is provided nearly instantaneously :

$$M_{avail} = M_{i,avail} - M_{fric}(N) - M_{aux}. \tag{4.2}$$

The available torque at crankshaft is calculated similar to equation (3.36) with the same values for friction and auxiliaries. Another signal of interest is the current torque reserve calculated from the signals above as

$$M_{reserve} = M_{avail} - M_{calc}. \tag{4.3}$$

This value represents the direct available additional torque at current operation.

4.2 Prediction of dynamic behavior

The main idea and calculation method is described in Danninger [5]. Engine dynamic behavior influences the quality of fulfilling the drivers demanded torque. Characteristic values defining the dynamic behavior of the engine torque are important for decision making within hybrid or transmission control. These can be e.g. the coefficients of a transfer function that specify the dynamic behavior, see Hülser [14]. The aim is to provide compressed information by the ECU in a standardized mathematical format.
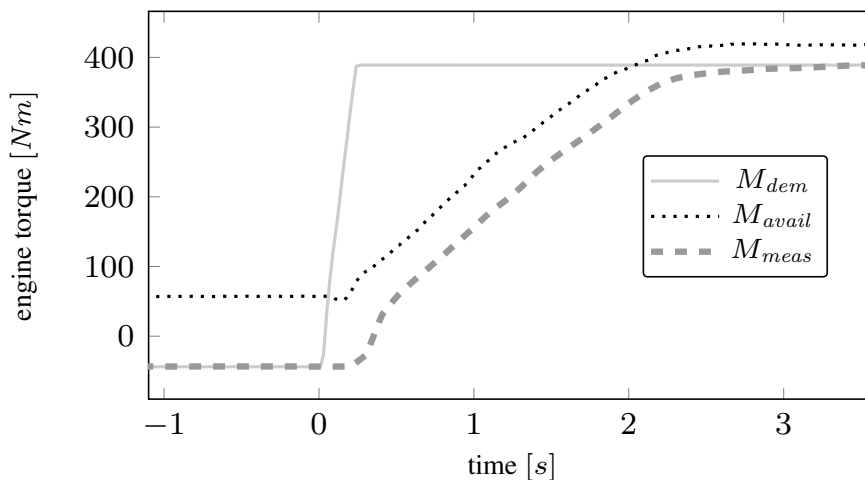

Figure 4.3: Step response from drag torque to full load and calculated time until demand torque with time delay in measurement signal.

The main processes of engine torque build up for a turbocharged diesel engine is illustrated in figure 4.3.

A torque build-up starts with a very fast torque increase up to the *available torque* M_{avail} defined by the smoke limit and actual air mass flow.

Torque requests beyond the torque reserve require an increase of air mass flow. With turbocharged diesel engines this implies either the acceleration of turbine and compressor, which requires increased exhaust gas enthalpy or the decrease of EGR or both. In order to have a fast torque response a reduction respectively deactivation of the EGR is a standard measure. Reducing EGR increases the air mass flow quickly in most operating conditions. This leads to higher gas temperature (less dilution with burned gas), faster and hotter combustion process and increases the exhaust gas energy. Acceleration of the turbocharger results from this. Finally increased compressor speed raises the air mass flow and by this higher fuel quantities can be injected what delivers more torque.

To derive a model characterizing the dynamic behavior, demand torque steps are analyzed using an example passenger car diesel engine of the 2 liters displacement class. Following analysis shows torque response measurement at constant engine speed. Fig. 4.4 summarizes the results of five different torque response tests.
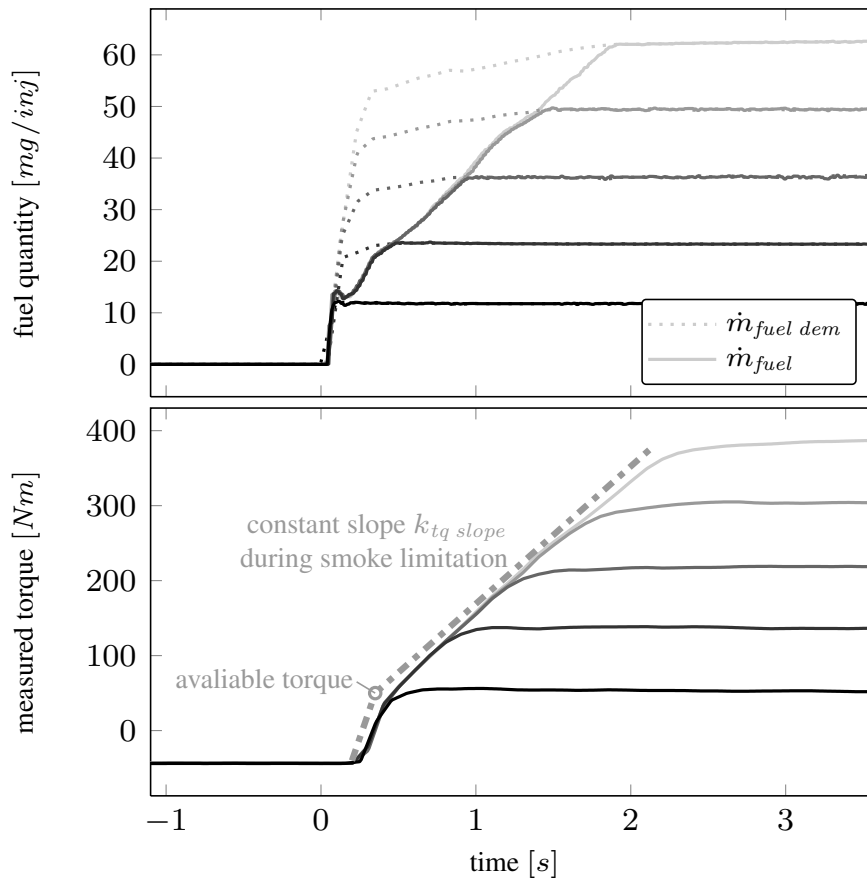

Figure 4.4: Fast torque requests from drag torque to five different torque levels.

All five tests start at zero fuel injection mass flow and end at different demand torque values. Upper plot shows requested (dotted) and injected fuel (solid). The lower diagram shows respective torque measured at testbed. Grey dash-dotted lines approximate the dynamic behavior: first phase (torque reserve) and second phase (smoke limitation). The signal of measured torque M_{meas} is time-delayed and low pass filtered by the testbed automation system. Nevertheless it is still possible to distinguish between the immediately available torque M_{avail} and the torque slope during smoke limitation $k_{tq\ slope}$ especially in Fig. 4.4. Simplified linear behavior of the torque build up during smoke limitation results from appropriate engine design and calibration. It is the target behavior as it provides best engine performance and driveability.

As analyzed extensively and presented in Schalk [21] the main influence factors on slope $k_{tq\,slope}$ are *engine speed n* and *EGR-ratio r_{egr}*. The latter depends on engine hardware and - calibration and represents the physical context whereas this value is explicitly not needed in the calculation. General behavior remains similar independent from engine speed or EGR-rate, as soon as the smoke limiter gets active the torque build-up follows a ramp (turbocharger acceleration).

To reach the demanded torque the required fuel quantity and the charge air must be available. As long as the latter one is not fulfilled, the smoke limiter remains active.

Provided figures have either common starting - or end point for comparing torque build-up behavior in different situations.

As can be seen from the lower diagram in Fig. 4.4 two values have been chosen to characterize and quantify the dynamic behavior of the engine torque:

- Immediately *available maximum torque*;
- *Slope* of the torque response in smoke limitation.

The available torque is calculated from *sensor values* and existing *calibration*. Based on the proposed three main signals shown in Fig. 1.2 the time that is required to fulfill a specific torque request can be derived

$$t_{tq\,dem} = \max\left(0,\, M_{dem} - M_{avail}\right) \cdot k_{tq\,slope}(n, r_{egr}). \tag{4.4}$$

Further analysis is done to validate this finding on its general applicability. Fig. 4.5 shows measurements starting at different torque levels with the target of full load. Upper diagram shows the demand and injected fuel quantity at constant speed. Torque reserve can easily be identified as the injected fuel quantity follows the demand value until this level and then follows the time constant of the air path.

The lower diagram presents the measured torque. Time constant is confirmed as independent from torque level as all different steps lead to the same behavior.

By this e.g. the transmission control can observe shifting times and decide to start a shift process or to inhibit shifting, see Bachinger [3]. A hybrid control unit can use this information to estimate the electric energy required to assist the combustion engine during transient operation.
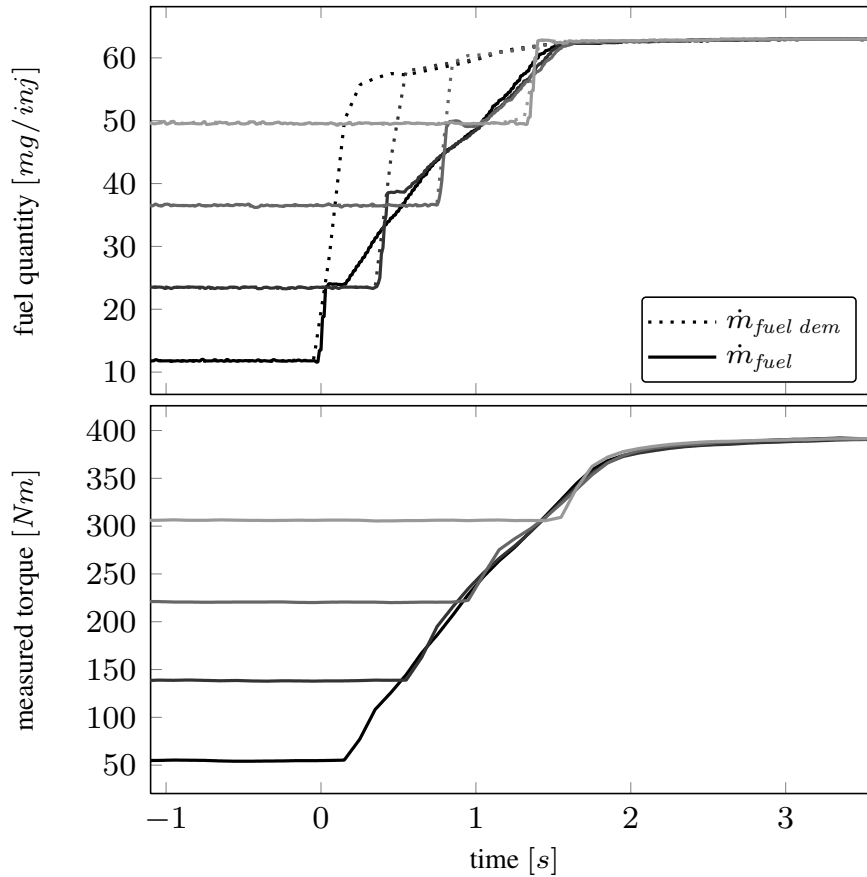
Figure 4.5: Fast torque requests from four different levels to maximum torque.

A big advantage is that neither TCU nor HCU need their own data set which describes the engines dynamic behavior. Also there are no parameters regarding the engine torque dynamic within the TCU and HCU which have to be kept consistent to the engine calibration.

4.3 Dependency on engine speed

Engine dynamics depend on the injection quantity as this is the main energy source for the combustion. Higher engine speed lead to increasing number of injections per time. Therefore it is obvious that engine speed has a significant impact on engine performance and higher speed enables a faster response on a requested torque increase.
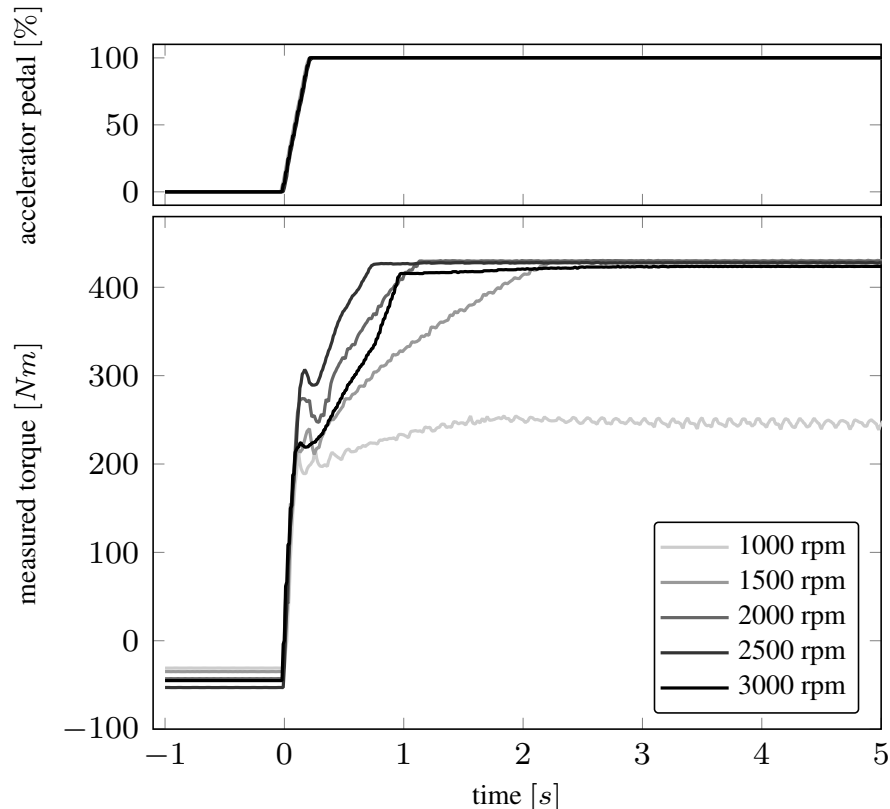
Figure 4.6: Step response measurement at different engine speeds from engine motoring to full load.

Figure 4.6 illustrates the perspicuously different torque response behavior in the time domain depending on engine speed resulting in different maximum torque level and performance. At 1000 rpm the maximum torque is limited what leads to different final values. The torque reserve from motoring condition is almost independent while increasing engine speed leads to a steeper slope of the torque response.

4.4 Dependency on EGR rate

The recirculation of exhaust gas has positive and negative effects on the engine behavior. On one hand it is a very effective measure to reduce pollutant emissions as explained in section 2.3. On the other hand this incombustible gas reduces the maximum available torque and engine performance. For this reason the EGR is reduced to a calibrate-able minimum value, depending on engine speed and injection quantity, as soon as the torque demand exceeds the available maximum torque.
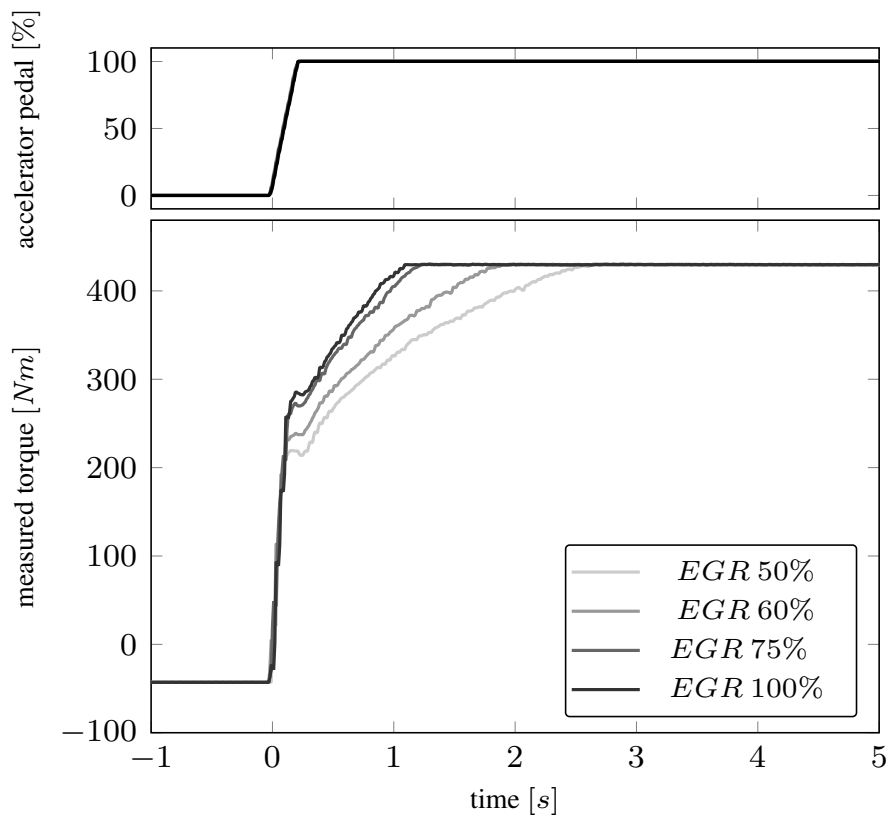

Figure 4.7: Step response measurement at 2000 rpm with different fixed EGR valve positions.

Figure 4.7 shows measurement results for different levels of minimum EGR valve position to show the influence. In respect to step response measurement in normal operation the effect of EGR on the torque is reduced to the time until the intake manifold is completely emptied and refilled once.

4.5 Model for air path dynamics

From chapter 3 we know that the cylinder mass flow $\dot{m}_{cyl}$ is a main input value for torque calculation. During operation the pressure in intake manifold p_{im} is responsible for the magnitude while the EGR-rate is accountable for the composition respectively the amount of air available for combustion. This section describes an approach to model the air path for determination of the amount of air available for combustion as well as the dynamics. Volumetric efficiency η_{vol} of an ICE gives the ratio of the gas mass in the cylinder divided by the mass that would ideally be in place based in the density of the intake manifold. Therefore it represents the efficiency of the gas mass flow from the intake manifold into the combustion chamber.

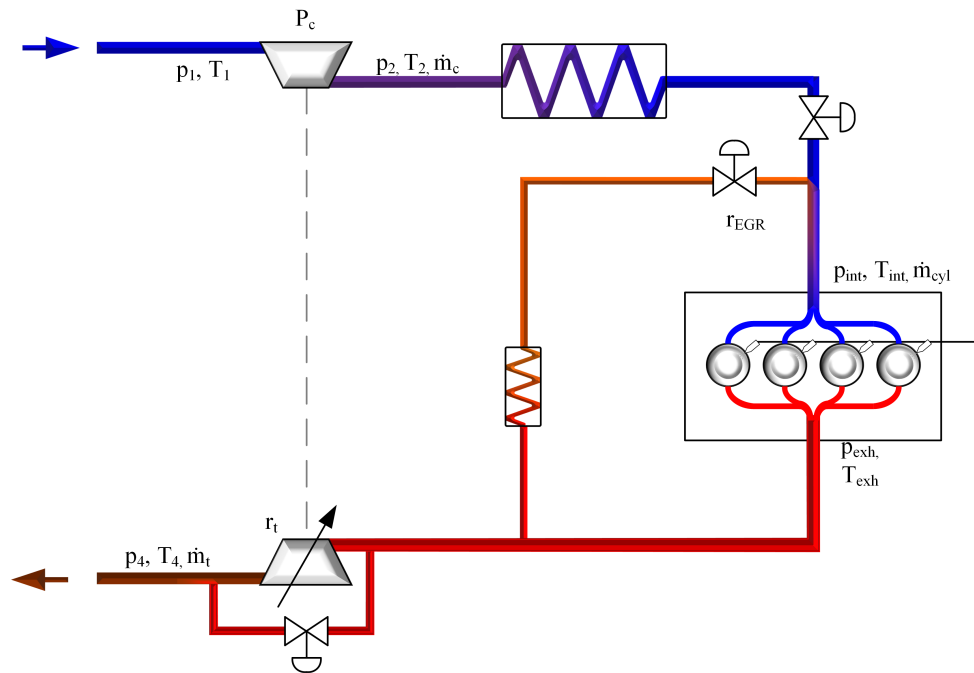Figure 4.8: Air path model with state variables and actuators.

Figure 4.8 shows the system and main influencing parameters. The power consumption of the compressor P_c depends on the enthalpies before h_1 and after compressor h_2 and the mass flow rate in the compressor and is calculated as

$$P_c = \dot{m}_c(h_2 - h_1). \tag{4.5}$$

By using the equations from chapter 3 the enthalpy difference can be rewritten. The

function depends on inlet temperature T_1, pressure difference of inlet pressure p_1 and outlet pressure p_2, compressor efficiency η_c and specific heat capacity c_p and the ratio of specific heats κ

$$h_2 - h_1 = \frac{1}{\eta_c} c_p T_1 \left[\left(\frac{p_2}{p_1} \right)^{\frac{\kappa-1}{\kappa}} - 1 \right]. \tag{4.6}$$

According to Boost Theory [2], the combination of formula 4.5 and 4.6 the compressor power can be written as

$$P_c = \dot{m}_c \frac{1}{\eta_c} c_p T_1 \left[\left(\frac{p_2}{p_1} \right)^{\frac{\kappa-1}{\kappa}} - 1 \right]. \tag{4.7}$$

The power of the turbine P_t can be calculated very similar to the compressor with the additional introduction of the turbine efficiency η_t

$$P_t = \dot{m}_t \frac{1}{\eta_t} c_p T_{exh} \left[1 - \left(\frac{p_4}{p_{exh}} \right)^{\frac{\kappa-1}{\kappa}} \right]. \tag{4.8}$$

In stationary operation the power of compressor and turbine must be the same by the application of the first law of thermodynamics (energy conservation) and the mean power of turbine and compressor can be set equal.

$$P_c = P_t \quad \dots \quad \text{stationary operation} \tag{4.9}$$

Starting point for the physical calculation is the use of ideal gas equation to represent the main elements as described in Kuzmych [16].

Change of the intake pressure p_{int} is modeled depending on the temperature T_{int}, the intake manifold volume V_{int}, displacement volume V_d, volumetric efficiency η_{vol} and engine speed N as

$$\dot{p}_{int} = \frac{R_{air} T_{int}}{V_{int}} \left(\dot{m}_c + \dot{m}_{EGR} - \frac{\eta_{vol} V_d N}{R_{air} T_{int}} p_{int} \right) \tag{4.10}$$

by using the EGR mass flow rate $\dot{m}_{EGR}$ and the mass flow rate over the compressor $\dot{m}_c$. Similar approach is used for the exhaust manifold pressure p_{exh}

$$\dot{p}_{exh} = \frac{R_{exh} T_{exh}}{V_{exh}} \left(\frac{\eta_{vol} V_d N}{R_{air} T_{int}} p_{int} - \dot{m}_{EGR} - \dot{m}_t + \dot{m}_{fuel} \right) \tag{4.11}$$

using exhaust manifold temperature T_{exh} and turbine mass flow rate $\dot{m}_t$.

The change of compressor power P_c is defined by introducing the time constant τ as

$$\dot{P}_c = \frac{1}{\tau}\left(\eta_t P_t - P_c\right). \tag{4.12}$$

Inserting turbine power equation 4.8 leads to

$$\dot{P}_c = \frac{1}{\tau}\left(\dot{m}_t c_p T_{exh}\left[1 - \left(\frac{p_4}{p_{exh}}\right)^{\frac{\kappa-1}{\kappa}}\right] - P_c\right). \tag{4.13}$$

Adopting conversion of κ, R and c_p as defined in equation 2.14 the equation can be rewritten as

$$\dot{P}_c = \frac{1}{\tau}\left(\dot{m}_t c_p T_{exh}\left[1 - \left(\frac{p_4}{p_{exh}}\right)^{\frac{R_{exh}}{c_{p,exh}}}\right] - P_c\right). \tag{4.14}$$

Using the ODEs from formula 4.10, 4.11 and 4.14 and using a state vector $x = [p_{int}, p_{exh}, P_c]'$ the system can be written as nonlinear state space model

$$\begin{bmatrix} \dot{x}_1 \\ \dot{x}_2 \\ \dot{x}_3 \end{bmatrix} = \begin{bmatrix} \frac{R_{air}T_{int}}{V_{int}}\left(\dot{m}_c + \dot{m}_{EGR} - \frac{\eta_{vol}V_d N}{R_{air}T_{int}}x_1\right) \\ \frac{R_{exh}T_{exh}}{V_{exh}}\left(\frac{\eta_{vol}V_d N}{R_{air}T_{int}}x_1 - \dot{m}_{EGR} - \dot{m}_t + \dot{m}_{fuel}\right) \\ \frac{\dot{m}_t c_p T_{exh}}{\tau}\left[1 - \left(\frac{p_4}{x_2}\right)^{\frac{R_{exh}}{c_{p,exh}}}\right] - \frac{x_3}{\tau} \end{bmatrix}. \tag{4.15}$$

Using the sum of mass-flows similar to Kirchhoff's law leads to $\dot{m}_{cyl} = \dot{m}_c + \dot{m}_{EGR} = \dot{m}_t + \dot{m}_{EGR} - \dot{m}_{fuel}$. The system can be rewritten now as

$$\begin{bmatrix} \dot{x}_1 \\ \dot{x}_2 \\ \dot{x}_3 \end{bmatrix} = \begin{bmatrix} \frac{R_{air}T_{int}}{V_{int}}\left(\dot{m}_{cyl} - \frac{\eta_{vol}V_d N}{R_{air}T_{int}}x_1\right) \\ \frac{R_{exh}T_{exh}}{V_{exh}}\left(\frac{\eta_{vol}V_d N}{R_{air}T_{int}}x_1 - \dot{m}_{cyl}\right) \\ \frac{\dot{m}_t c_{p,exh}T_{exh}}{\tau}\left[1 - \left(\frac{p_4}{x_2}\right)^{\frac{R_{exh}}{c_{p,exh}}}\right] - \frac{x_3}{\tau} \end{bmatrix}. \tag{4.16}$$

The dynamic of the air path system depends on the change of the intake pressure. This value can be used directly from this state space model. Further on the relation of current - to the stationary full load conditions at a specific engine speed shall be taken into account

to derive the slope of torque response

$$k_{tq\,slope} = \dot{p}_{int} \frac{p_{int,max} - p_{int,act}}{M_{N,max} - M_{act}} = \dot{x}_1 \frac{x_{1,max} - x_1}{M_{N,max} - M_{act}}. \tag{4.17}$$

By the use of calculation methodology from sections 3.7 and 4.1 and using equation 4.4, time to fulfill a torque request can be calculated based on physical methodology as

$$t_{tq\,dem} = \dot{x}_1 \frac{x_{1,max} - x_1}{M_{N,max} - M_{act}} \cdot \max\left(0,\, M_{dem} - M_{avail}\right). \tag{4.18}$$

4.6 Conclusion

This section focused on the dynamic behavior of the diesel engine with turbocharger and exhaust gas recirculation.

Based on the torque calculation methodology from chapter 3, torque reserve is provided by applying the method on the instantaneously available injection quantity from smoke limitation.

The prediction of dynamic performance by distinguishing between available torque and a constant slope during smoke limitation is described.

Use of following characteristic values is presented:

- actual torque;
- available torque;
- time to fulfill of torque request.

Limitation of the engine torque by a full load curve and its effect on the calculation methodology and measurement results is outlined. Main dependencies on performance that aren't directly considered in the calculation methodology were presented.

Finally a physical model on the air path dynamics is derived and given in state space notation. The use to calculate the slope of engine torque increase is given in this chapter.

5 Implementation and simulation results

5.1 Model structure

The calculation methodology as described in the previous chapters is implemented in Matlab Simulink. The operation uses blocks from the standard library exclusively. Therefore the implementation is independent from the used version of Matlab Simulink and it enables a simple conversion into executable code for embedded control.
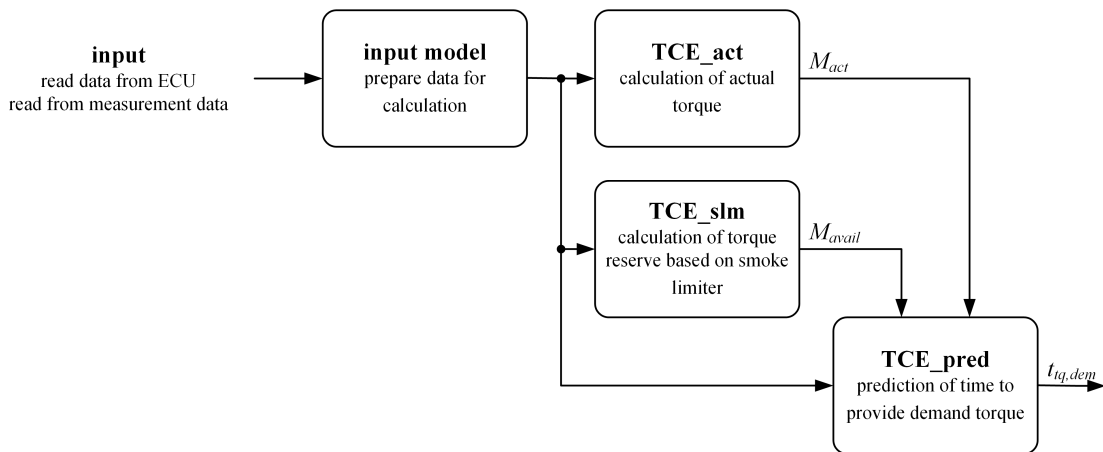

Figure 5.1: Top level architecture of Simulink implementation.

Figure 5.1 shows the top level architecture of the calculation methodology that provides the three main signals M_{act}, M_{avail} and $t_{tq,dem}$.

The *Torque Combustion Engine (TCE)* calculation algorithm collects the data from measurement files in case of offline simulation. The online version uses data from the ECU. As the model is implemented generically the input model takes care about unit conversions and required sensor-specific adaptation. This input model provides data for the torque

calculation.

This algorithm is calculated two times in parallel. The first calculation uses current engine operation conditions to calculate the actual torque of the engine. The second calculation follows the same algorithm but uses the values given from smoke limitation to calculate the instantaneously available torque.

Based on actual and available torque the time to provide the demand torque is calculated. Figure 5.2 provides a deeper insight on the torque calculation algorithm. Again the model starts with a common input model that is used to calculated air- and cylinder mass flow as well as the air fuel equivalence ratio λ based on actual or smoke limitation conditions. While intake enthalpy and engine inertia calculation follow direct implementation of the given equations, the combustion requires a more sophisticated approach.

At first the angle of MFB50 is calculated based on injection timing and shape parameter. Injection power based on the fuel injection quantity and the lower heat value is provided. Using the equivalent room ratio function the separation between isochoric and isobaric combustion is evaluated. Then the combined working process from compression via combustion to the expansion is calculated and results in the exhaust enthalpy. In parallel the surface and volume at MFB50 is provided as geometric data.

Calculation of gas exchange closes the combustion cycle with providing the energy of the low pressure cycle when the valves are opened and closed.

Wall heat loss calculation at first calculates the wall temperature based either on the empirical approach or on the thermal state estimation.

All these inputs are collected and summed up for energy conservation and provides the IMEP and inner torque of the diesel engine. By subtracting friction torque and auxiliaries the available torque at crankshaft is calculated.
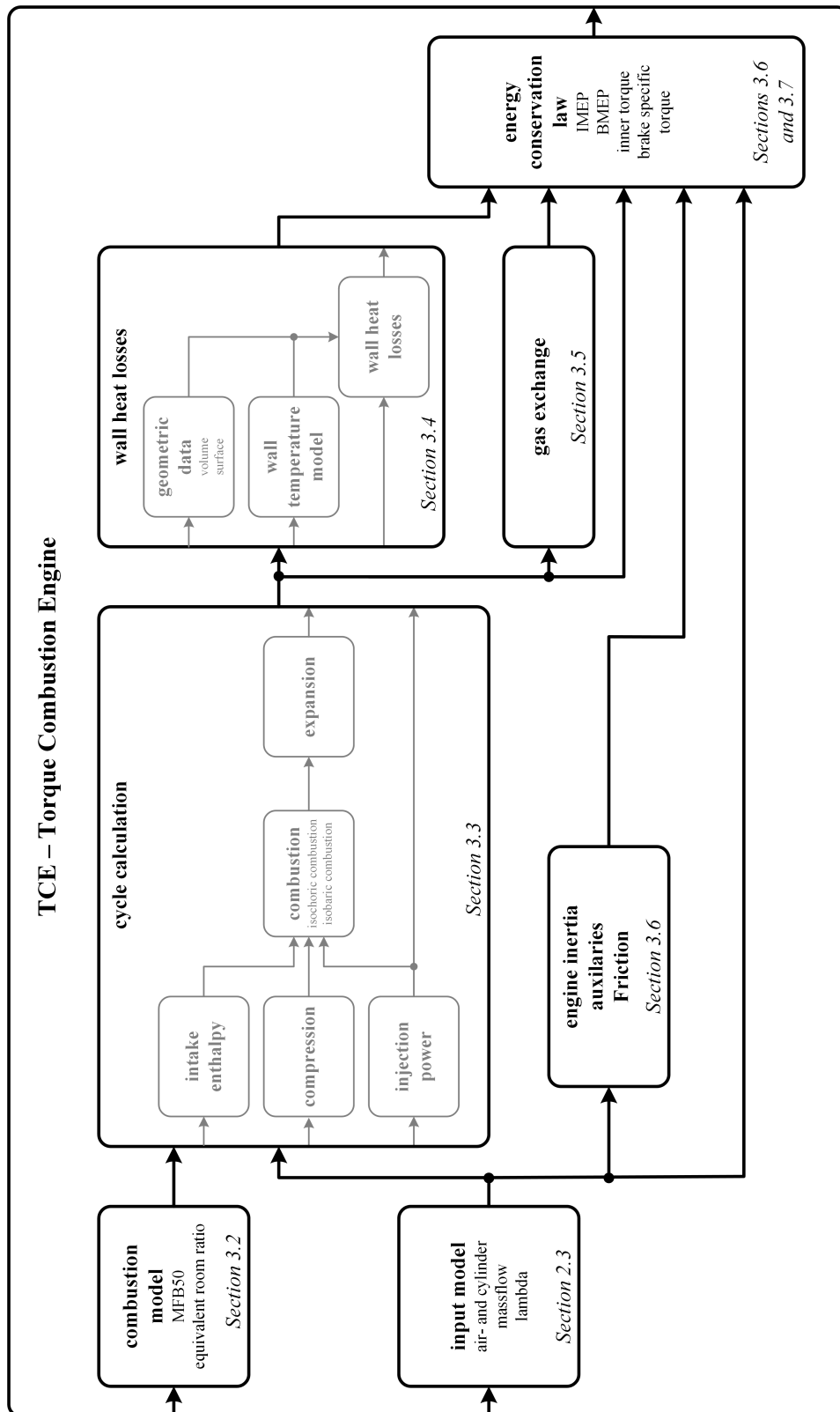
Figure 5.2: Structure of the torque calculation methodology in Matlab Simulink.

5.2 Model parametrization

Parametrization is the application of a model with specific calculation values that the overall model matches well to the defined application. Uncertainties on model parameters or boundary conditions are the most common source of error in on- and offline simulation. The model as described in chapter 3 is based on physical correlations in the diesel engine. To fit the outcome of the model to a specific engine several parameter to be introduced. The basis are values defined in table 4.1 as well as general parameters given in appendix C and D.

Combustion calculation requires further parameters for start and end of combustion and the shape parameter β, see section 3.2. The values of these calibration maps can be identified by the use of cylinder pressure based signals e.g. from indication system on engine testbed. As an initial basis for calibration, the approximation $\beta = \frac{\varphi_{MFB50} - \varphi_{SOC,ref}}{\varphi_{MFB50} - \varphi_{MFB90}}$ can be used.

To check the calculation of gas exchange the indicated mean effective pressure of the low pressure loop $IMEP_{low}$ can be used and the calculation can be confirmed.

Wall heat losses calculation (see section 3.4) requires a basis calibration of the gas-wall heat transfer coefficient.

The inertia need to be introduced to cover torque loss or increase by speed changes.

To finally come to the brake specific torque at the crankshaft the auxiliaries and friction need to be considered. These values are already available in state of the art ECUs, for offline calculation the effects are covered by empirical maps derived from measurement on engine testbed.

5.3 Step response measurement

Based on an initial state of the system a change of demand value in very short time is applied and the dynamic behavior is evaluated. Applying this method to the turbocharged diesel engine with excitation on the accelerator pedal provides the time behavior of the engine states and outputs. Step response is used to identify how the system responds on sudden changes on demand values.

These results have important practical value because complexity in real life can be reduced

to artificial, reproducible test cases.

The behavior differs mainly on engine operation point defined by speed and accelerator pedal position. For deep analysis the measurement procedure must cover the relevant influencing parameters.
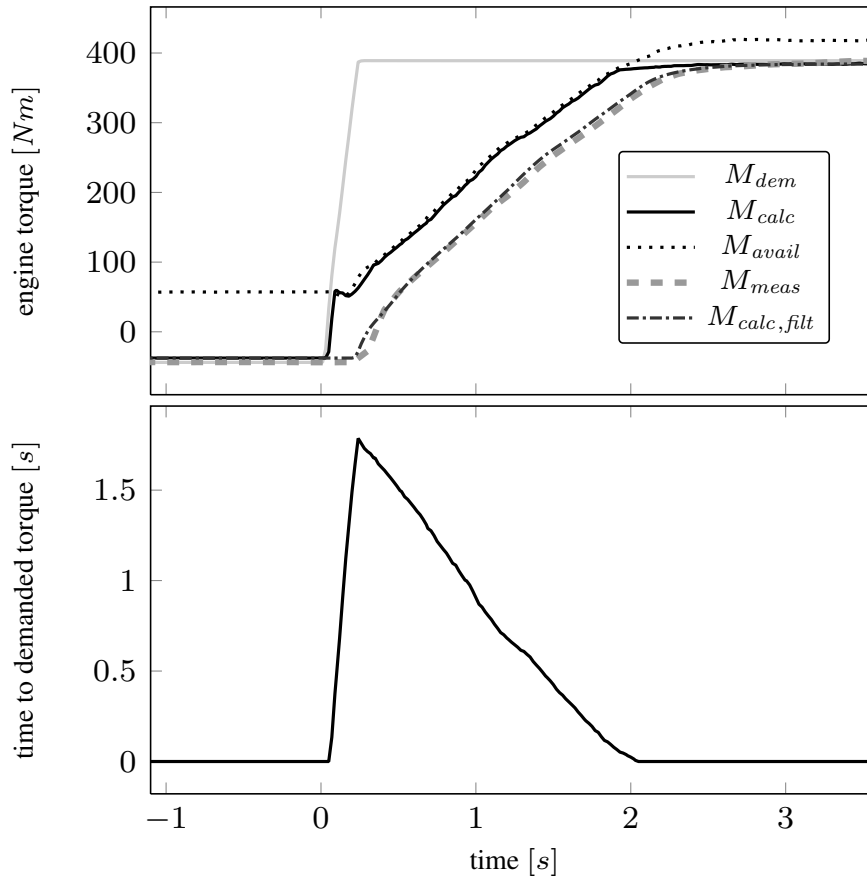

Figure 5.3: Step from engine motoring to full load including filter and delay time of 150 ms

Recorded testbed measurements as already shown in figure 4.4 and 4.5 are used as input data for the proposed calculation method. To compare the simulation results with measurements one single step response is selected for analysis in figure 5.3. For the engine torque a delay time of ∼150ms and low pass filtering with a time constant of again ∼150ms shows up in testbed measurements compared to to the calculated torque signal.

Time delay and time constant result from a summation of various different effects: data transfer times, sampling time of the testbed, built-in filtering for signal smoothing, time delay until all cylinders inject the new fuel mass flow as well as physical distortion from crank shaft to torque measurement. For validation reasons, delay time and filtering were both also applied to the results of the calculation algorithm.
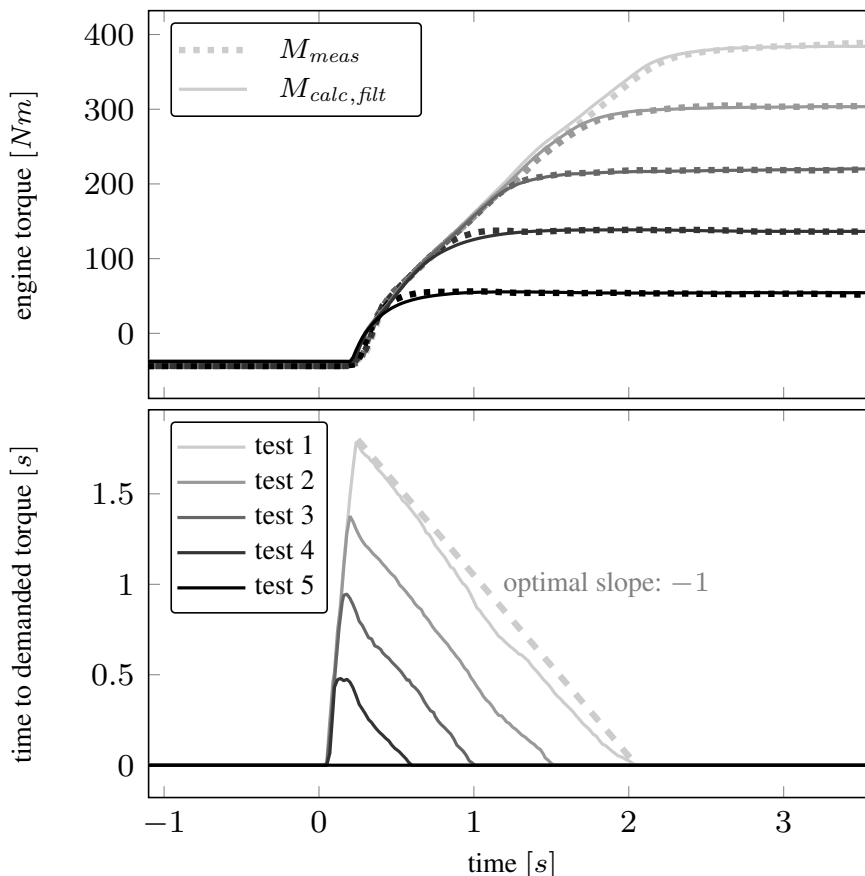
Figure 5.4: Step response from motoring mode to different demand values with measurement and calculated values.

Figure 5.3 shows a step from engine motoring to full load at 3000 rpm engine speed with demanded value, calculated torque signals and measurement from engine testbed.

The results confirm that the relevant effects for step response measurement in standard condition are covered by the shown method. Simplifications as shown in chapter 3, e.g. the use of the ideal working cycle, do not significantly affect the quality of the calculated results. Additional validation of the algorithm is done using different excitations and are summarized in figure 5.4 and figure 5.5. The slope of the *time to reach the demanded torque* during smoke limitation is independent from starting and final value. Note that - considering a smooth parameterization of smoke limitation - a slope around (-1) during smoke limitation implies an optimal estimation of the remaining time until the demanded torque is finally reached.

This confirms approach stated in figure 4.4 by separation of *available torque* and *torque slope* during smoke limitation.
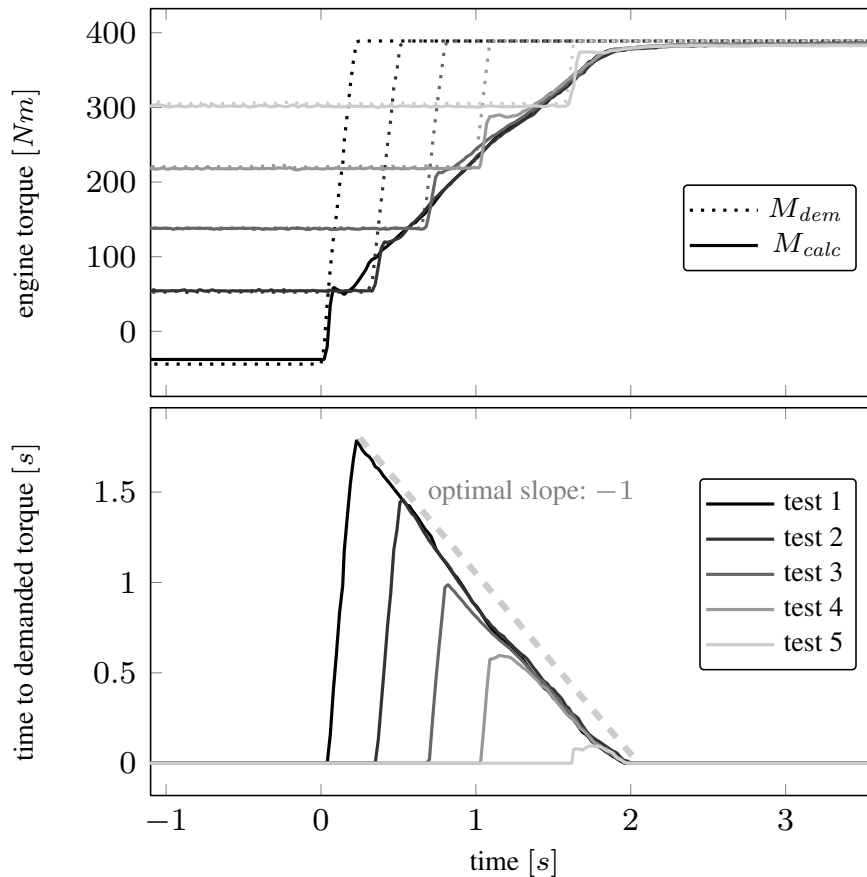
Figure 5.5: Torque steps from different starting point to full load.

5.4 Systematic analysis of transient response

Based on the results of single step measurement a more detailed analysis has been executed to validate the behavior in different operation conditions. This section discusses the main dependencies that influences the torque calculation without being directly considered in the formulas. Based on the analysis also the effect on calculation methodology is investigated and analyzed if the effects are considered sufficiently.

For this analysis a detailed measurement program on engine testbed was done on engine 1. The operation points and modes as given in table 5.1 were selected based on experience as outlined. Each measurement was executed with two sequences of steps on the accelerator pedal.

The first sequence given in the upper part of figure 5.6 shows the step response measurement with different steps on the accelerator pedal from 0% to the levels 25%, 50%, 75% and full load 100%.

EGR valve position	engine speed				
	1000rpm	1500 rpm	2000 rpm	2500 rpm	3000 rpm
Standard EGR	✓	✓	✓	✓	✓
50% EGR	✓	✓	✓		
60% EGR	✓	✓	✓	✓	✓
75% EGR	✓	✓	✓	✓	✓
90% EGR		✓	✓	✓	✓
100% EGR	✓	✓	✓	✓	✓

Table 5.1: Measured operation points and test conditions for systematic analysis of transient response.
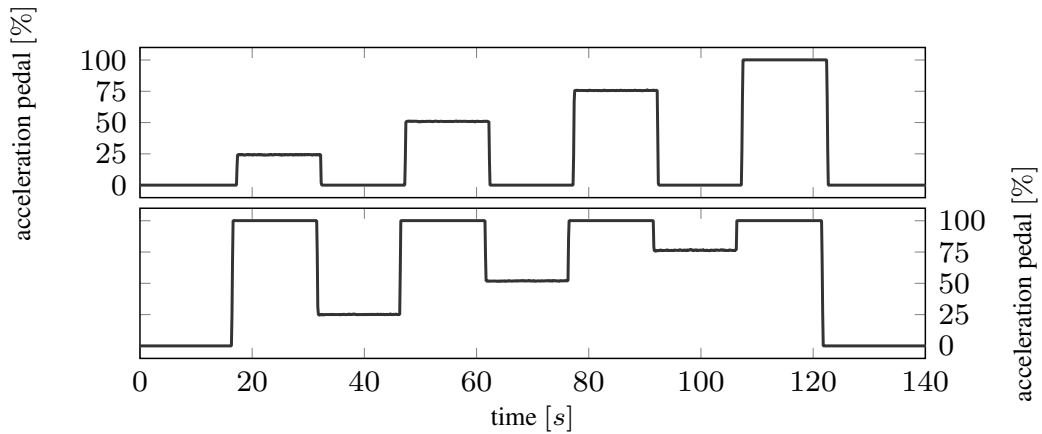
Figure 5.6: Sequences of step response measurement from engine motoring operation with different step magnitude.

The second sequence given in the lower part of figure 5.6 shows the step response measurement with different starting levels and the target of full load operation.

During this measurement the engine testbed system stabilizes the engine speed at the selected value.

Measurement results are used for analysis and as input signals for simulation.
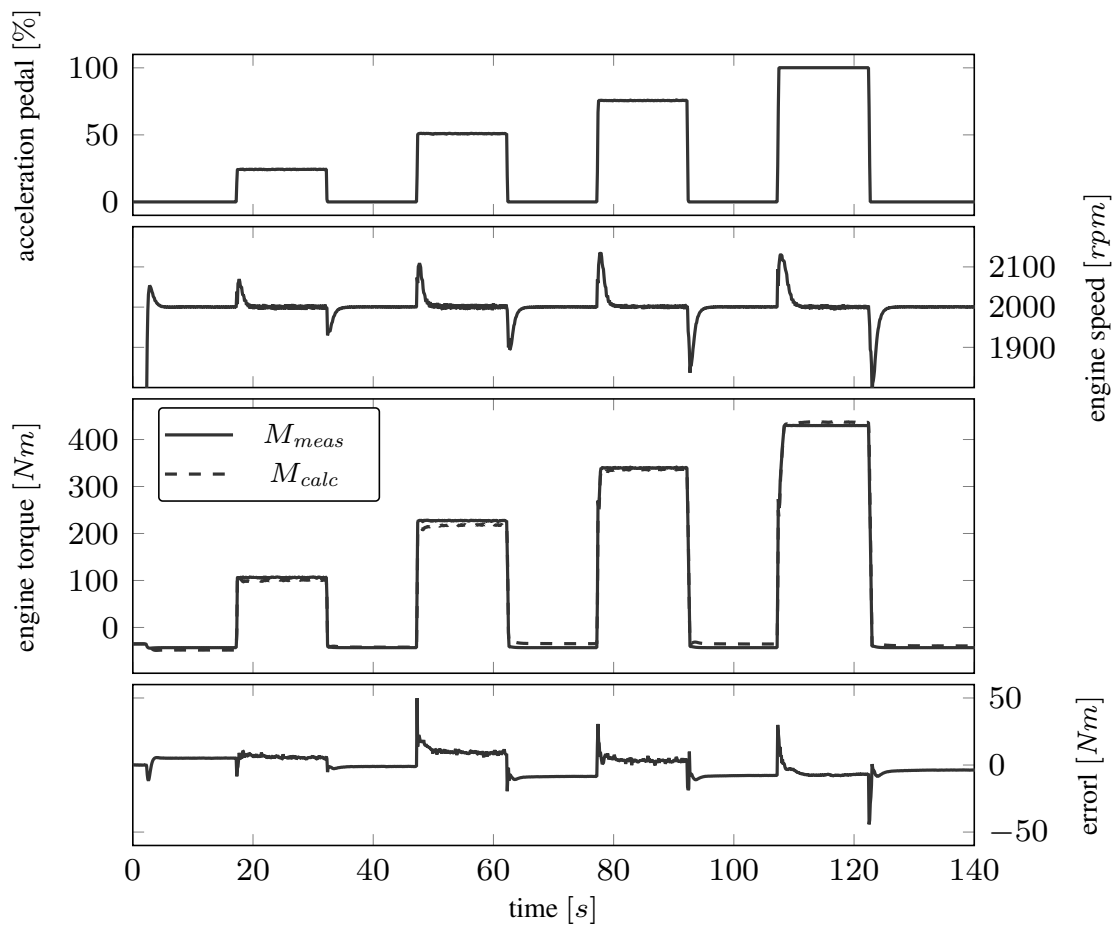
Figure 5.7: Example for the first sequence of step response measurement from engine motoring operation with different step magnitude at 2000 rpm.

Figure 5.7 shows the measurement sequence at 2000 rpm engine speed as defined in the upper diagram of figure 5.6 with load steps from engine motoring condition to different load levels.

The upper diagram shows the actuation of the accelerator pedal. Second diagram shows the engine speed and one can see that the testbed control takes care on keeping the engine speed constant by a closed loop control.

The third diagram shows the engine torque. The solid line represents the measurement signal from engine testbed, the dashed line gives the calculation result from the given torque calculation methodology.

Assuming the measurement to be correct, the lowest diagram provides the calculation error as from measurement and calculated value. Within high transient conditions the calculation error raises for a short time. At this point it shall be reminded that measurement of the

engine torque has some dead time.
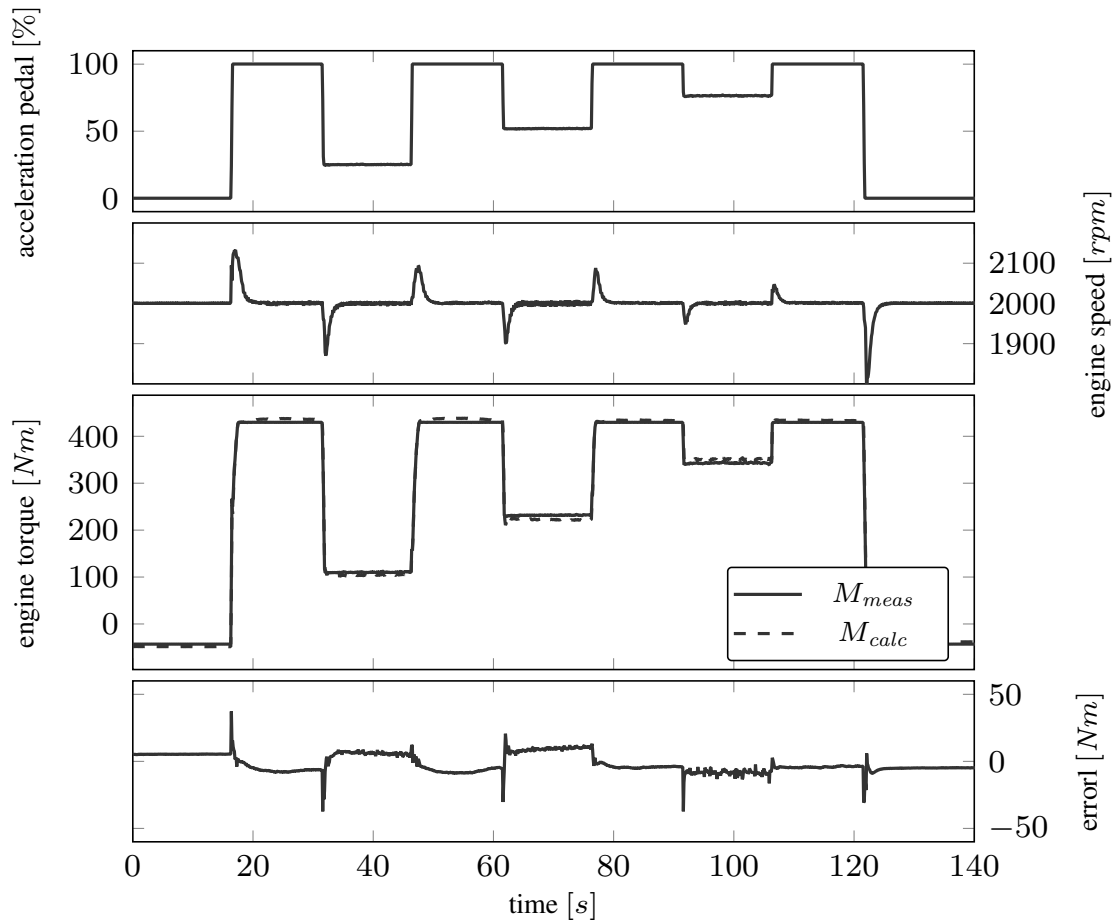
Figure 5.8: Example for the sequence of step response measurement from different starting points to full load at 2000 rpm.

Figure 5.8 presents the torque response. Based on the sequence as defined in the lower diagram of figure 5.6, again at 2000 rpm. The upper diagram shows the accelerator pedal position, second diagram provides the engine speed that is controlled by the testbed operation control.

The third diagram gives the engine torque measured from engine testbed (solid line) and from calculation (dashed line).

Although the different actuation leads to slightly different results, the calculation represents measurement. The calculation error is given in the last diagram of this figure.

5.5 Variation of engine speed

The investigations from section 4.3 analyses the calculation results at a single engine speed. This section gives insight on behavior at different engine speeds.
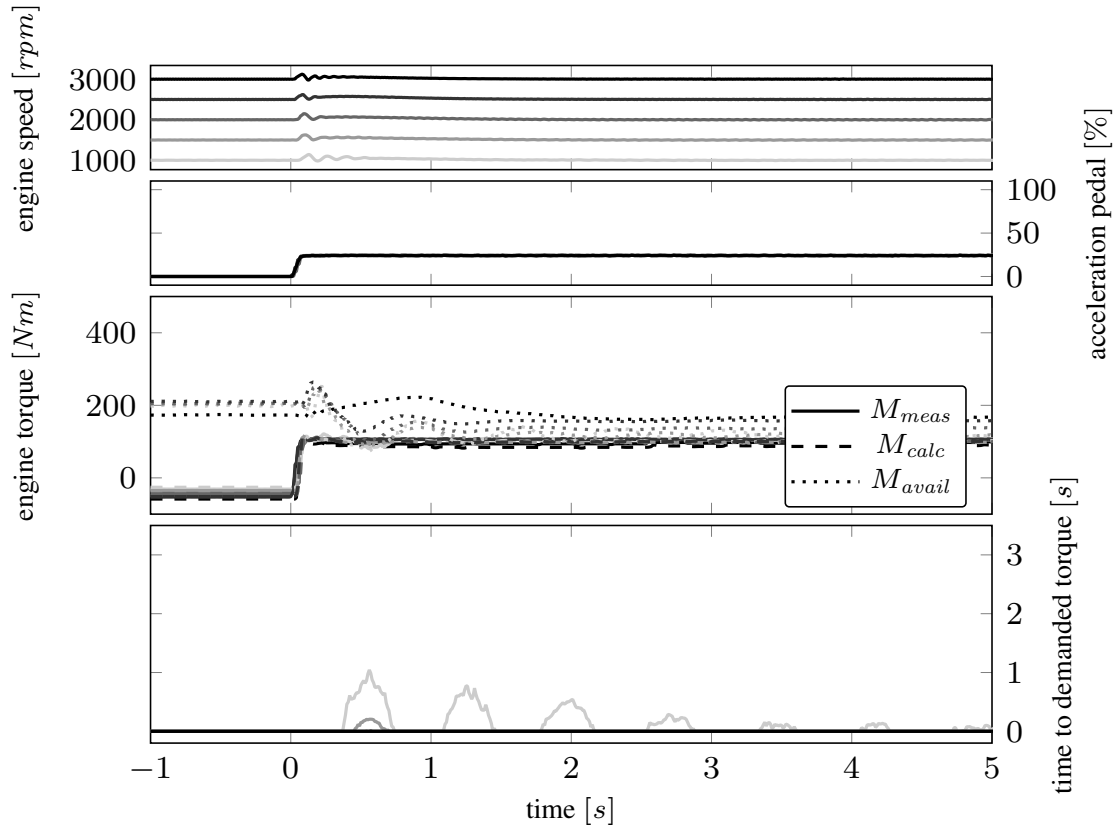
Figure 5.9: Torque build-up at different engine speed with accelerator pedal step from 0% to 25%.

Figure 5.9 starts the analysis of the calculation at different engine speeds.

The upper diagram shows the engine speed with different levels of brightness for the analyzed engine speed levels. Second diagram provides the requested step in the accelerator pedal position.

The third diagram provides the measurement (M_{meas}, solid line), the calculated actual value (M_{calc}, dashed line). Smoke limitation based on air fuel equivalence ratio leads to available torque (M_{avail}, dotted line). Due to the fact that available torque is higher than the requested torque, the time to available torque remains zero. At lowest engine speed the torque is already near the full load operation and due to oscillation in the air mass, time to demanded torque shows some values beyond 0.

The upper diagram of figure 5.10 shows the brightness indicator as dependency of engine speed for the 5 measured levels from 1000 to 3000 rpm with steps of 500 rpm.
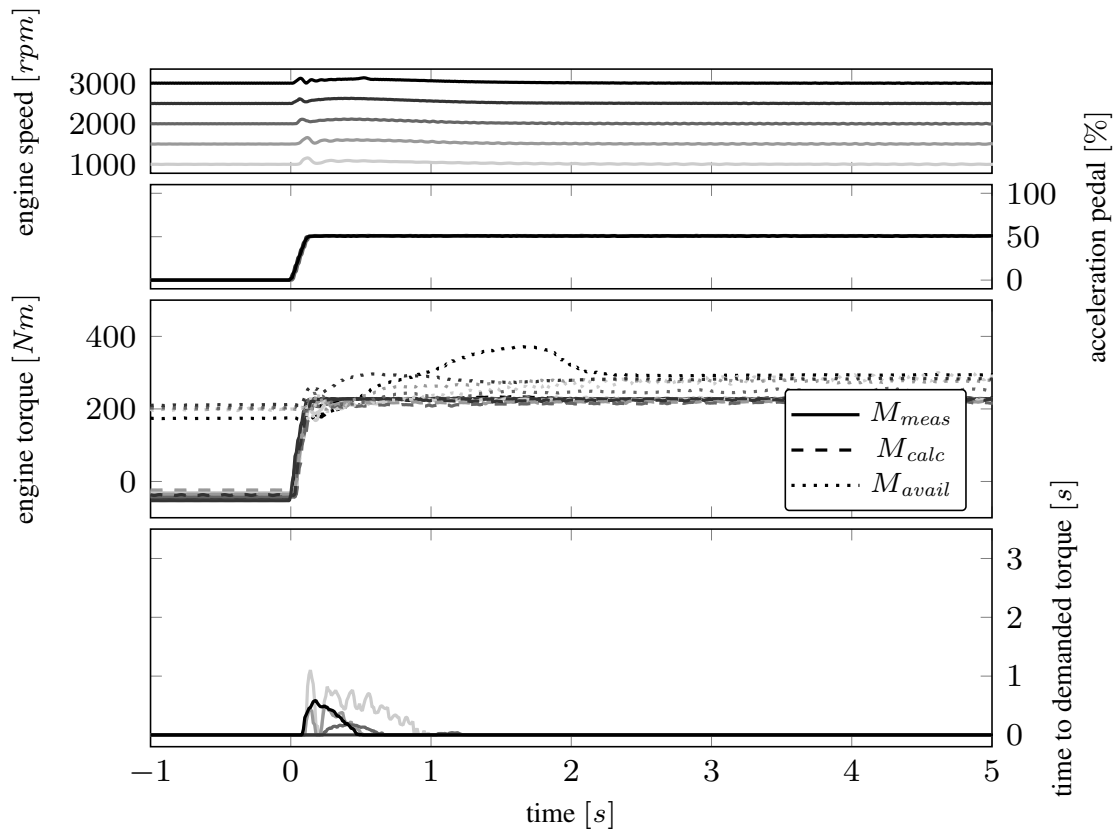
Figure 5.10: Torque build-up at different engine speed with accelerator pedal step from 0 to 50%.

Second diagram shows the excitation of the accelerator pedal by a step from 0% to 50% for each engine speed.

Engine torque is presented in the third diagram. Available torque M_{avail} (dashed line) almost meets the level of final torque. The diagram shows almost immediate raise of engine torque to the target value.

At 50% accelerator pedal position the engine calibration generally provides a small torque reserve. By this the available torque at this operation point raises very few above the actual torque, independent from engine speed.

Few time to demanded torque is necessary to increase the air excess ratio as calculated in the lowest diagram as almost sufficient torque reserve is available before the request.

Figure 5.11 shows the step response behavior with a step on the accelerator pedal from zero to 75% as illustrated in the second diagram.

Measurement is done at different engine speed levels from 1000 rpm to 3000 rpm and are presented by different intensity to distinguish the relation to each other in the following diagrams.
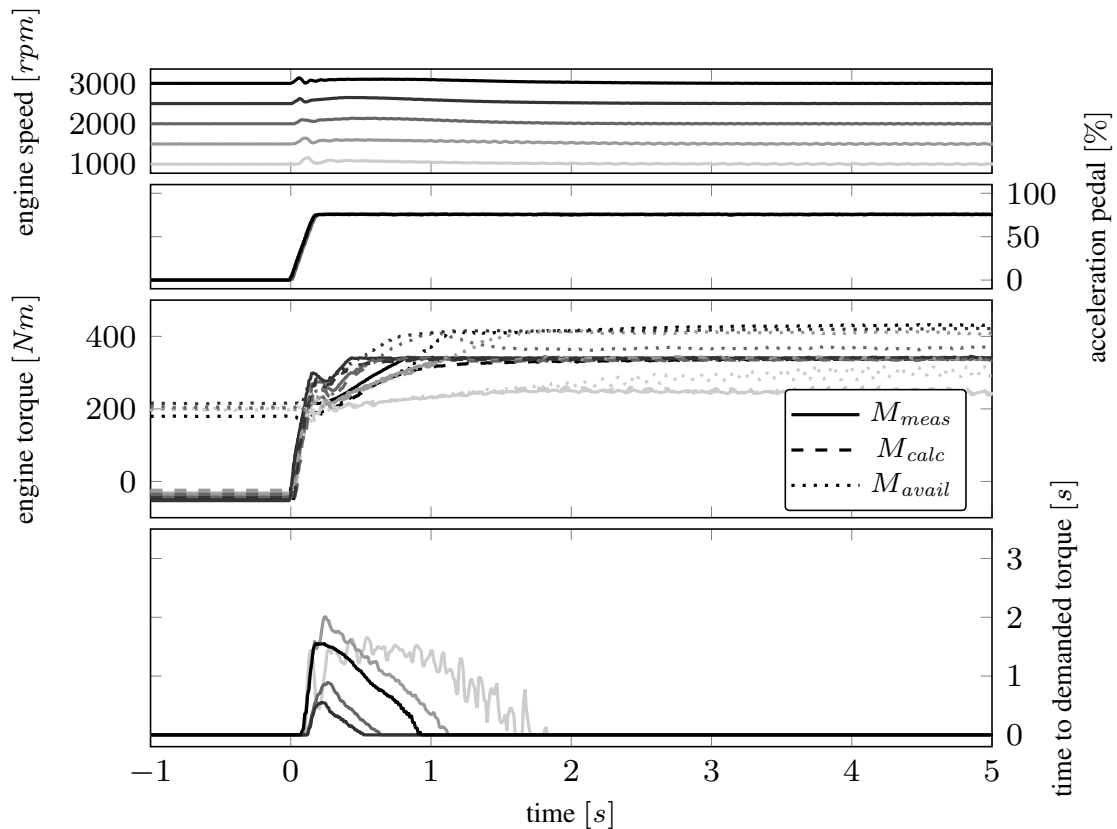
Figure 5.11: Torque build-up at different engine speed with accelerator pedal step from 0% to 75%.

The available torque before excitation is lower than the final torque level, so the torque reserve is not sufficient to immediately provide the requested output. Therefore the output instantly changes to the available level and then raises with the time constant of the air system.

The influence of engine speed can be clearly seen by the different transient behavior. Lower engine speed lead to longer times to reach the target value.

The bottom diagram shows the time to required time to demanded torque. The bright colored line of the measurement visualizes the behavior that a longer timespan is needed to reach the demand torque at low engine speeds. Differences due to engine speed can be

clearly seen by the diversity of the magnitude and shape of time to demand torque. At 1000 rpm the target torque is significantly lower due to physical limits.
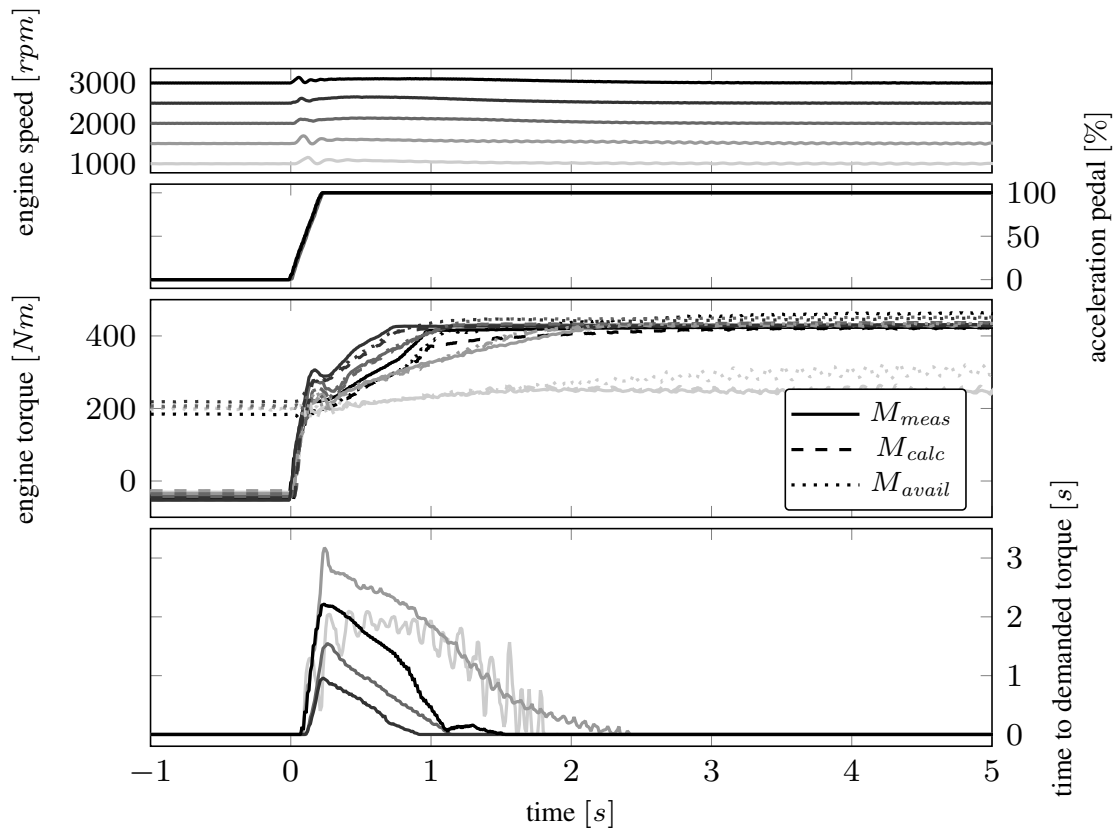
Figure 5.12: Torque build-up at different engine speeds steps from motoring to full load.

The step from engine motoring mode to full load at different engine speeds is shown in figure 5.12. Top diagram presents the engine speed levels, the brightness of the curves enable to distinguish between the tests in other diagrams. Second diagram provides the excitation by the accelerator pedal as common step from 0% to 100% for each test. Engine torque is illustrated in the third diagram. Again the influence from engine speed can be clearly identified whereas higher speed leads to faster times to demand torque. Especially in low engine speed with reduced maximum torque the measured, calculated and available torque are very noisy. This leads to very agitated prediction of time to demand torque at 1000 rpm. At highest speed an increase of torque buildup at the end of the torque buildup can be seen that results into a fast decrease of time to demand torque. This results from thermodynamic reasons like change of turbocharger efficiency and is not represented in the simplified approach of the air path model.

While previous figures in this chapter show the transient torque behavior at different speed from 0% accelerator pedal, now sequence in figure 5.13 starts at a level of 25%.
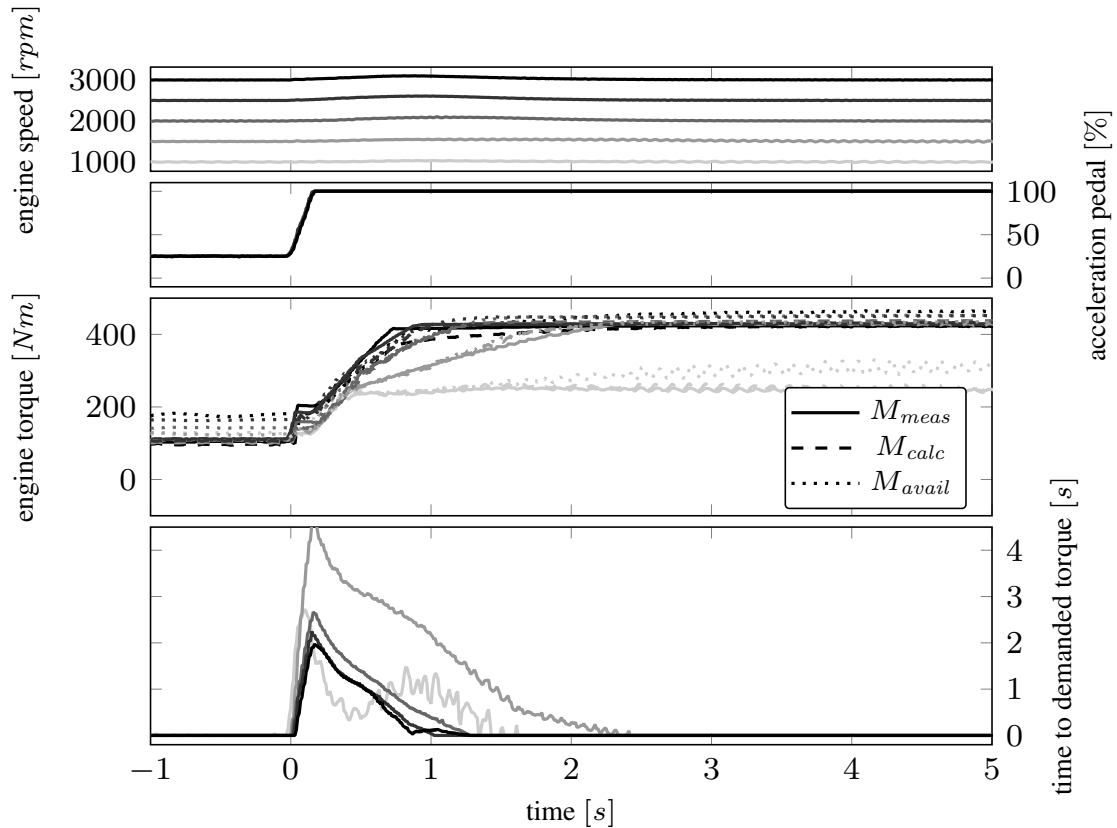
Figure 5.13: Torque build-up at different engine speeds steps from 25 % to full load.

Depending on engine speed, given in first diagram, the starting conditions are very different as the torque reserve is very small in current situation. This leads to significant longer time prediction than the really needed time. Again a clear change of the ramp inclination depending on engine speed level can be seen as a result of unpredicted change of turbocharger efficiency. Modeling of this behavior requires nonlinear model-predictive algorithms of the thermodynamic air system. Due to massive increase of calculation time of this approach this step is not taken within this work.

Online calculation reduces the error in time to demanded torque in each calculation step as the nonlinear thermodynamic effects are included in the torque calculation methodology.

Starting the step response measurement from 50% acceleration pedal position leads to the behavior is given in figure 5.14. First diagram shows the engine speed. Calculated torque matches well to the measurement although the system behaves very nonlinear.
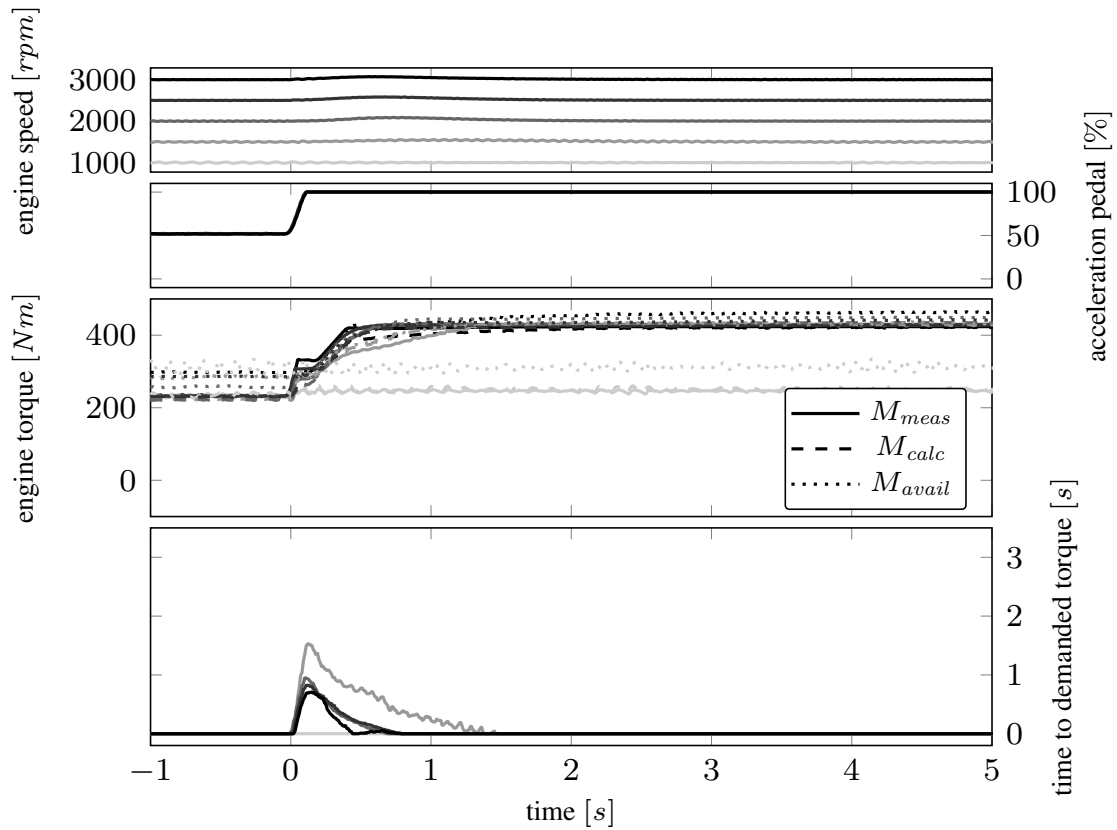

Figure 5.14: Torque build-up at different engine speeds steps from 50 % to full load.

Limitation of full load torque leads to very small torque increase at 1000 rpm engine speed. The predicted time to reach demand torque does not fully follow the ideal gain, nevertheless it gives a useful estimation on the required time to reach the target value.

5.6 Variation of EGR rate

Calculation of torque reserve in section 4.1 presented the importance of air mass flow for combustion and its effect on available torque due to smoke limitation.

Recirculation on exhaust gas reduces is a powerful measure to reduce pollutant NO_X emission. The drawback is a reduction of air mass flow at the same operation point and lower exhaust gas enthalpy what results in worse transient performance.

This section shows the effect of different EGR-levels on engine torque in step response test. The capability of the proposed calculation to represent this effect is validated. Measurement and analysis in this section is done on engine 1, see engine specification in table 4.1. Air mass flow is increasing while the EGR rate is decreasing.

Following figures show the EGR valve position that is defined as opened with 0% and closed with 100%.

5.6.1 Analysis of EGR rate at 1500 rpm

Section 4.4 outlined the effect of EGR on the measured engine torque. This section analyses the influence of EGR on calculated and available torque and the predicted time to reach demanded torque in detail.

The following figures illustrate several measurements as overlay to visualize the effect of different EGR valve positions in same operation conditions respectively the effect on engine torque in a step response test. The top diagram provides the air mass flow. The brightness of the graphs indicate the relation to the specific measurement.

Second diagram shows the accelerator pedal. This gives initial condition and excitation on the system.

Third diagram presents the system answer with the engine torque as the main output. Three signals are given for each test. First is the measured torque from engine testbed M_{meas} with solid line. The diagram is completed by calculated torque M_{calc} with dashed and maximum available torque M_{avail} with dotted lines as signals calculated by the algorithm as proposed by this work.

Lowest diagram displays the time to demanded torque in the role of the main outcome derived from air system dynamics.

Figure 5.15: Torque build-up at 1500 rpm and different EGR rates with an accelerator pedal step from 0% to 50%.

Figure 5.15 shows the influence of different EGR levels. The top diagram show the air mass flow as this measurement signal is the strongest indicator on the EGR rate at a specific engine operation point. In the third diagram the engine torque is illustrated. The initial and final torque level is independent from the EGR valve because in stationary conditions the air excess ratio is higher than the smoke limitation. Requested torque can be provided but torque reserve is influenced significantly.

Although the available torque is almost sufficient to implement the demanded torque increase, some time to reach the target value is needed. The lowest diagram displays this time and shows the increasing values with when the EGR valve is opened wider.

Figure 5.16 presents a step from motoring mode to 75% acceleration position with different EGR valve positions.
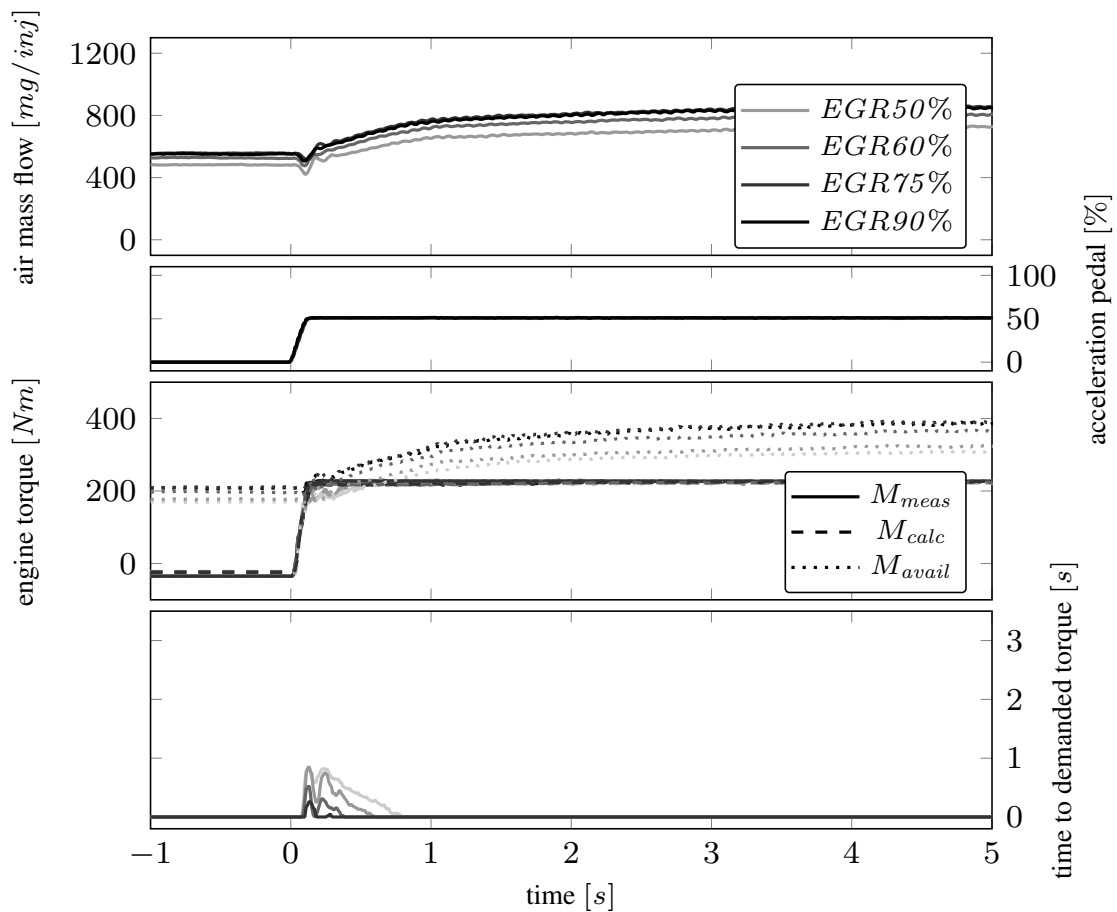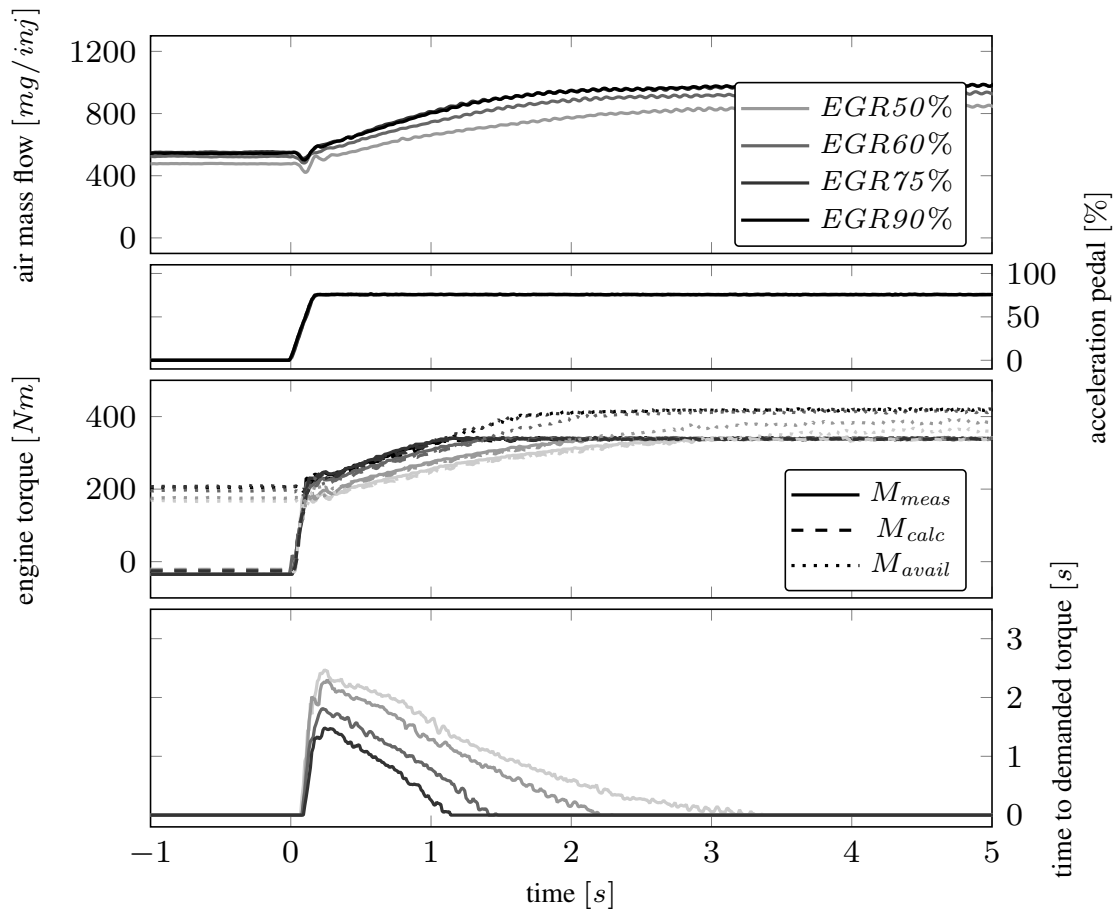

Figure 5.16: Torque build-up at 1500 rpm and different EGR rates with an accelerator pedal step from 0% to 75%.

First diagram shows the increase of air mass flow. It can be clearly seen that closed EGR valve (dark lines) show much faster raise than 50% open position of the EGR valve (brightest line).

Third diagram illustrates the related engine torque. The different level of available torque caused by exhaust gas recirculation lead to lower step height with wider opened EGR valve. Additionally it leads to longer times to build up the requested torque. This can be seen in the lowest figure.

Although the EGR rate is considered only indirectly, the relevant information is available in the calculation methodology.

Figure 5.17 illustrates the step to full load. Here the absolute influence of the air mass flow on the engine torque can be seen very clearly in the top diagram. After 3 s the target air mass flow becomes stationary with closed EGR but increase is slower the wider the EGR valve is opened.

Figure 5.17: Torque build-up at 1500 rpm and different EGR rates with an accelerator pedal step from 0% to full load.

The third diagram provides the engine torque signals. With closed EGR the stationary air mass flow is reached at approximately 2.2 s while with the EGR valve opened at 50% only $^3/_4$ of the demand value is provided.

The lowest diagram illustrates the time to demanded torque. Lower torque reserve leads to higher initial calculated time values. Secondly the dynamic of the air system is decreased by high EGR rates what leads to longer times for torque buildup.

5.6.2 Analysis of EGR rate at 2500 rpm

Figure 5.18 shows the influence of EGR rate at an engine speed of 2500 rpm. Air mass flow level becomes lower the wider the EGR valve is open. The available torque is related to the air excess equivalence ratio. Due to changed EGR rate lower torque reserve is available with higher EGR rate.

Figure 5.18: Diesel engine torque build-up at 2500 rpm and different EGR rates with an accelerator pedal step from 0% to 50%.

Third diagram illustrates the engine torque response on the requested change of accelerator pedal from second diagram. The available torque clearly behaves as a function of the EGR rate.

In comparison to figure 5.15 the torque reserve is sufficient to provide the requested torque instantaneously. Therefore increase of measured and calculated torque are almost congruent for all tests. Due to this fact the time to demanded torque remains practically zero.

The step in the accelerator pedal from 0% to 75% is presented in figure 5.19. Depending on the EGR valve position the absolute level of air mass flow varies. Absolute level or air mass flow is slightly higher compared to the measurement at 1500 rpm. The shape of air mass flow in the top diagram indicates the time constant of the air path system. Higher engine speed leads to significant lower time constant in the air path.
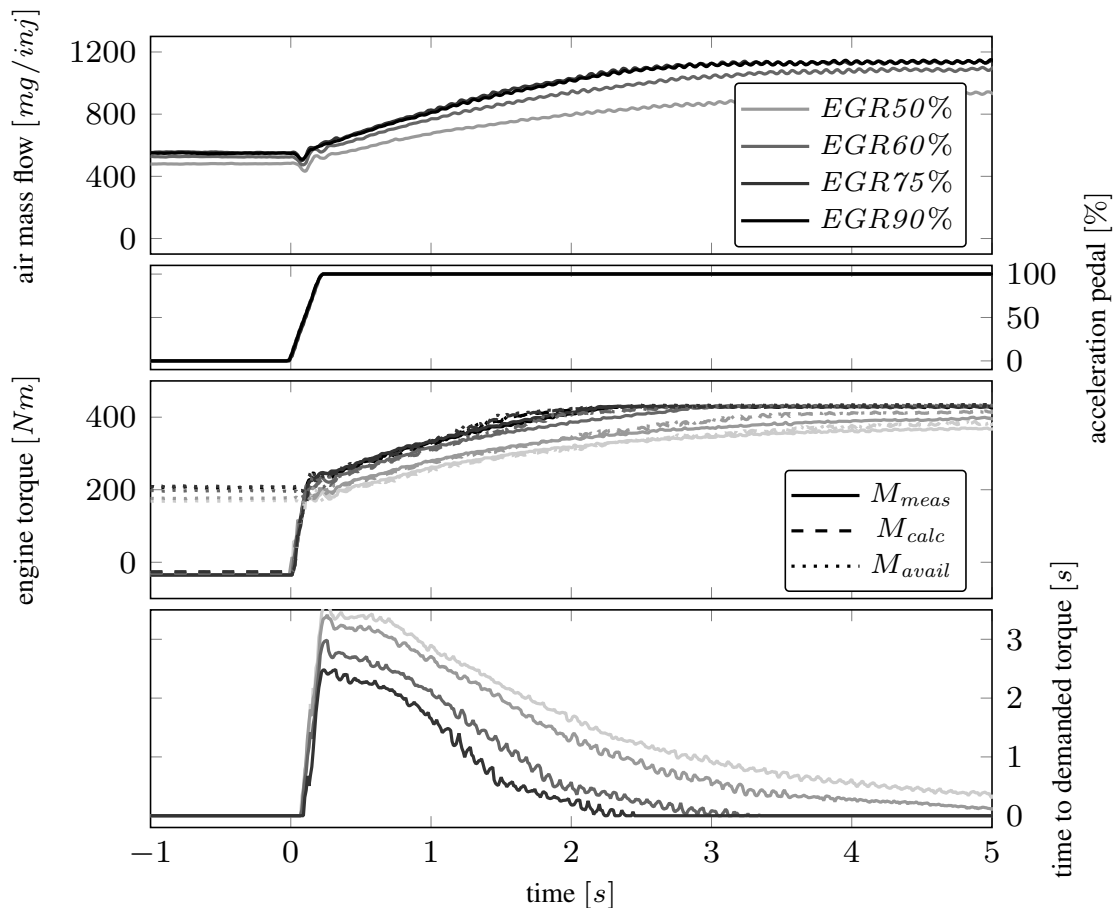

Figure 5.19: Diesel engine torque build-up at 2500 rpm and different EGR rates with an accelerator pedal step from 0% to 75%.

The third diagram shows that the available torque at starting conditions is lower than the requested final torque. Therefore the air system needs to increase the air mass flow by speeding up the turbocharger before the requested torque can be provided.

Estimated time to demand torque can be seen in the lowest diagram of this figure. Its dependency on EGR lead to differences in the prediction representing the state of the air path system.

Figure 5.20 shows the step from zero to full load. As for every turbocharged engine the torque reserve is not sufficient for this request. The air system need to build up the necessary intake pressure to provide sufficient amount of air to stay within the limits of air excess equivalence ratio.
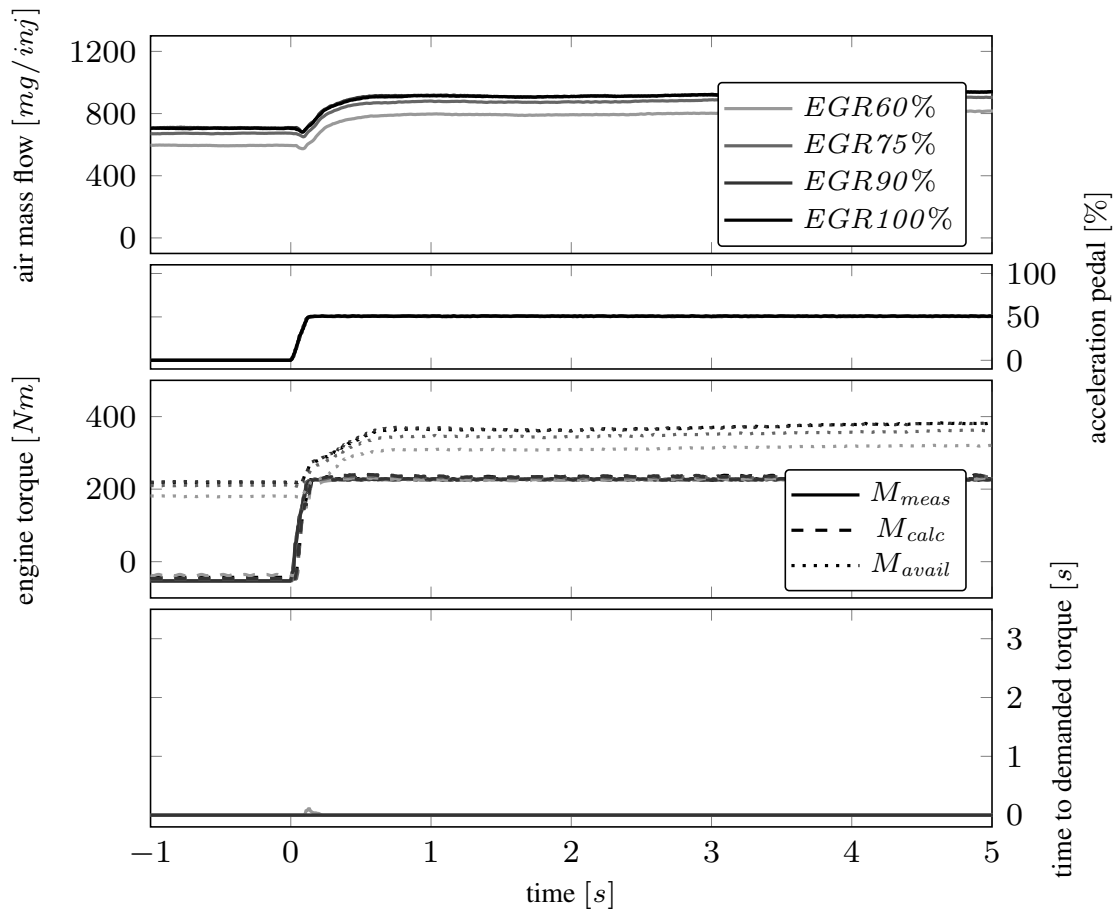

Figure 5.20: Diesel engine torque build-up at 2500 rpm and different EGR rates with an accelerator pedal step from 0% to full load.

In general the higher engine speed reduces the time to demanded torque but the effect of EGR rate still results in slower torque buildup. First diagram shows the air mass flow. EGR valve position of 60% leads to significant less air and extended time constant in the air path system to increase the amount of available air.

Torque shapes in third diagram provide the fast raise by the use of torque reserve. Increase beyond this level follows the dynamics of the air system. With the EGR valve position of 60% the requested torque cannot be fully reached. Time to demanded torque remains on a low level as a steady state deviation as displayed in lowest diagram.

At starting point of 25% acceleration pedal the available torque is almost equivalent to engine motoring mode. This means that the torque reserve in the measurement sequence shown in figure 5.21 is significantly lower than previously shown in figure 5.20. Increase of fuel energy up to the smoke limit provides a smaller ascent of exhaust gas enthalpy by the excitation of the accelerator pedal. This leads to lower performance of the turbocharger and as a result to less dynamic in the air system.
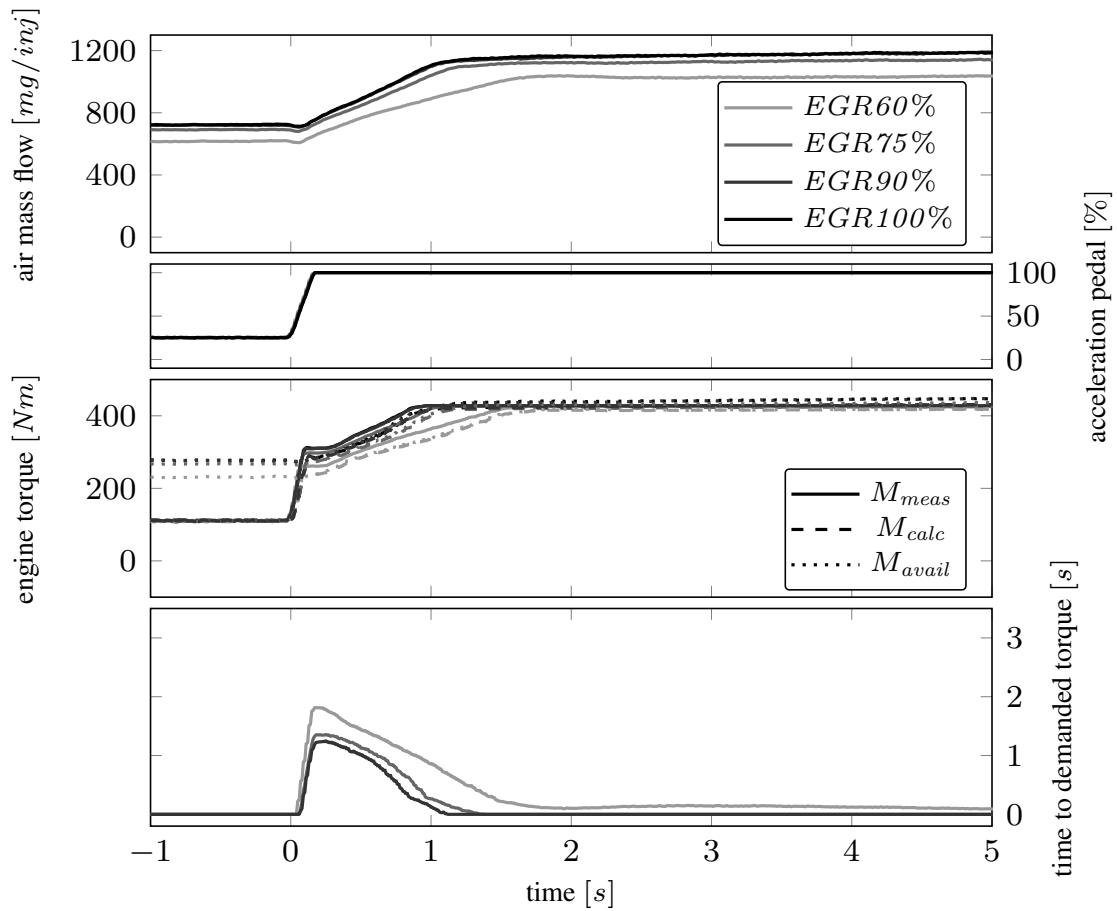
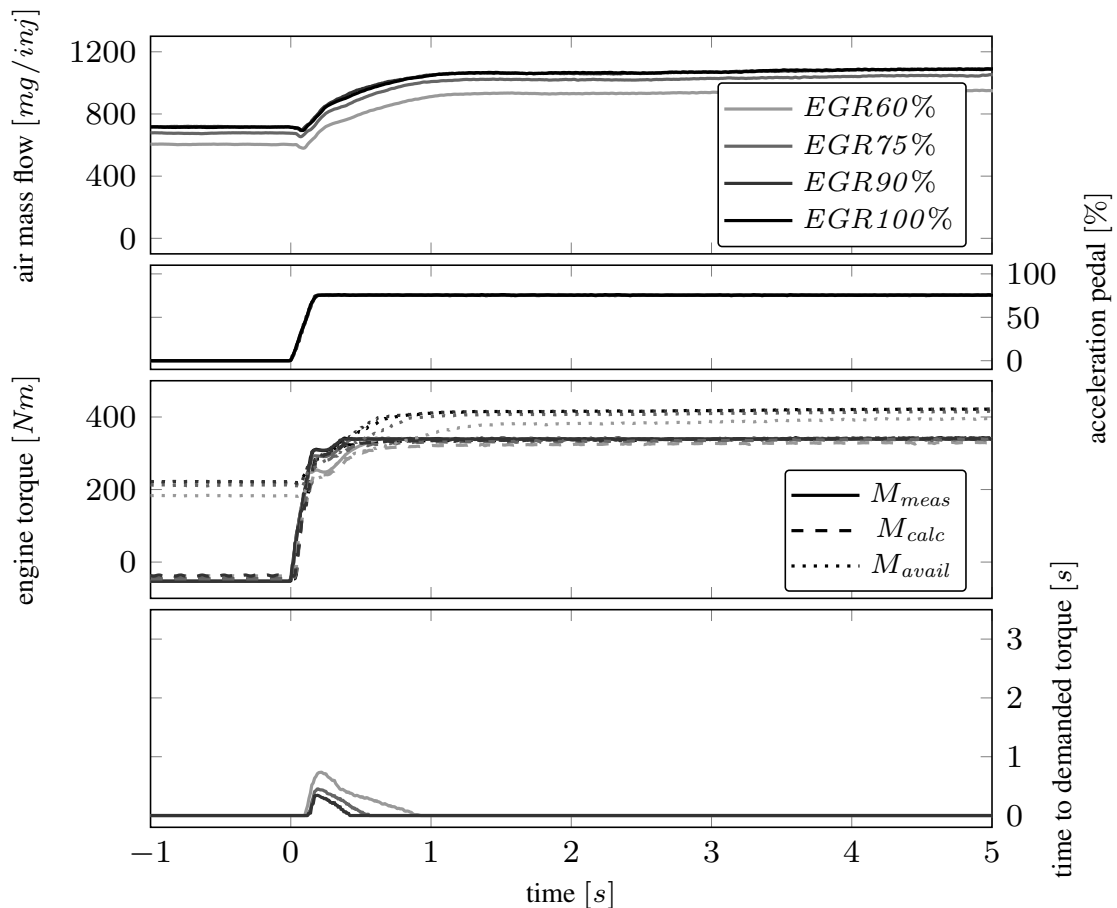
Figure 5.21: Diesel engine torque build-up at 2500 rpm and different EGR rates with an accelerator pedal step from 25% to full load.

The calculated torque at high EGR rates is lower than the measurement in this operation condition, whereas the shape remains representative.

The lowest diagram in figure 5.21 presents the longest time to demand torque in the analysis of EGR rate at 2500 rpm. Highest EGR rate leads to the slowest torque build-up. With EGR valve position of 60% the demanded torque cannot fully be provided and the time to demanded torque doesn't drop to zero for this reason.

Figure 5.22 shows the transient step response starting with 50% acceleration pedal position. Section 5.3 presented the independence of initial condition in air path dynamics. This analysis stresses that this learning is valid for same EGR level. Different EGR rates lead to divergent time constants in the air path.
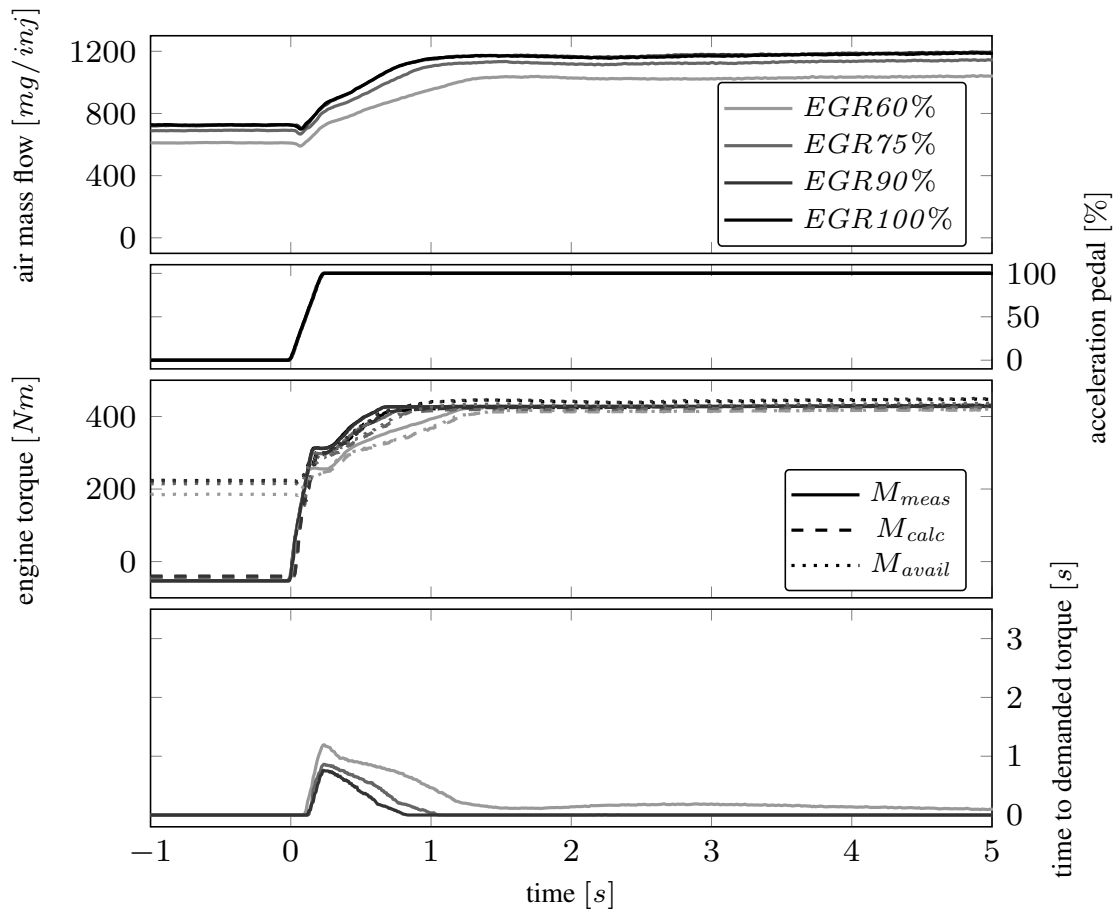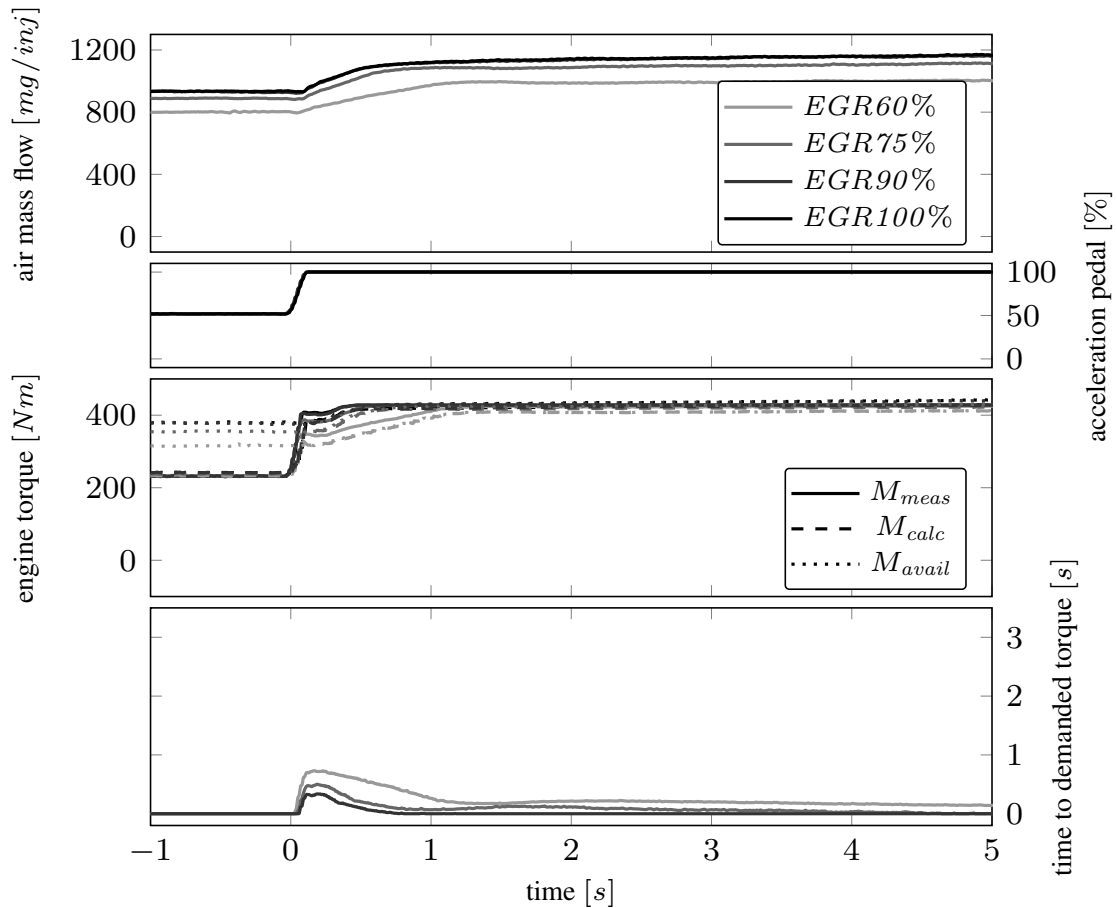

Figure 5.22: Diesel engine torque build-up at 2500 rpm and different EGR rates with an accelerator pedal step from 50% to full load.

The EGR valve position has a very significant impact on the available torque and resulting also on the time to provide the required torque. Again the calculated torque at 60% EGR valve position is slower than the measurement. Additional it shall be remarked that also for 75% EGR valve position the full load torque can hardly be reached.

Time to demanded torque as shown in lowest diagram provide useful estimation for transient operation but doesn't cover stationary deviation.

5.7 New European Transient Cycle

For passenger cars the certification cycle for European applications is the New European Driving Cycle (NEDC), defined in UNECE R101 [7] and [28]. It consists of two main parts as shown in figure 5.23.

At first there are 4 times 195s of urban operation, each with three accelerations to 15, 32 and 50 km/h followed by a short cruise at 32 km/h interrupting the last deceleration.

This sequence is followed by part 2 with 400s extra-urban velocity profile and a maximum speed of 120 km/h.

The total length is 11.007 km, total duration of 1180s with average speed of 33.6 km/h.
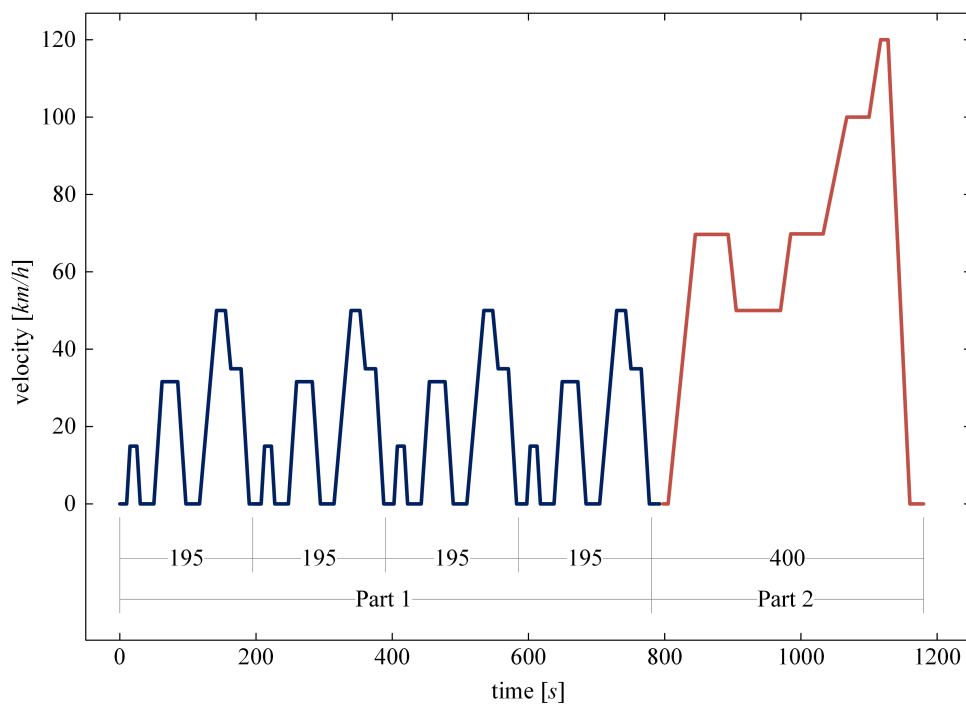
Figure 5.23: Definition of NEDC driving cycle

The definition includes boundary conditions for clutch actuation and selected gear. Using gear ratio of the transmission and a defined gear shift program and sequence, this vehicle cycle is converted into an engine cycle. Engine speed and accelerator pedal are used to execute the test on engine testbed. Basis for this conversion is the application of engine 1 in an European compact executive car with automated transmission.

The upper two diagrams of figure 5.24 show the definition of the NEDC for engine speed and accelerator pedal. The sequence of urban and extra-urban operation can be

clearly distinguished. Gear changes according the shift program can be seen during phases of vehicle accelerations and decelerations in the engine speed signal. This results from adaptation of engine speed to velocity.
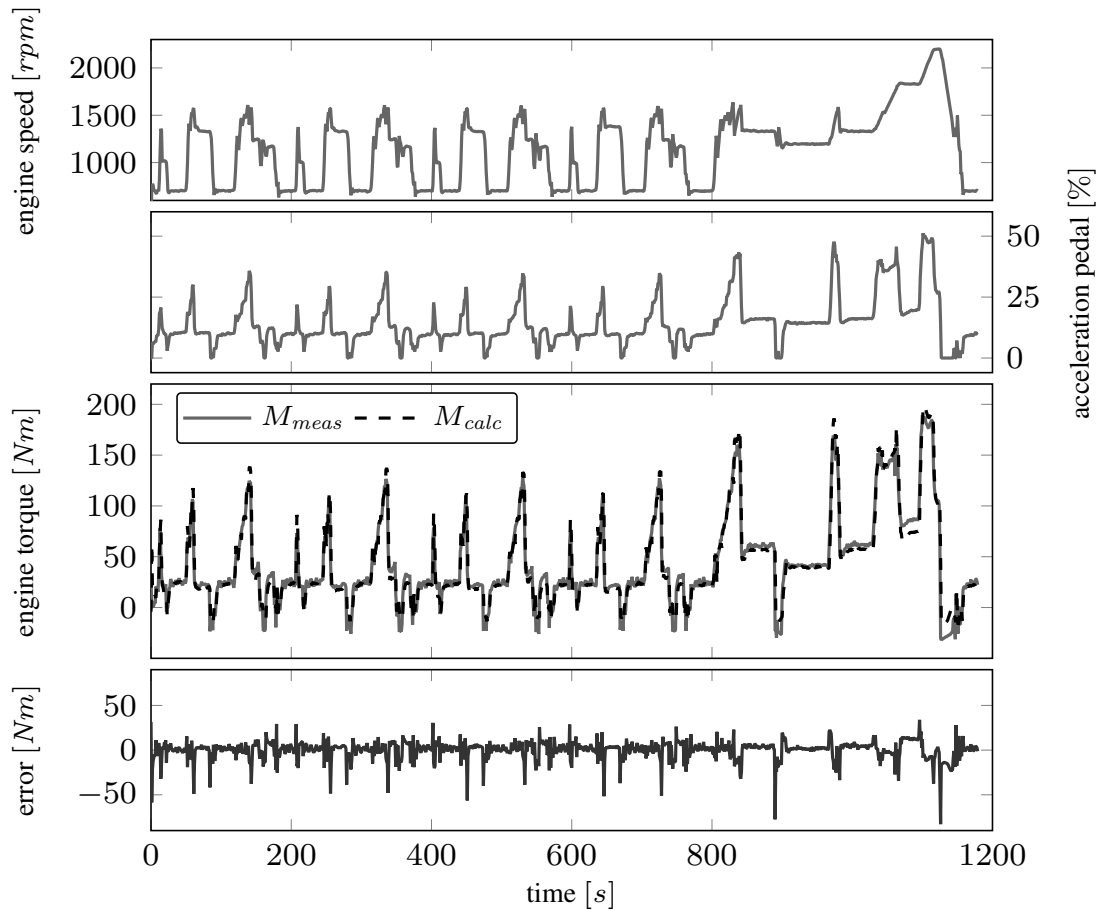
Figure 5.24: Comparison of measurement from testbed and calculated torque in NEDC test cycle.

The third diagram illustrates the engine torque from measurement and the calculation methodology in this work. As visually the difference is hard to appraise, the absolute error is given in the lowest diagram of this figure. Deviation results from torque differences by temporal shifts and by error of absolute values. Especially in vehicle deceleration temporal shift leads to large peaks of negative deviation.

Mostly the error is within in the range of $\pm 5 Nm$. The arithmetic average error considering the whole NEDC is $-0.0345 Nm$.

As the first part of the NEDC is a repetition of the urban sequence, a detailed view on the starting 190s is given in figure 5.25. Engine speed and accelerator pedal in the upper two diagrams show the three accelerations.
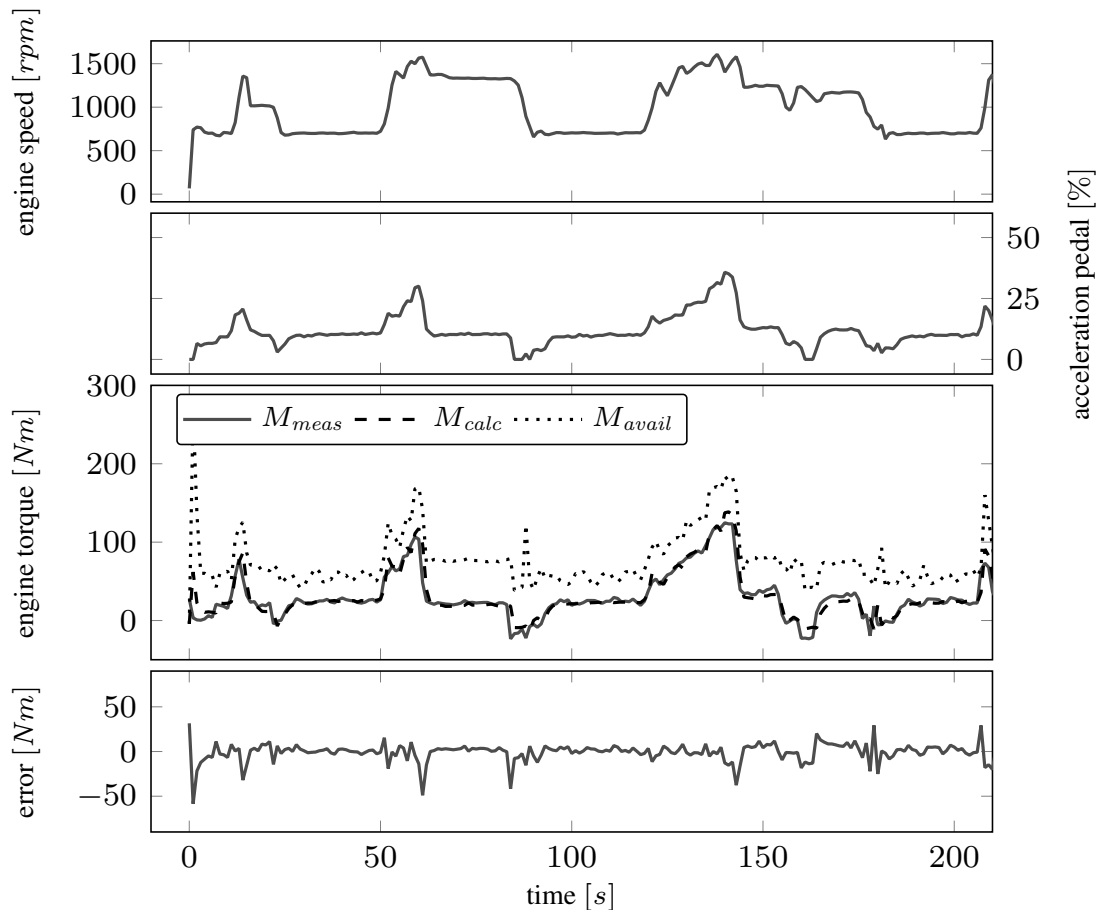
Figure 5.25: Detail from the beginning of NEDC with comparison of calculated and available torque

The third diagram shows the available torque based on smoke limitation in addition to the measurement and calculation. During the engine calibration process the required engine and vehicle performance is considered. The engine dataset is created to ensure that the torque reserve is large enough to fulfill the requested torque increase all over the cycle. Error between measurement and calculation shows most negative deviation when changing from deceleration to stationary condition. This results from time shift between signals from engine testbed and ECU.

Figure 5.26 shows the extra-urban part of the NEDC. Top diagram shows sawtooth-shape in the speed signal as a result from gear shift events. High velocities of 130km/h lead to operation at high engine speed up to 2200 rpm.
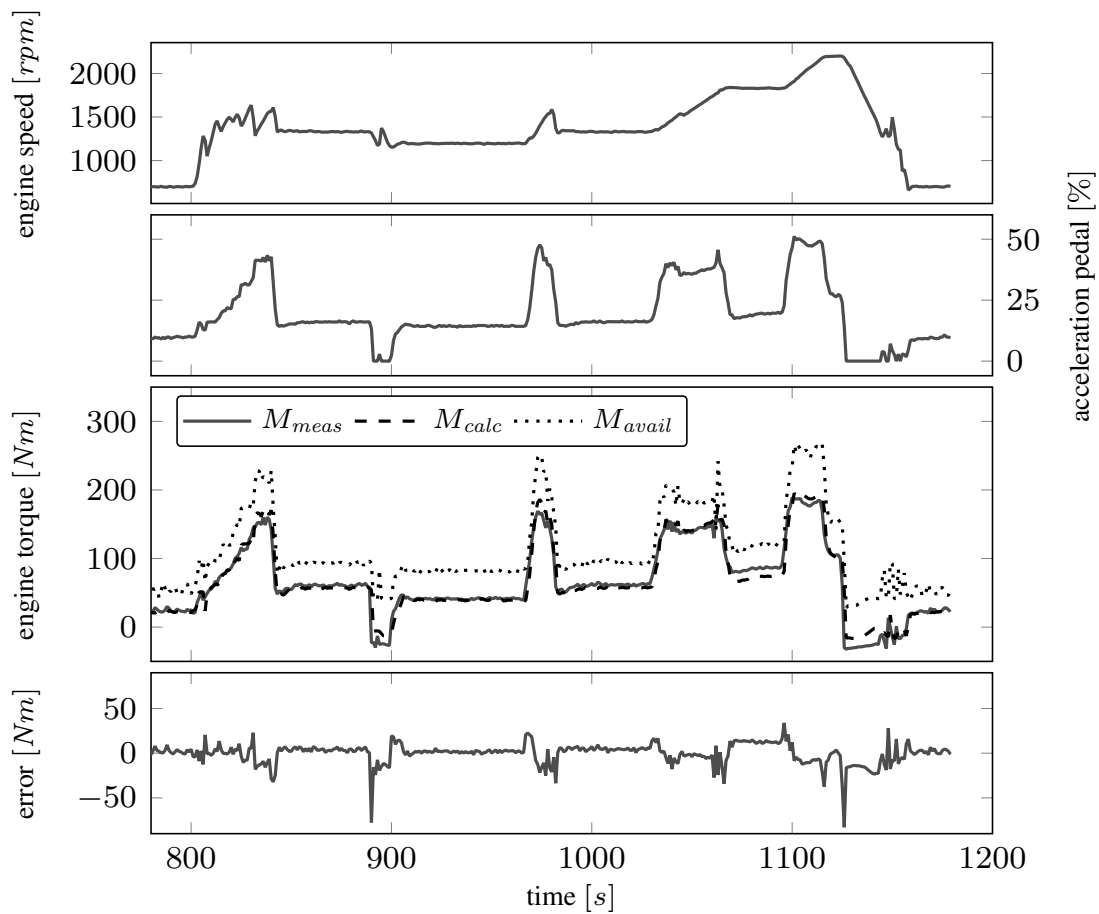
Figure 5.26: Detail of last acceleration in NEDC with comparison of calculated and available torque

The third diagram presents engine torque from calculation and measurement as well as the available torque. Again the torque reserve is sufficient to fulfill the requested torque at every time.

The error between measurement and calculation again has negative spikes during deceleration. This is a result of high dynamic and small time shift between the two signals.

5.8 World harmonized light vehicle test procedure

The *Worldwide harmonized Light-duty vehicle Test Procedure (WLTP)* is established for uniform testing of vehicle pollutant and green house gas emission. Experts from European Union, Japan and India developed the cycle according the guidelines of UNECE World Forum for Harmonization of Vehicle Regulations [27] and finally confirmed it in 2015. The developed procedure defines a global harmonized standard for the evaluation of green house gas and pollutant emission for passenger cars and light duty vehicles. The test procedure consists of 4 parts as shown in figure 5.27.
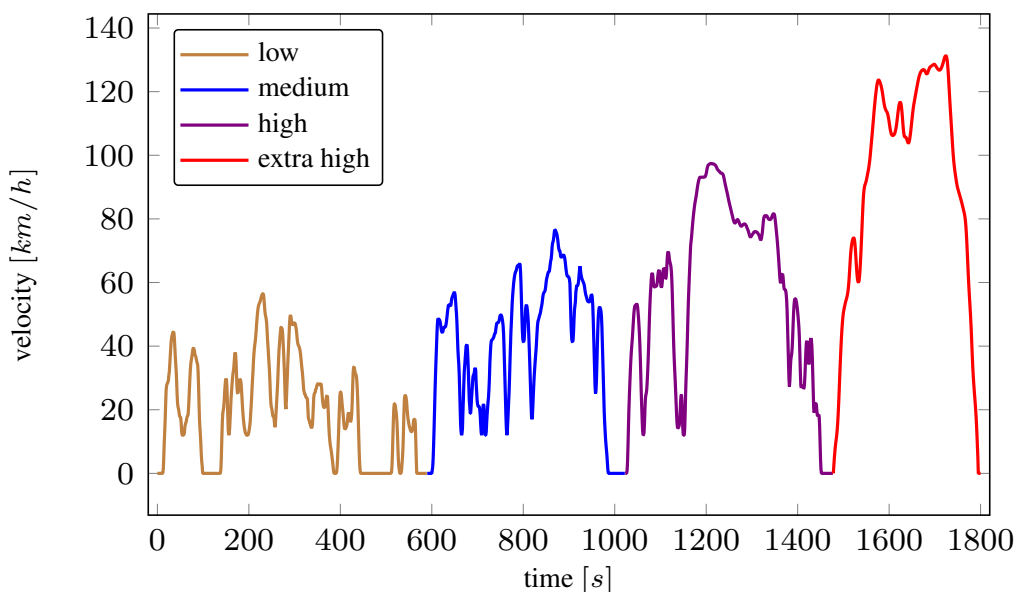
Figure 5.27: Velocity profile of Class 3 WLTP including the 4 parts for low, medium, high and extra high phase according the definition of UNECE [27].

property	low	medium	high	extra high	total
duration $[s]$	589	433	455	323	1800
distance $[m]$	3095	4756	7162	8254	23266
ratio of stops $[\%]$	26.5	11.1	6.8	2.2	13.4
maximum velocity $[km/h]$	56.5	76.6	97.4	131.3	
average velocity $[km/h]$	25.3	44.5	60.7	94	53.5

Vehicles are sorted into 3 different classes by the ratio of rated power PWr in W/kerb mass in kg. WLTP definition as given in [29] defined that Class 1 vehicles with $PWr \leqq 22$ only need to run the low and medium part. Class 2 vehicles with $PWr \leqq 34$ extend the

cycle with the high part and high powered vehicles with $PWr > 34$ execute the full cycle including the extra-high part.

This test is a severe improvement compared to NEDC. Velocity profile represents city traffic, urban, rural and highway operation and covers a wide operation range in the engine map, although the transients are still slower than in real world operation.

Simulation is executed on standard desktop computer with real-time factor of 0.012 therefore no detailed runtime analysis is displayed in this work.
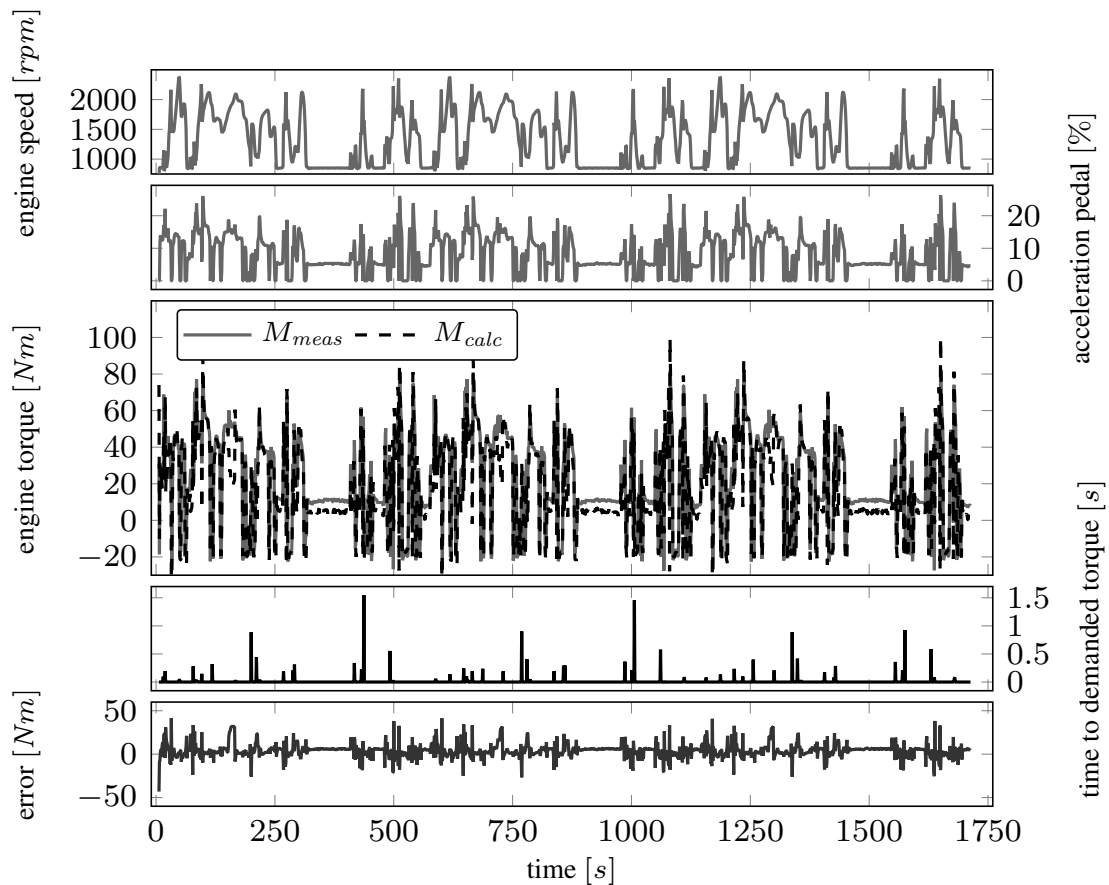
Figure 5.28: Full WLTP test cycle of engine 2 - comparison from testbed and calculated data.

The conversion of the vehicle velocity profile to engine speed and accelerator pedal of engine 2 as provided in figure 5.28 is done based on an European family car with manual transmission. Although the vehicle and engine combination leads to a class 1 definition, all parts of the WLTP are executed. The fourth diagram shows multiple events where the time to demanded torque is greater than zero.

The lowest diagram in figure 5.28 presents the absolute torque calculation error.

The next pages analyze the sections of WLTP separately for more detailed view.

Figure 5.29 shows the low-part of WLTP.
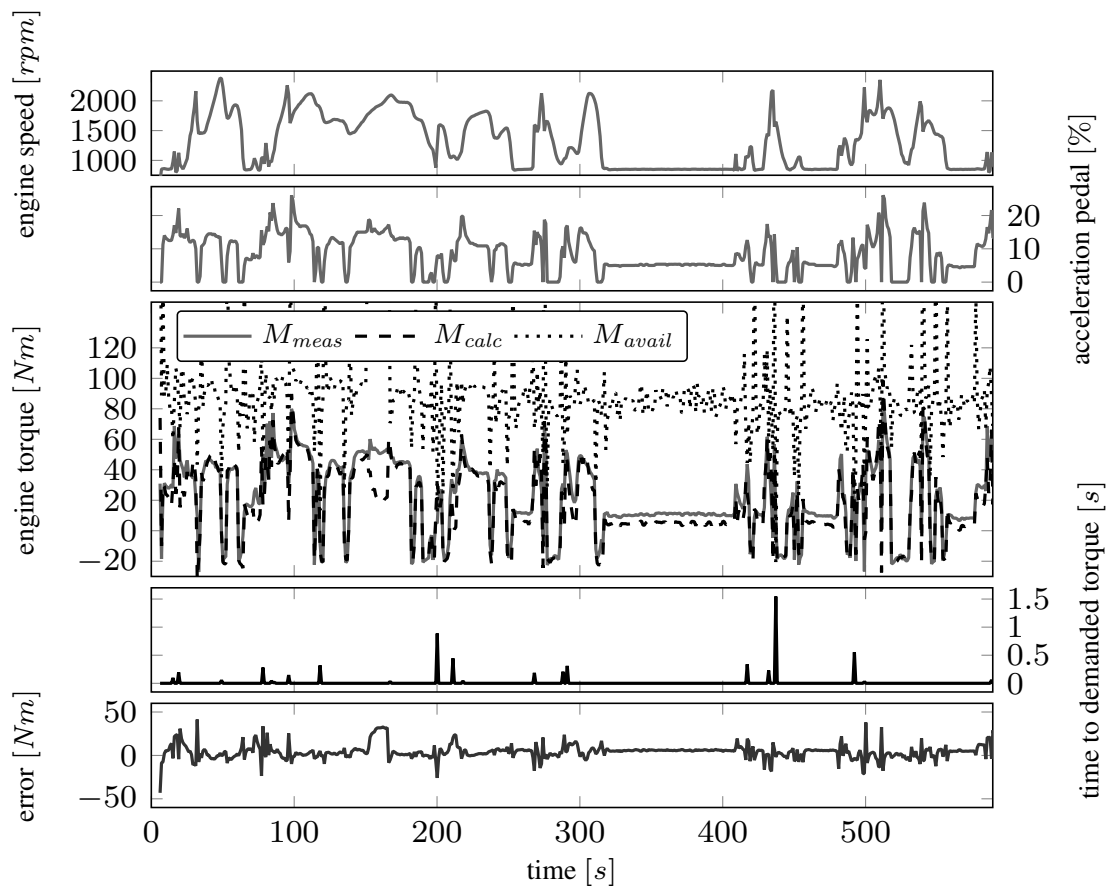
Figure 5.29: Low-part of WLTP test cycle of engine 2 - comparison from testbed and calculated data.

Here in more detail the high transients in engine speed and accelerator pedal are visible in the upper two diagrams. Gear shift events lead to steep changes in engine speed.

The third presents the measured (solid), calculated (dashed) and shows the available torque (dotted). Torque reserve is not sufficient in all operation conditions to fulfill requests of demanded torque. These sections can be identified in the fourth diagram as in these conditions the time to demanded torque become larger than zero.

The lowest diagram illustrates the absolute error of measured and calculated torque.

Figure 5.30 presents a transient section for detailed analysis. The timeframe starts with a deceleration when engine is in motoring condition. It is followed by power requests from accelerator pedal and after some seconds by an increase of engine speed.
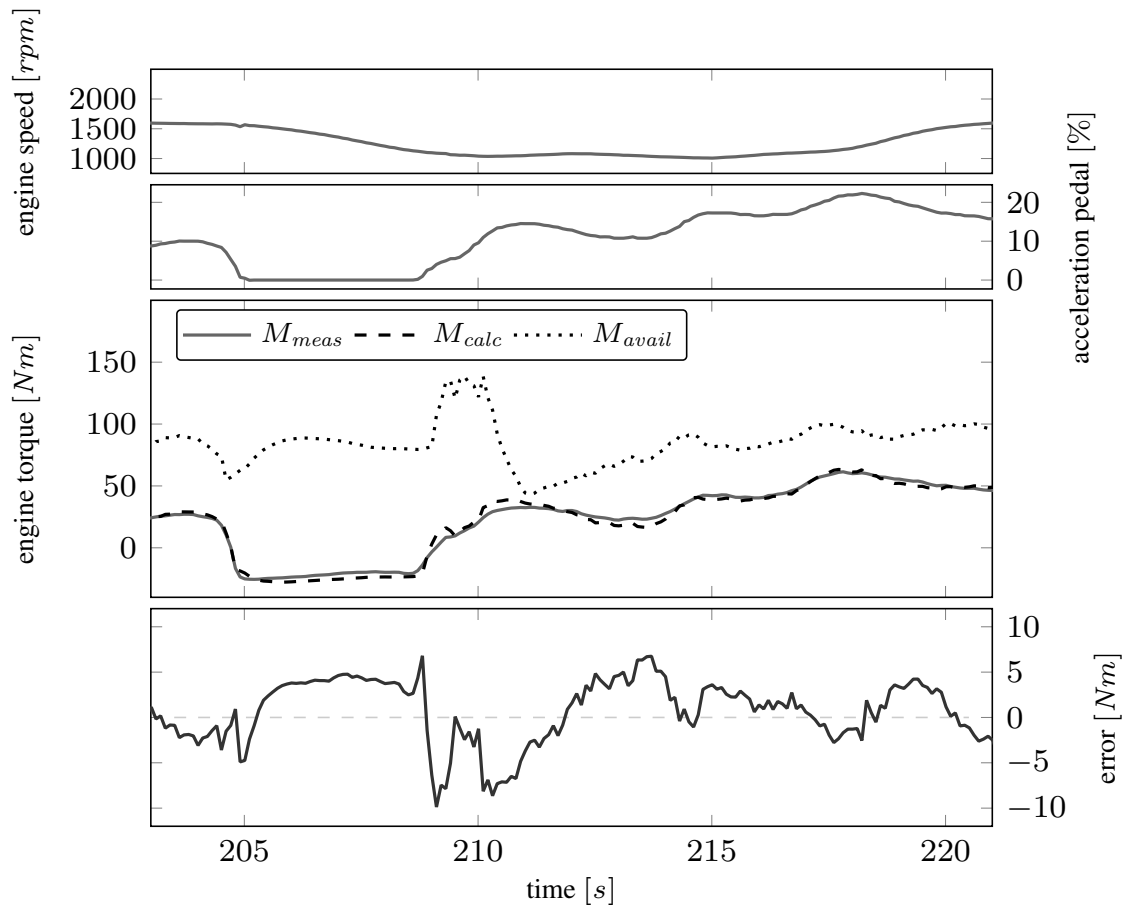
Figure 5.30: Detail of torque - comparison from testbed and calculated torque in WLTP test cycle of engine 2.

Third diagram illustrates the engine torque. Calculated signal (dashed line) and measurement (solid line) show similar behavior. At 211 s available torque almost touches the current value but all demanded torque can be provided by the torque reserve. The lowest diagram show the absolute error between measurement and calculated torque given in the diagram above. During deceleration with fuel cut-off only motoring torque remains. This operation condition shows positive deviation of about 5 Nm as a result of inaccuracy of friction torque calibration. After re-entering the firing-operation negative deviation is detected while after some seconds the error is commuting a around zero in transient operation.

The medium part of the WLTP is given in figure 5.31 and shows engine speed range from idle to 2500 rpm. Compared to the low part, velocity and therefore the torque level in general is higher.
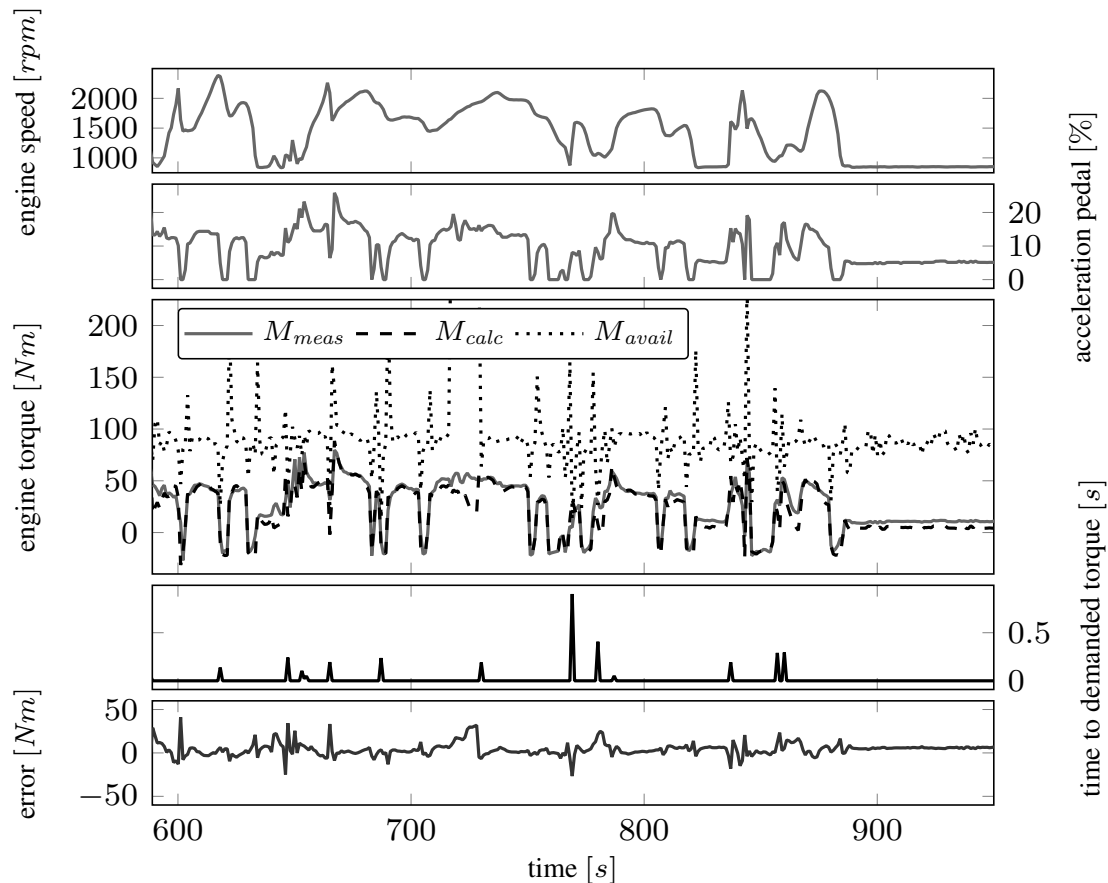
Figure 5.31: Medium part of WLTP test cycle of engine 2 - comparison from testbed and calculated data.

The measured and calculated torque as well as the available torque is presented in the third diagram. Torque reserve is mostly sufficient to provide the requested torque instantaneously whereas several times a time to requested torque of 0.2 s is detected. Nevertheless no significant limitation with respect to engine torque arises from the air path system.

The error is calculated as measurement torque minus calculated torque; these values are illustrated in the lowest diagram. Maximum deviation e.g. at 600 s occurs during fuel cut-off in shift events as a result from minor time shift between measurement and calculation signal. Smoke limit is calculated by the ECU and provided as input-signal. The effect at 720 s with sudden increase of available torque results from computation error as this value changes to the upper calculation limit of 1000 mg/inj.

Figure 5.32 shows the high part of the WLTP with rural traffic conditions. Higher average speed and many transients in the accelerator pedal characterize this section.
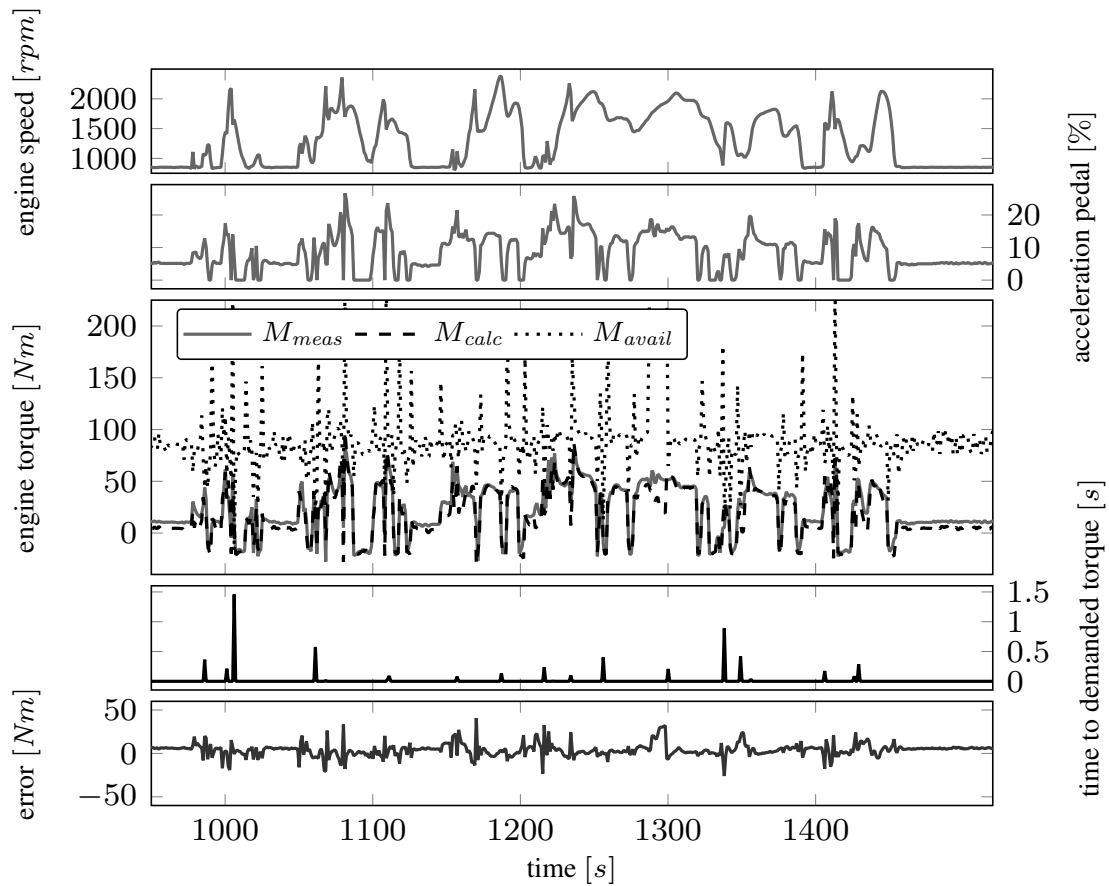
Figure 5.32: High part of WLTP test cycle of engine 2 - comparison from testbed and calculated data.

Calculated (dashed) and measured (solid) torque are presented in the third diagram. The dashed line provide the maximum instantaneously available torque. At time-stamp of 1010 s the torque reserve becomes zero for some time and further torque requests would not be available. As there is no additional request, the demanded values can still be provided by the combustion engine.

In the fourth diagram several times the torque reserve becomes zero. As a result time to demanded torque beyond zero occurs multiple times. The lowest diagram in this figure illustrates the error as the measured minus the calculated torque. Short time shift during high gradients in the torque signals lead to short term deviation. This effect doesn't have negative impact on the application of the proposed algorithm for the target applications.

The extra high part of the WLTP represents highway traffic with velocity up to 130 km/. The engine speed signal as given in figure 5.33 shows multiple peaks that result from gear shift events. Up-shift lead to fast speed reductions that can be clearly identified.
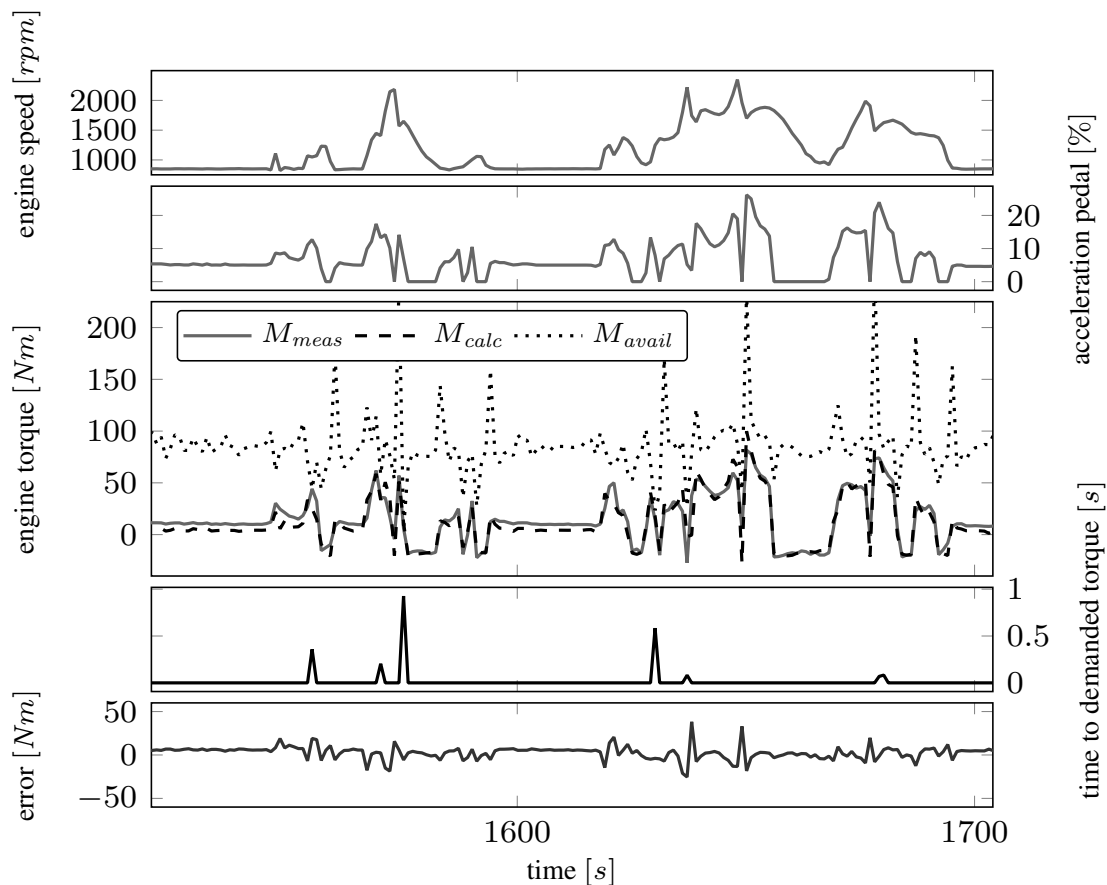
Figure 5.33: Extra high part of WLTP test cycle of engine 2 - comparison from testbed and calculated data.

The average acceleration pedal position is significantly higher than in the previous parts of the WLTP. From torque signal it can be seen that acceleration lead to increased torque demand whereas constant cruising require only few permanent torque, e.g. in the time-frame around 1600 s.

Acceleration right after deceleration lead to the most challenging situation with respect to torque reserve. This is a result of the intake pressure control strategy as deceleration reduces the pressure in the intake manifold that is then further on required for torque increase. Unless the availability of predictive information this usually is covered by gain scheduling of the intake pressure controller with respect to the sign of deviation.

The bottom diagram gives the error of measured and calculated torque.

5.9 Conclusion

This chapter shows the implementation of the methodology as provided in chapter 3. The torque calculation is implemented to compute the actual torque M_{act} as well as the available torque M_{avail}. Both follow the same structure as given in section 5.1.

Engine dynamics as given in chapter 4 is used to calculate the time to demanded torque $t_{tq,dem}$.

The algorithms are implemented in Matlab Simulink. This platform is used for simulation and analysis of the proposed method.

At first single step response measurement is used to validate the torque calculation. Based on the satisfactory results the dynamic behavior is discussed. The analysis of time to demanded torque identifies the optimal gain of *-1* for perfect prediction.

The method was analyzed with different excitation of the accelerator pedal. Systematic torque increase first immediately the use of torque reserve and further on the torque buildup according the time constant of the air path was proven. This behavior is independent from starting or target torque.

At next the dependency on engine speed was checked. Therefore an intense measurement program was executed and multiple sequences of steps in the accelerator pedal and the result on real hardware were measured. Based on this data the provided method was applied and the effect of different engine speed was shown to be covered sufficiently for good estimation of available and actual torque and the time to demanded torque.

Based on engineering experience the EGR rate has significant influence on the dynamic behavior of the internal combustion engine. This effect was at again firstly measured on engine 1 and further on the calculation method was applied to these data. The calculation results are representative although it is not directly considered in the algorithm.

Time to demanded torque cannot fully predict the behavior of changed air path as this is neither taken into account by the calibration of the input values nor by a nonlinear predictive air path model.

Finally measurement data of the legislative driving cycles NEDC and WLTP are used to validate the methodology in transient cycles. As the dynamics of NEDC is very low only the error on torque calculation can be proven and shows comparable results. WLTP

is designed to represent real driving behavior and consists of 4 parts, low and medium representing urban traffic, high for rural operation and extra high for highway. Torque calculation with comparison to measurement data from engine 2 is shown for the whole cycle, each part and some detail.

Engine calibration is performed to enable transient operation without running into the soot limiter. A couple of event when time to demanded torque is above zero occur in WLTP. In these situations no additional torque is requested and therefore no real time delay results.

The three main output signals - calculated and available torque and the time to torque demand - are proven in the simulation environment by using measurement data from engine testbed. These signals are identified to be important input for powertrain control, especially for torque intervention and prediction during gear shift.

6 Experimental validation

6.1 Implementation in rapid prototyping ECU and testbed setup

Code generation in Matlab Simulink

This section describes the work-flow from the Simulation environment in Matlab Simulink to the executable code in the rapid prototype control unit.
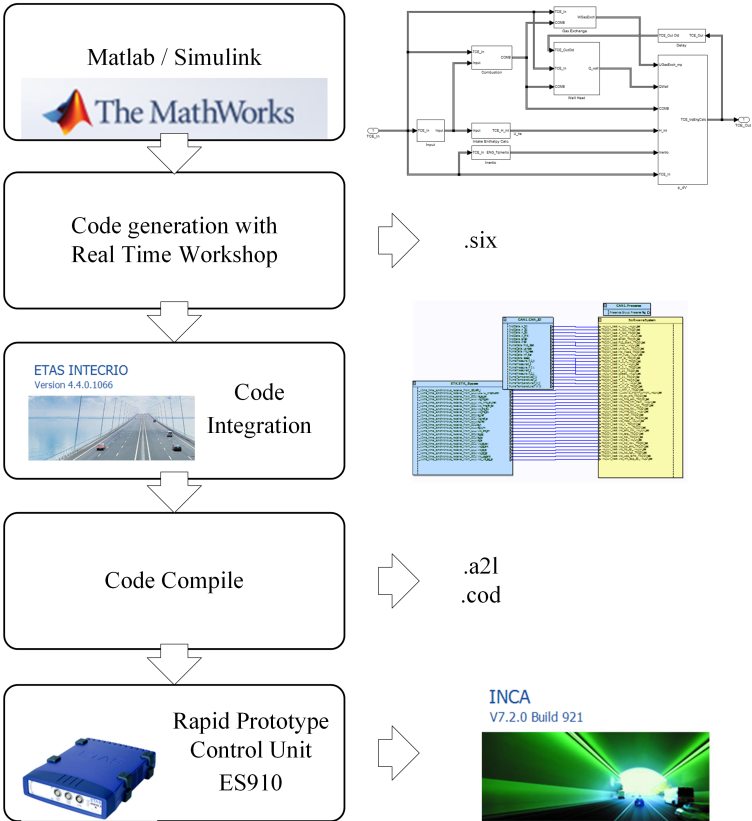
Figure 6.1: Compile process to generate executable code for rapid prototype control

At first each calibration and measurement label including name, unit and range is defined.

The next step assigns the label definition with the blocks and lines in the calculation model.

The inputs and outputs of the model have to be connected with the according INTECRIO inports and outports. The resulting label of the in- and out-ports in the derived code is defined by the line connected to the block.

Finally the compiler settings needs to be set for the INTECRIO Real Time Workshop. With the correct settings the build process can be started to compile the Simulink model into the .six file.

INTECRIO build environment

The tool INTECRIO from ETAS provides the configuration options to connect code from Matlab Simulink, ETAS ASCET or handwritten c-code with the inports and outports of the rapid prototyping hardware.

The connection with the ECU is done using the data definition file (.a2l) and program file (.hex) via ETK or CAN. With this definition is's possible to select defined ECU labels and connect it to the in- and outports of the code elements in the INTECRIO environment. The occurrence time / raster must be defined for each label and code element.

After successful definition the code compile process to generate the executable files is started and results in the data definition (.a2l) and code (.cod).

Rapid Prototype Control Unit (RPS)

The platform for the execution of the calculation algorithm is the rapid prototyping control unit ES910 from ETAS. This device is equipped with a double precision floating point processor and a real time operating system. ETK, CAN and Ethernet interface enable connection to the ECU, testbed and calibration system.

Engine Control Unit

The engine control is done by an EDC17 from Bosch with prototype access for measurement and calibration. The basic software, complex device drivers and injection control are provided by the Tier1 supplier, the torque - and air - path as well as the exhaust aftertreatment control is based on an OEM specific algorithm.

INCA Measurement and Calibration System

The calibration and measurement tool INCA from ETAS is mainly used for engine applications as it is also done in this case. At first the two ECU projects - for the

combustion engine and the rapid prototype control unit - need to be added by introduction of the .a2l and .hex respectively .cod file.

Secondly the workspace need to be created, connected to the ECU projects and the hardware setup with the ES910 is defined. Then finally the experiment environment as a graphical representation is set up. Therefore the specific measurement labels that are defined in the a2l-file are selected with the target update rate. They can be assigned to measurement windows with a numerical representation of the actual value or to an oscilloscope that gives the temporal history in a graphical way.

Calibration labels can be selected similar whereas scalar variables are presented in tables, curves or maps can be displayed either in tables or as a combined editor with table and 2D / 3D graphic.

In online operation the measurement can either be done with or without recorder. Usually during calibration only temporal values are used and recording is activated for specific test runs e.g. stationary map or transient test measurement.
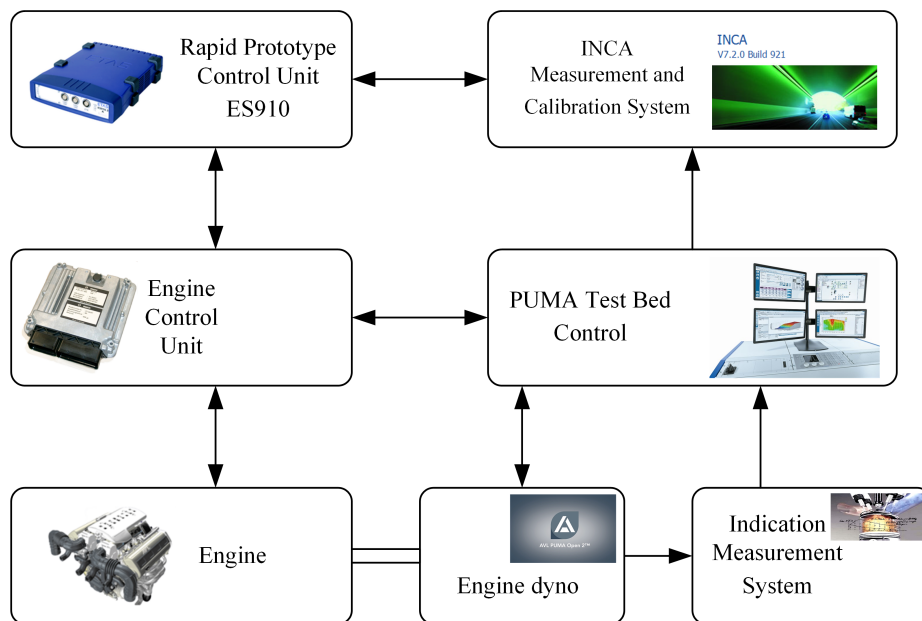
Figure 6.2: Setup for validation in bypass operation on engine testbed

Puma testbed control

The used transient testbed is equipped with AVLs PUMA Open testbed automation system. This system is proven at many OEMs and enables high productivity, quality and efficiency. The engine can be operated in different modes e.g setpoint for engine speed

and accelerator pedal, speed and torque setpoint, manual and automated definition of operation mode and test sequences.

Several control loops e.g. brake torque control or speed control are implemented and accessible in different operation modes.

Testbed measurement equipment like temperature and pressure sensors, injection quantity balance and sampling of exhaust emission according diluted with air using the CVS method are integrated and directly accessible.

Engine dyno

The engine dyno from the DynoExact APA Series is a cradle-mounted asynchronous machine. Excellent torque measuring accuracy of $\pm 0.1\%$ final scale and control stability is reached by the measuring based by means of a bending lever.

Zero inertia simulation and four quadrant operation enable the execution of all relevant use cases for steady-state testing, dynamic vehicle and driver simulation in transient operation including emission testing.

Indication Measurement System

For optimization of the combustion process by combustion experts and calibration engineers, the Indication Measurement System IndiCom based on cylinder pressure signal and integrated measurement data processing is installed.

Data acquisition, detailed cycle by cycle analysis and online information of characteristic values enable optimization of the combustion process during all phases of the engine development.

Engine

Online measurement used for the analysis in this chapter is based on the engine 2 (see Table 4.1). Further attributes are a cooled low pressure exhaust gas recirculation and a pipe-integrated indirect charge air cooler. The calibrated emission level corresponds to Euro 6c legislation.

6.2 Stationary operation

This section provides the results from online testbed measurement. For this analysis and calculation, measurement data of the warm engine are used to validate the method. Each operation point is approached and then operated until the conditions like pressures and temperatures become stable.
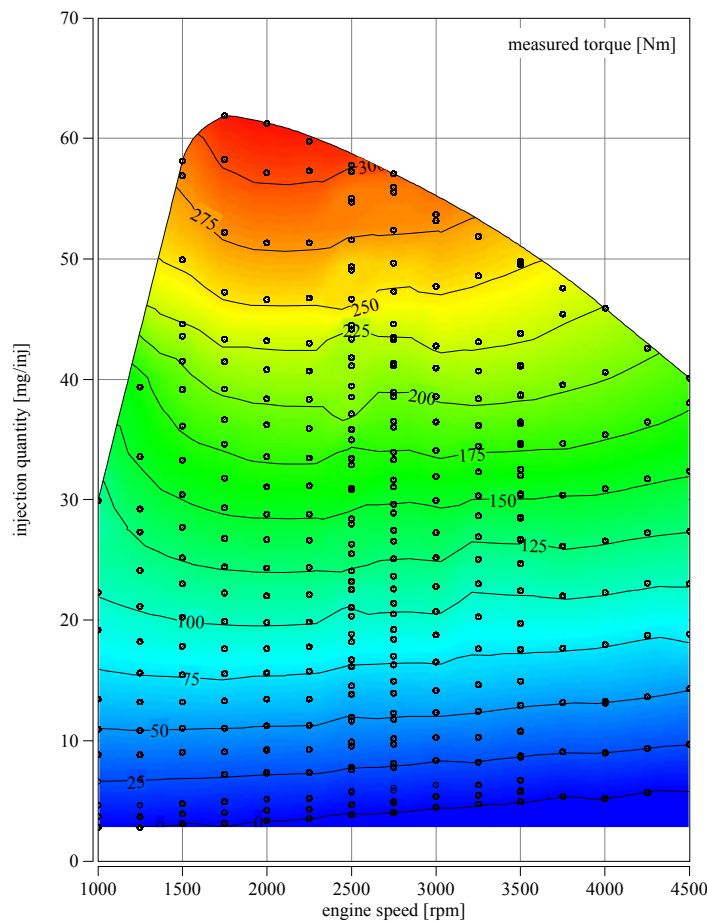
Figure 6.3: Measured engine torque from testbed automation in stationary operation.

Testbed automation triggers the storage of average values of some seconds as measurement point shown in measured torque in figure 6.3 as black circles.
Measurement is started at 1000 rpm in motoring condition, then the engine torque request is stepwise increased up to rated speed. After reaching the full load torque, the operation
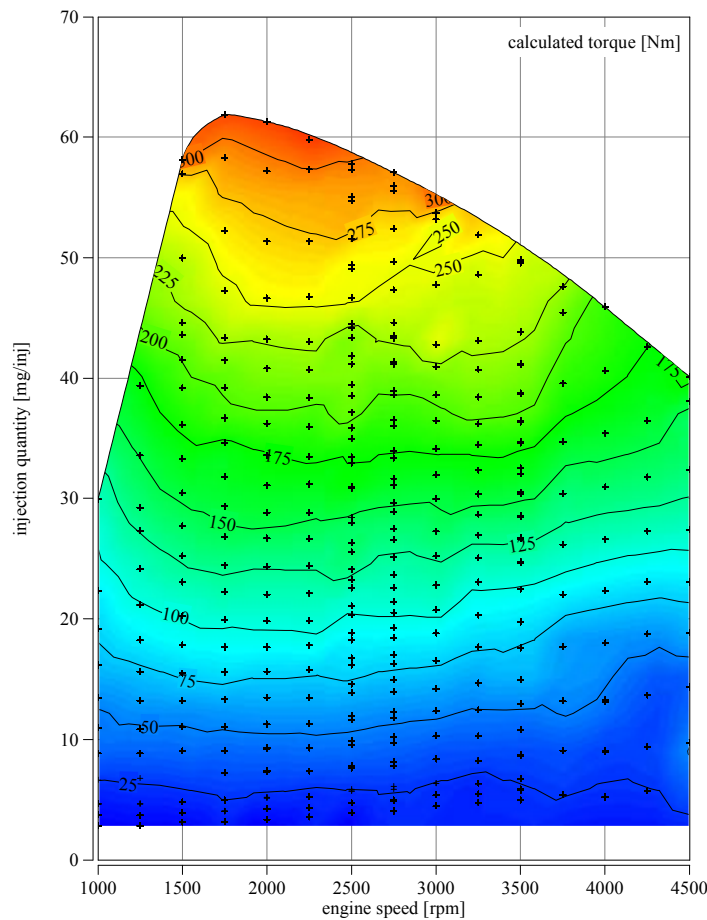
Figure 6.4: Calculated engine torque from algorithm in rapid prototype ECU in stationary operation.

point is changed to motoring mode and next engine speed. The torque sweep at engine speeds 2500 to 3500 rpm was measured two times. By this measurement procedure in total 350 engine operation points are measured.

Figure 6.3 illustrates the measured engine torque. The level is represented by color indicator, isolines show the level of torque equivalence. Black dots indicate the measurement points for engine map analysis of engine 2.

The calculated torque is given in figure 6.4 where the torque level is represented by color indicator, isolines show the level of torque equivalence. Cross indicators display the stationary operation points at engine map analysis on engine testbed.

Figure 6.5 presents the difference on MFB50. The measured value from Indicom measurement system is subtracted by the calculated values from the calculation algorithm in the RPS. Isolines show the deviation in °CA with the color indicator for the difference level.
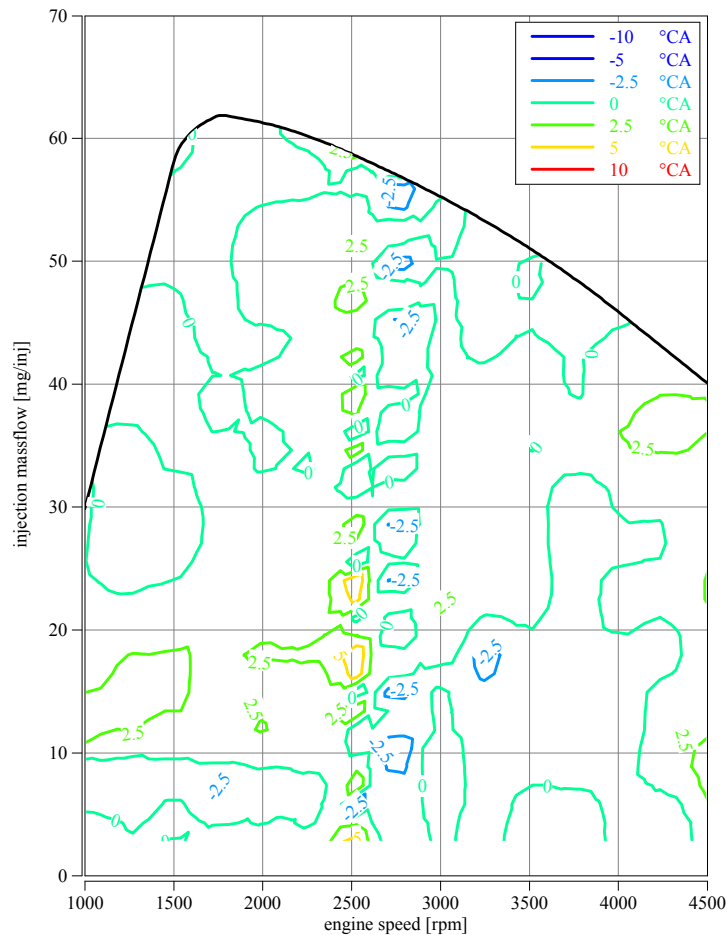
Figure 6.5: Difference of combustion center MFB50 in stationary operation.

As mentioned above, engine speeds of 2500 rpm and 2750 rpm were measured twice. This introduces deviations as due to system and measurement tolerances its not possible to reproduce exactly equivalent conditions. The resulting measurement and calculation levels were averaged in post-processing. Distinctive behavior in this area compared to single measurement than the rest of the operation map. Interpretation of results need to consider a deviation of ± 2.5%.

Figure 6.6 presents the deviation of IMEP. Measured value from Indicom measurement system is subtracted by the calculated values from the calculation algorithm in the RPS. Isolines show the deviation in hPa with the color indicator for the difference level.
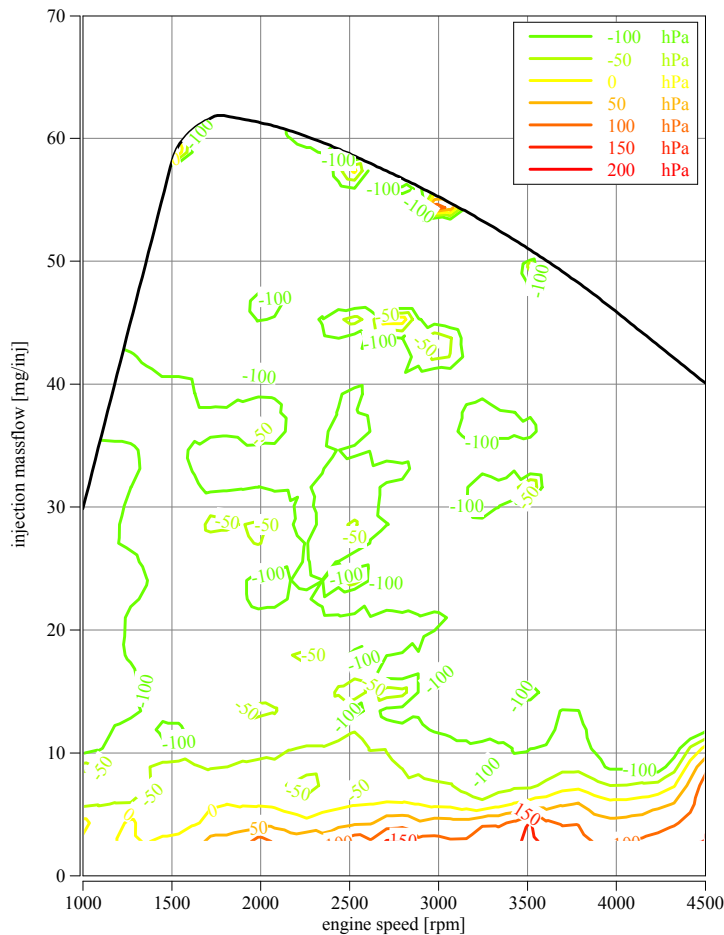
Figure 6.6: Difference of calculated and measured indicated mean pressure IMEP in stationary operation.

Engine operation at low torque show most inaccuracy, especially at high engine speed. Relative uncertainty of injection quantity determination becomes very large at low fuel mass-flow. The proposed algorithm uses this signal as main input signal with direct impact on Q_{fuel} and exhaust gas enthalpy $U_{h,exh}$ as they are main contributors in the energy balance equation. For broad areas the correlation between measured and calculated IMEP is within ± 100 hPa.

Deviation of torque calculation is computed by subtraction of measured value from Puma testbed automation (compare figure 6.3) and calculated values from the proposed algorithm in the RPS as given in figure 6.4. Isolines show the deviation in Nm with the color indicator for the difference level.
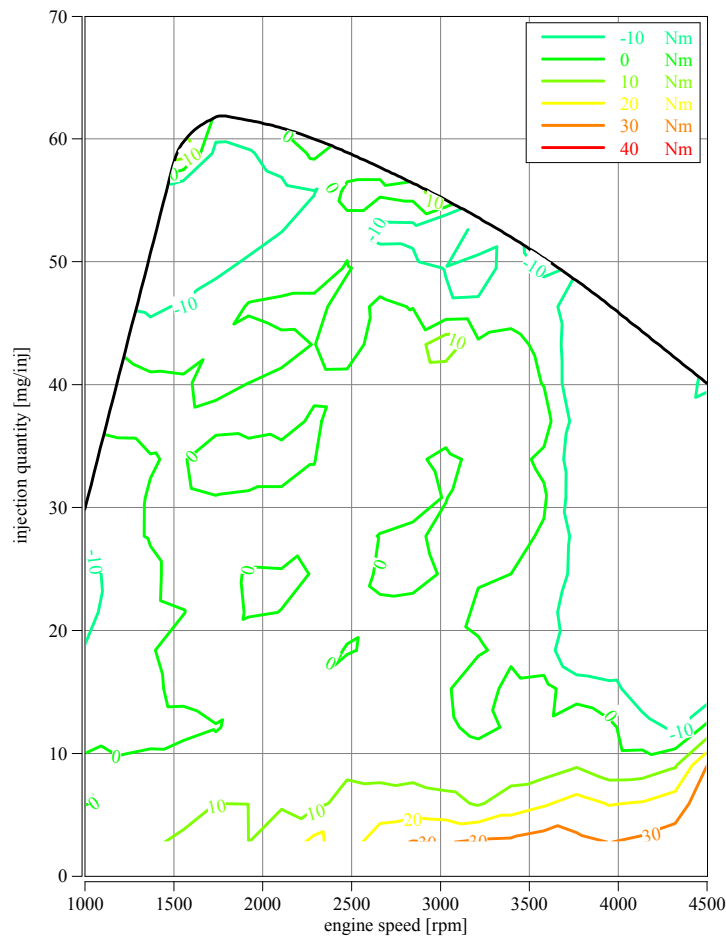
Figure 6.7: Difference of calculated and measured engine torque at stationary analysis with engine 2.

As brake specific torque is calculated from IMEP by consideration of friction, auxiliaries and inertia, the comparison on torque level leads to similar results as discussed above; engine operation at low torque levels show most inaccuracy, especially at high engine speed.

Area with most relevance in respect to emission cycles and real life operation show an accuracy of ± 10 Nm.

Figure 6.8 shows the relevant torque labels as surface with color indicator. The lines in x- and y-direction represent the interpolation raster used in post-processing analysis.
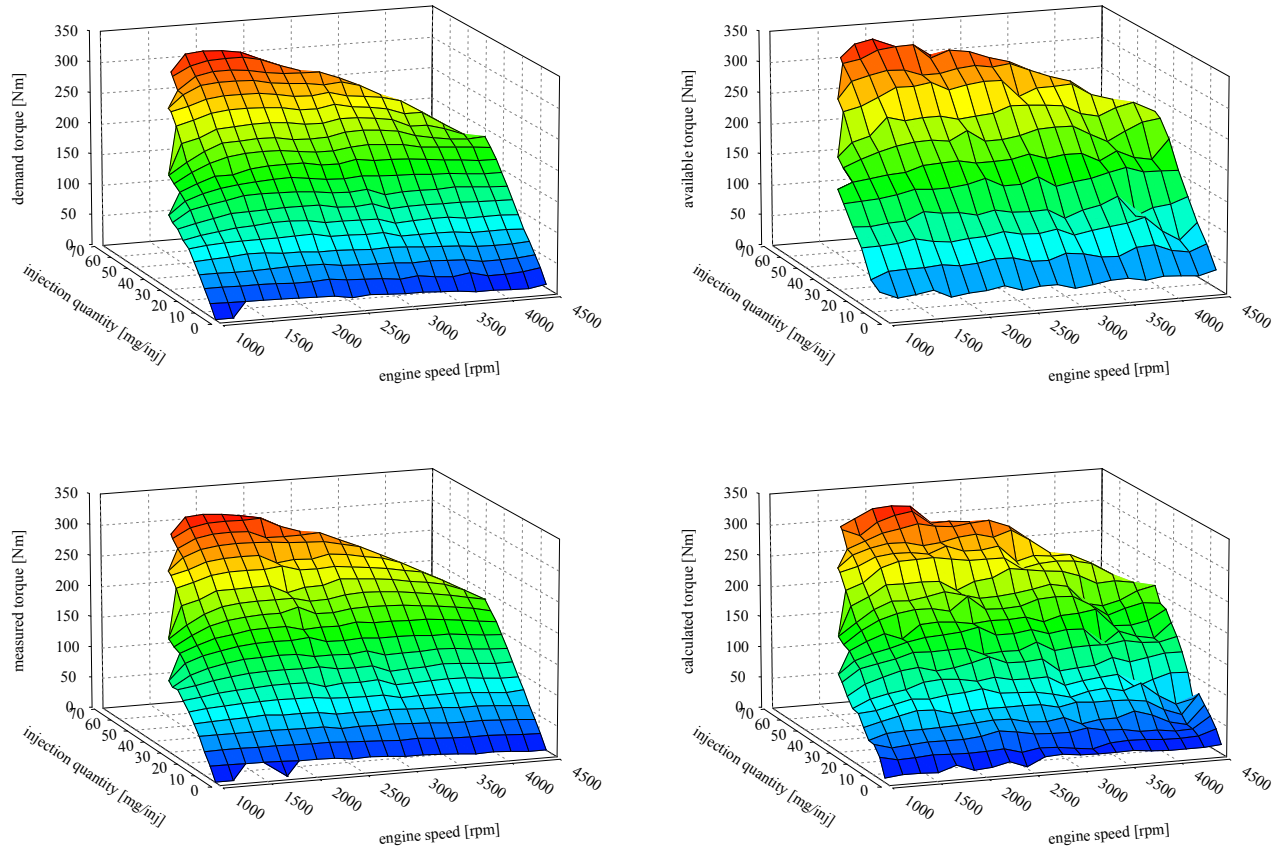
Figure 6.8: Surface diagram of demand, available, calculated and measured torque derived in stationary operation.

Top left diagram presets the demand torque derived from accelerator pedal and its relation to engine speed and fuel injection quantity.

Measurement torque as reference value is displayed in the diagram below. Comparison of these two maps show the influence of reproducibility in the engine speed of 2500 and 2750 rpm as these were measured twice and show most deviation.

Bottom right diagram illustrates calculated torque. The method based on the proposed algorithm directly uses input signals without any filtering or inertia. Therefore the surface is less smooth than demand and measurement signals.

Top-right diagram provides the level of instantaneously available torque as outcome from the proposed algorithm.

6.3 Transient test

The final validation is done based on a WLTP with all 4 phases that is executed on the engine testbed. Measurement is executed on engine 2 with the use of the setup according figure 6.2.

This test was selected as it combines critical circumstances that occur also on real life with respect to transient performance, covers a wide engine speed ranges and requests to high torque levels.
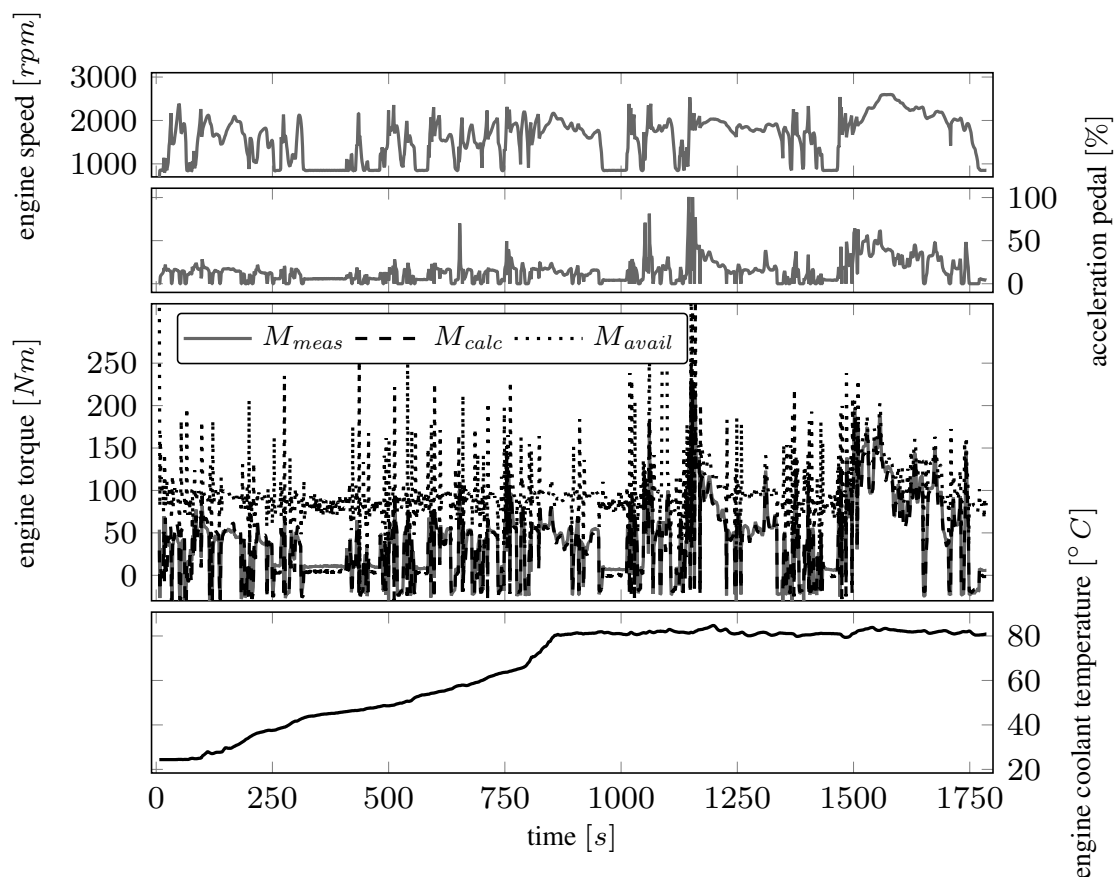
Figure 6.9: WLTP cycle from testbed and calculation with engine warmup.

Figure 6.9 shows that influence of engine temperature is covered. Measurement starts with the engine at ambient temperature, covering the engine warm-up and the operation hot engine.

An other view on the test is given in figure 6.10 with analysis on the measured and calculated torque. To identify engine operation the upper two diagrams again show engine speed and accelerator pedal.
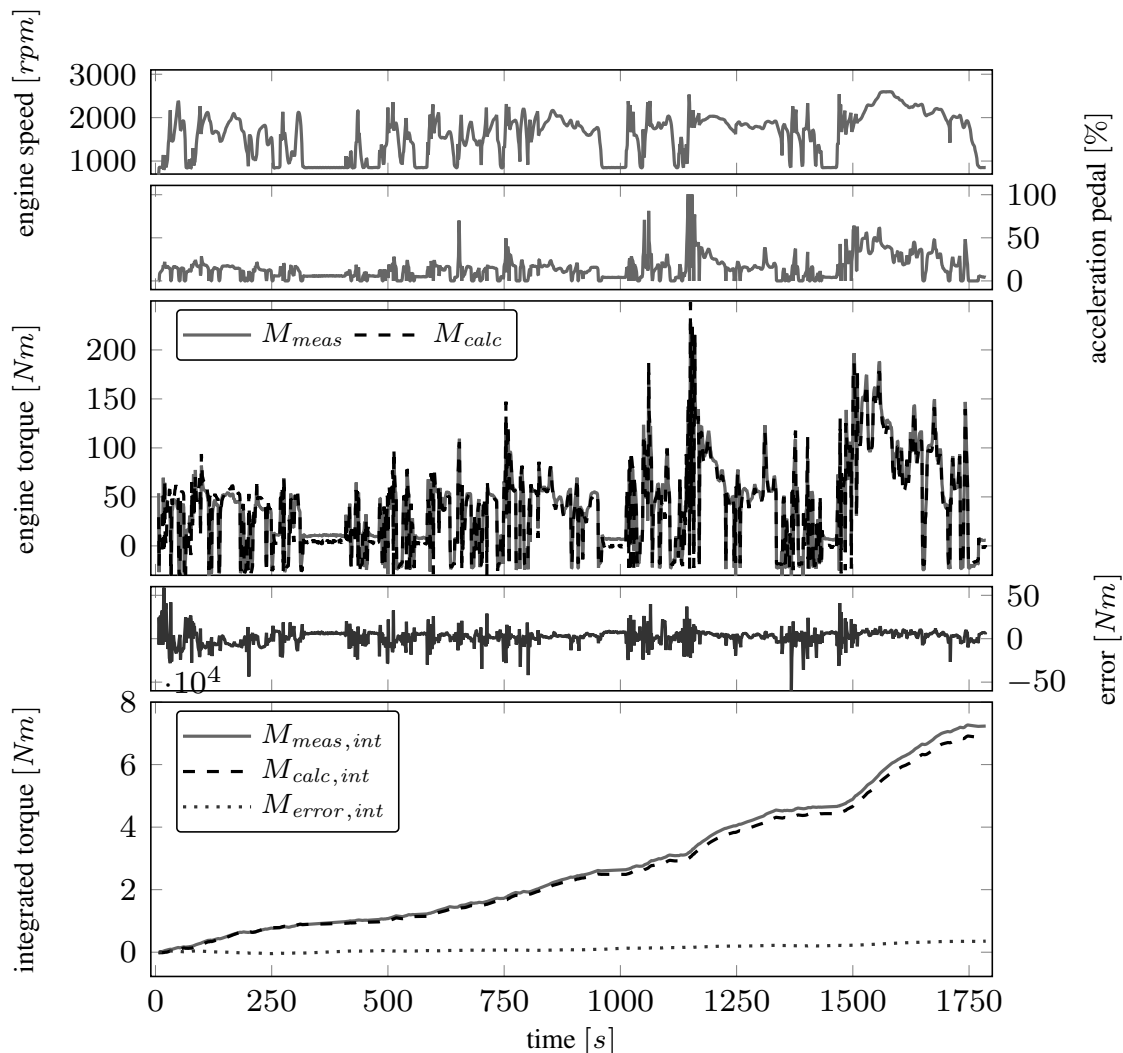
Figure 6.10: WLTP cycle torque from testbed and calculation and torque deviation.

Third diagram shows the comparison of measurement and calculated torque. The graph below illustrates the absolute deviation between these two signals. In the majority of the time the error is within ± 10 Nm, several time ranges show error or up to 30 Nm. This deviation is exceeded only 3 times. Lowest diagram presents integrated torque values over the test cycle. The integrated error (dotted) becomes positive in small steps what leads to increasing difference between the integrated measured (solid) and the calculated (dashed) torque. Final deviation of the integrated error in cold WLTP is 5.4 %.

Figure 6.11 shows intermediate results from the calculation algorithm. The top diagram provides the combustion center. As result of the measurement principle, the $\varphi_{MFB50,meas}$ drops to $-30°$ when the injection quantity becomes zero what is the case in motoring mode. The calculation algorithm remains in calculating the signal similar to fired operation.
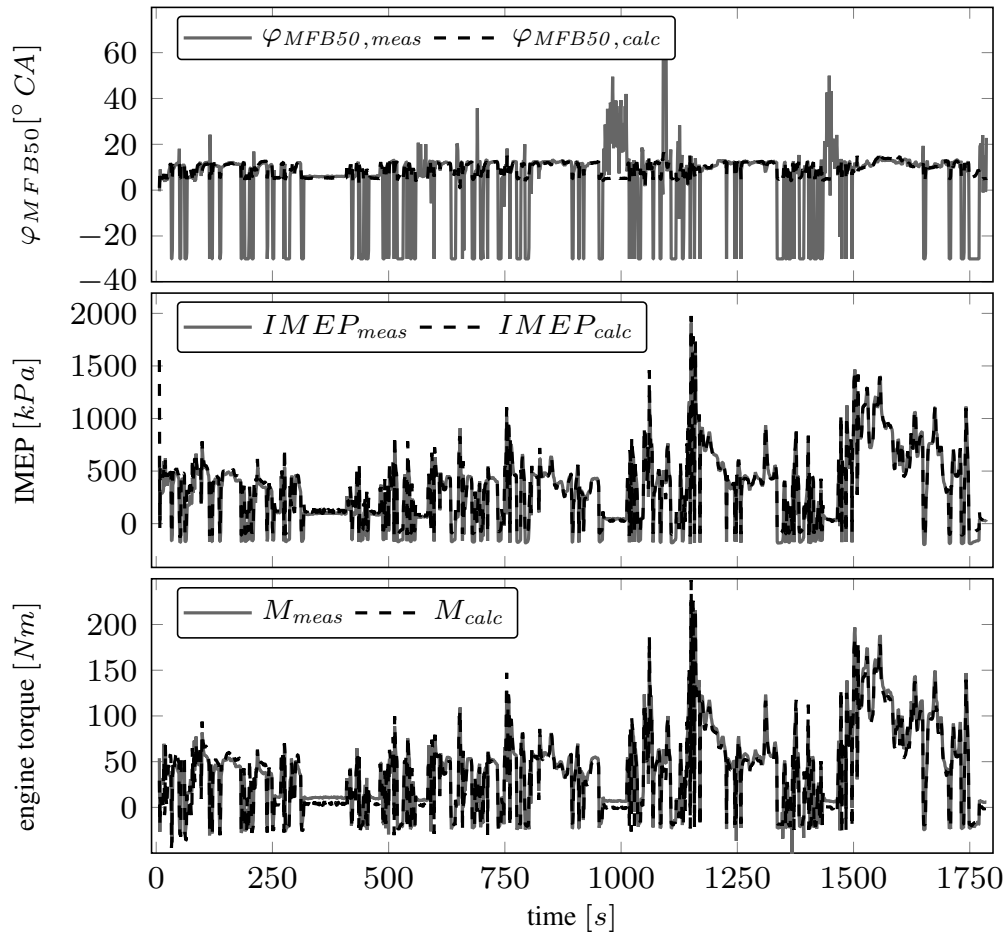
Figure 6.11: MFB50, IMEP and engine torque from testbed and calculation in a WLTP.

Although both behavior is physically correct, the calculated signal is more smooth and better for control tasks. While combustion is active the signals correlate.

The middle diagram illustrates the IMEP from measurement and calculation. More detailed analysis will give insight about the calculation error.

The correlation of the comparison on engine torque in the lowest diagram is very similar. Most difference occurs during idle phases. This results from inaccuracy of friction torque calibration.

Figure 6.12 shows more detailed analysis between 100 s and 250 s. This is a section with still cold engine temperature. The time frame is characterized by very transient operation conditions with lots of motoring phases followed by torque requests.
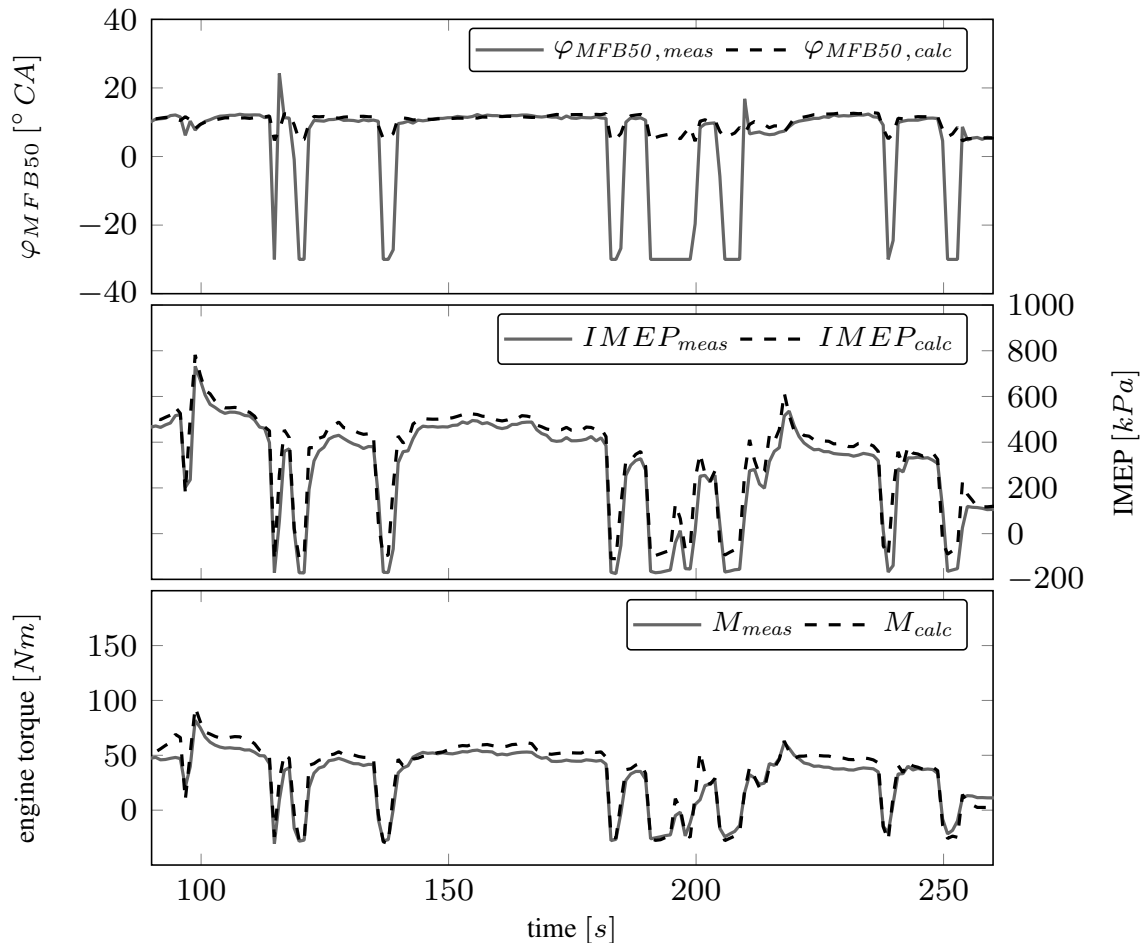
Figure 6.12: Detail of MFB50, IMEP and engine torque from testbed and calculation at 100 to 250s in WLTP.

The top diagram illustrates the MFB50 from measurement and calculation. Drop to the lowest value during the motoring phase can be clearly identified. The relation to IMEP in the middle diagram confirms the to the statement that this occurs when the engine is not fired. These phases are characterized by a drop of IMEP to zero.

Middle and lowest diagram show the comparison of measured and calculated values in engine warm-up. The influence is considered by the use of intake temperature sensor and coolant water temperature. As the calculation represents the measurement with few deviation, no further warm-up correction is implemented.

Hot engine conditions are analyzed in detail in the time from 1100 to 1300 s.

Figure 6.13 illustrates provisional results of the calculation algorithm and their comparison to measurement.
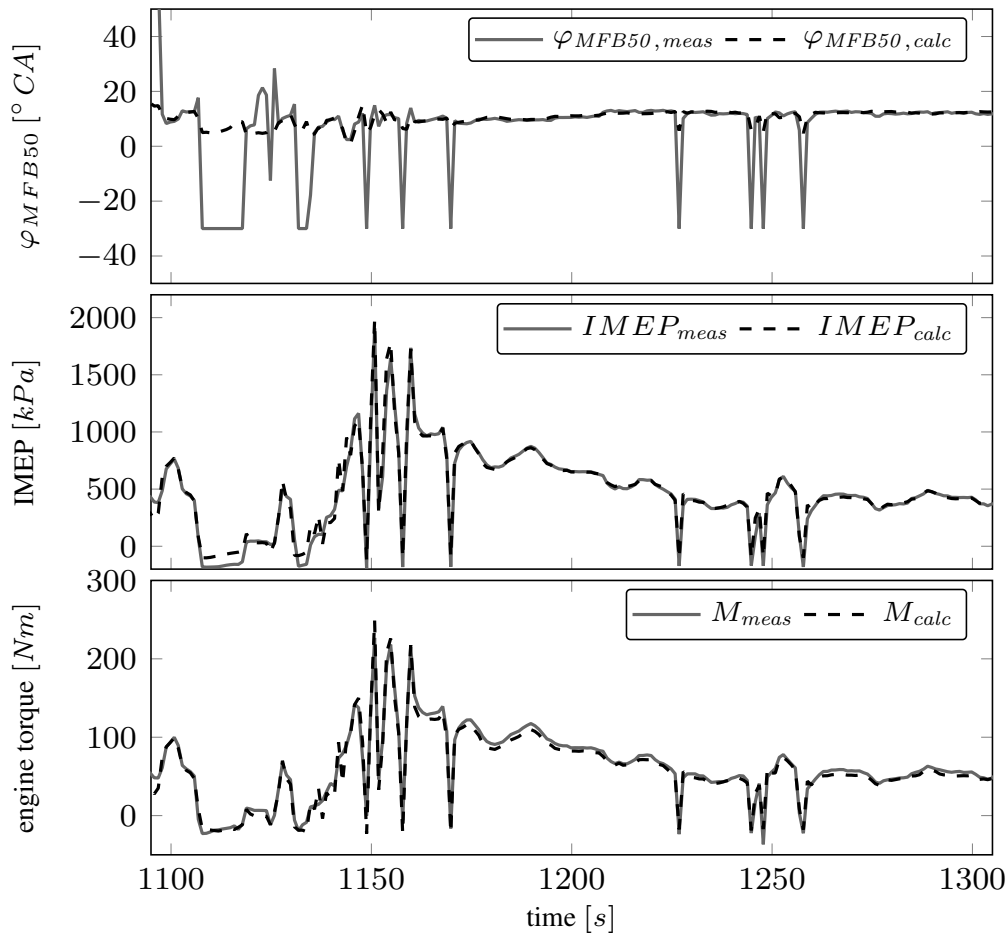
Figure 6.13: Detail of MFB50, IMEP and engine torque from testbed and calculation at 1100s in a WLTP.

The top diagram shows correlation of MFB50. Neglecting the deviation in motoring mode, the values in fired operation represent the measurement with small deviation.

Indicated mean effective pressure represents the inner work of the internal combustion engine. Although this signal is only available by special measurement equipment, the correlation to calculation from energy balance is used for validation. It validates the calculation to be representative.

Similar behavior is illustrated in the lowest diagram by the torque comparison. These signal additionally considers engine inertia, auxiliaries and friction. The correlation confirms that effects influencing the engine torque within transient operation are covered in the proposed calculation.

Finally figure 6.14 presents an analysis in the period from 1100 to 1200s. This section was selected as it contains highly transient operation. First and second diagram displays engine speed and accelerator pedal request.
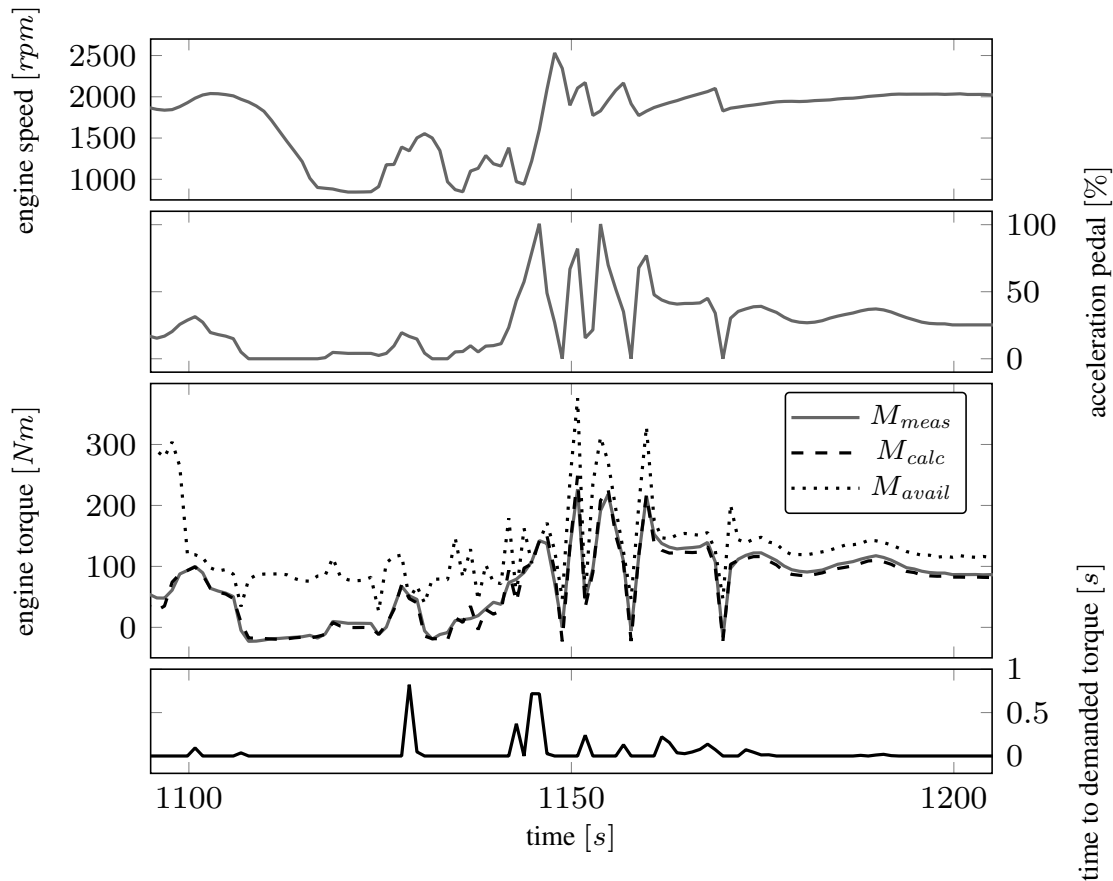
Figure 6.14: Detail of engine torque and time to demanded torque at 1100s in a WLTP.

The third diagram displays the measured, calculated and available torque. When available torque drops down to the actual torque, further torque requests can only be fulfilled with time delay. At 1128 s torque reserve becomes zero and time to torque demand of up to 1.1 s is estimated. As in parallel demand and actual torque is reduced, no effect on engine performance results. Accelerator pedal demand ramps up from 10% at 1140s up to 100% at 1145s. The engine is not able to provide the requested torque. At 60% accelerator pedal position the torque reserve becomes zero. Further raise of demand torque is faster than increase of torque. Therefore a time to demand torque of up to 0.85 s is predicted in lowest diagram. Furter times beyond 0.5 s only occur when no additional torque is requested and therefore no effect on engine torque is detected.

6.4 Conclusion

This section summarizes the results of the experimental validation on testbed. At first the process to enable execution of the proposed algorithm in the rapid prototype control unit is explained. Step by step explanation from Matlab-Simulink via INTECRIO to the executable software is shown. The setup at the engine testbed including measurement and calibration environment is presented and each device is described.

Measurement in stationary operation is performed. The whole engine map is evaluated by 350 measurement points. Measurement and calculation results of MFB50 and IMEP were compared.

At next the WLTP transient test including engine warm-up conditions was used for validation of the given algorithm. Analysis on torque calculation error is given in several figures. Detailed determination in cold and warm conditions at selected time segments for engine torque and intermediate signals were presented. Results in cold and warm condition were analyzed and validate the correlation between calculation and measurement.

7 Summary and conclusions

7.1 Summary

This work presents an algorithm to calculate the torque of a diesel engine. Chapter 2 starts with the description of basics as the working principle of the internal combustion engine and the characteristics of the four strokes. At next it shows the thermodynamic principles including system definition and the basic equations on energy conservation and the principle of irreversibility. The explanation contains equations as well as related figures to express the context between pressure, volume, temperature and entropy and their relation to work.

Explanation of the formulas for ideal gas and its properties as well as elementary system parameters of the reciprocating working process like compression ratio, mean effective pressure, power, torque, gas mixture are described. Fuel and combustion properties like heat value, energy, rate of heat release prepare for the description of the standard cycle process.

Chapter 3 presents the algorithm for the online torque calculation method. The description starts with the combustion modeling using a single vibe function. Based on the determination of combustion center the equivalent room ratio function that is used to separate equivalent room - and equivalent pressure combustion.

Then the used working cycle including restrictions and simplifications is defined and the steps in the working process and all related formulas are illustrated. Calculation of wall heat losses are identified as a significantly influencing element in the torque calculation. The work provides algorithms for the computation of volume and surface at MFB50 by geometric context of the crank - rod system kinematics. The heat transfer coefficient leads to estimation of wall heat losses either with the presented empirical approach or by a

thermal state estimation

Gas exchange calculation enables the summation of energy balance that leads to the inner work of the combustion cycle. Derived from this the inner torque and indicated mean effective pressure were computed. Based on this and considering the friction losses, auxiliary torque and inertia the current torque at engine crankshaft is computed.

While the working cycle is mainly static, chapter 4 takes care about engine dynamics. The given algorithm is applied to calculate the maximum available torque based on smoke limitation in parallel to the current torque. This enables the estimation of torque reserve. For a given air path system the dynamic behavior respectively the required time have a demand torque request implemented is expressed by the instantaneously available torque and a slope during smoke limitation. Analysis and validation using measurements determine a dependency of the slope of engine speed and EGR-rate.

A state space model representing the air path system to determine the operation-dependent slope online and finally the formula for the time to fulfill a demand torque closes this chapter.

The implementation in Matlab Simulink for validation on desktop computer by the use of measurement data is the main focus of chapter 5. First section illustrates the model structure followed by the parametrization procedure.

Initial step response measurements and simulations are used for general validation of the methods described in previous chapters. The work presents the independence of the gradient for determination of time to demanded torque from starting or ending torque level.

By the analysis of a set of measurements with variation of the main parameters engine speed and EGR rate, a detailed comparison between measurement and calculation results is performed. The results confirm the capability to cover these influences indirectly.

New European Driving Cycle (NEDC) is currently uses for certification of passenger cars. Definition and results are presented by a comparison of torque from engine testbed and calculated torque in the whole cycle. More detail with selected time sections shows a good representation of the calculated torque.

Future passenger car certification will follow the new procedure WLTP as this is more representative with respect to real driving. Therefore this cycle is used in this work for

validation of the proposed algorithm. Measurement data is imported to the simulation environment and the calculated results are presented for the whole cycle as well as time sections with detailed results.

The process to transform the algorithm from simulation into the rapid prototype control unit is illustrated in chapter 6. The compiled code is used for online calculation at the engine testbed.

Detailed analysis at 350 stationary operation points with comparison of combustion center, IMEP and engine torque is given in the whole engine operation map from motoring mode to full load.

The finally presented online validation test is done based on a WLTP including warm-up conditions from ambient temperature up to standard engine temperature. Again analysis of combustion center, IMEP and engine torque in different conditions is given in whole cycle and selected time sections for detailed view.

7.2 Conclusions and contributions

The work presents an algorithm to calculate the engine torque, torque reserve and the time to demanded torque based on semi-physical approaches. Input values are commonly available in standard ECUs what enables a wide range of applications. The proposed algorithm is characterized by very low calibration effort due to intense use of physical and phenomenological models. Implementation in Matlab Simulink enable execution with real time factors around 0.01-0.02 on standard desktop computer.

To address optimization of gear shift behavior in modelbased transmission control the three main input signals are provided. By selecting demand values instead of sensor values, a prediction on future behavior can be done. Future vehicles will have algorithms estimating the near future and optimizing the vehicle setpoints with respect to fuel consumption and pollutant emission. The presented algorithm can be used for high quality prediction with low calibration and calculation effort while providing information on combustion process.

7.3 Present limitations and constraints

Model calibration requires information from cylinder pressure measurement system. Although this data usually is available during engine development phase and required data is available within the engine development process. If this data is not available extra measurement requires huge efforts for engine instrumentation, installation on engine testbed and operation.

High relative deviation of injection massflow determination at small quantities is known. As this signal has direct impact on the accuracy of the proposed algorithm, uncertainty on the calculated signals at very low injection quantities need to be considered.

The calculation algorithm uses pressure sensor in exhaust manifold. Although it becomes common in production vehicles there are still applications that doesn't use this sensor in production. In these cases additional efforts are required to provide this signal based on exhaust pressure model. The influence is limited to gas exchange calculation with low impact on the final result. Effect on air path dynamics calculation and related to this on the time to demand torque would need further investigation.

7.4 Outlook

The algorithm, especially the air path model for estimation of time to demand torque is going to be introduced into the demonstrator vehicle "Future Hybrid" for further improvements of transmission control. The proposed calculation is going to be used for optimization of combustion engine behavior within the EU project IMPERIUM for future power-train control optimization with major European OEMs in road transportation. Further application by the combination with engine out emission model for prediction of pollutant and greenhouse gas emission is intended.

Bibliography

[1] I. Andersson and T. McKelvey. A system inversion approach on a crankshaft of an internal combustion engine. In *Decision and Control, 2004. CDC. 43rd IEEE Conference on*, pages 5449 – 5454 Vol.5, 2004.

[2] AVL List GmbH. *Theory of Boost*. Graz, Austria, 11 edition, 2010.

[3] M. Bachinger. *Generic real-time model and embedded observer for automotive step-ratio transmission topologies*. Dissertation, TU Graz, 2016.

[4] H. Baehr and St. Kabelac. *Thermodynamik*. Springer, 13 edition, 2006.

[5] A. Danninger, M. Bachinger, M. Stolz, and M. Horn. Online Calculation of Diesel Engine Torque Dynamics. In *2014 IEEE International Conference on Control Applications (CCA)*, pages 669 –674, Antibes, France, 2014.

[6] A. Danninger, E. Schutting, and H. Hülser. Phänomenologische Berechnung des Drehmoments für den künftigen Einsatz in der Diesel-Motorsteuerung. In Alfred Leipertz, editor, *Berichte zur Energie- und Verfahrenstechnik*, pages 53–64, Ludwigsburg, 2013. ESYTEC Energie und Systemtechnik GmbH, Erlangen 2013.

[7] E/ECE/324/Rev.2/Add.100/Rev.3. Concerning the Adoption of Uniform Technical Prescriptions for Wheeled Vehicles, Equipment and Parts which can be fitted and/or be used on Wheeled Vehicles and the Conditions for Reciprocal Recognition of Approvals Granted on the Basis of these Prescriptions. Addendum 100: Regulation No. 101, Uniform provisions concerning the approval of passenger cars powered by an internal combustion engine only, or powered by a hybrid electric power train with regard to the measurement of the emission of carbon dioxide and fuel consumption

and7or the measurement of electric energy consumption and electric range, and of categories M1 and N1 vehicles powered by an electric power train only with regard to the measurement of electric energy consumption and electric range.

[8] Hohenberg. G. Experimentelle Erfassung der Wandwärme von Kolbenmotoren, 1983.

[9] L. Guzzella and Chr. Onder. *Introduction to Modeling and Control of Internal Combustion Engine Systems.* Springer Berlin Heidelberg, Berlin, Heidelberg, 2nd edition, 2010.

[10] H. Tschöke H. Hölz. *Dubbel - Taschenbuch für den Maschinenbau.* Springer, 22. edition, 2007.

[11] S. Hage. Modeling and validation of thermal state variables of a diesel engine, 2015.

[12] S.; Jin Z.; Jiang D. Huang, K.; Wang. Feedforward Method of Engine Torque Estimiation. In *Vehicular Electronics and Safety, 2006. ICVES 2006. IEEE International Conference on*, pages 246 – 249, Beijing, 2006.

[13] K. Huber. *Der Wärmeübergang schnellaufender, direkteinspritzender Dieselmotoren.* PhD thesis, Technische Universität München, 1990.

[14] H. Hülser, R. Fischer, A. Danninger, and M. Stolz. Verfahren zur Steuerung einer Antriebsmaschine für ein Fahrzeug, 2004.

[15] H.-M. Kögeler. *Zylindergleichstellung und Fehlerdiagnose an Verbrennungskraftmaschinen mit Hilfe der Energiepegelmethode.* Dissertation, TU Graz, 1996.

[16] O. Kuzmych, A. Hajjaji, A. Aitouche, and J. Bosche. Optimization of Control Lyapunov Function Using Sum-Of-Squares Technic . Application to Turbocharged Diesel Engine Model *. In *IEEE International Conference on Control Applications (CCA)*, pages 647–652, Antibes, France, 2014.

[17] P. C. Ma, T. Ewan, L. L. Jainski, A. Dreizler, V. Sick, and M. Ihme. Development and analysis of wall models for internal combustion engine simulations using high-speed micro-piv measurements. *Flow Turbulence and Combustion*, 2016.

[18] G. Merker and Chr. Schwarz. *Grundlagen Verbrennungsmotoren*. Springer Verlag, 4. edition, 2004.

[19] K. Mollenhauer and H. Tschöke. *Handbuch Dieselmotoren*. Springer, 3rd edition, 2007.

[20] R. Pischinger, M. Klell, and Th. Sams. *Thermodynamik der Verbrennungskraftmaschine*. Springer Wien New York, 3 edition, 2009.

[21] E. Schalk, St. Daum, P. Kislinger, H. Ofner, A. Danninger, Chr. Doppler, and E. Schutting. Limits for NOx Reduction by EGR in a Heavy Duty Diesel Engine at stationary and transient Conditions. In *ASME Internal Combustion Engine Division's 2012 Fall Technical Conference*, pages 1–7, Vancouver, Canada, 2012. ASME.

[22] G. Schopp, Th. Burkhardt, J. Dingl, R. Schwarz, and Chr. Eisath. Funktionsentwicklung und Kalibration für aufgeladene Motoren – Modellbasiert vom Konzept bis zur Serie. In Rolf Isermann, editor, *Elektronisches Management motorischer Fahrzeugantriebe*, pages 214–232. Vieweg+Teubner, 2010.

[23] E. Schutting, A. Neureiter, Chr. Fuchs, T. Schatzberger, and H.and Kammerdiener T. Klell, M.and Eichlseder. Miller- und Atkinson-Zyklus am aufgeladenen Dieselmotor. 06:480–485, 2007.

[24] G. Stiesch, Chr. Eiglmeier, G.P. Merker, and F. Wirbeleit. Möglichkeiten und Anwendung der phänomenologischen Modellbildung im Dieselmotor. *MTZ*, 60, 4 1999.

[25] A. Traussnig, M. Stolz, and M. Horn. MPC based Fan Control for Automotive Applications. volume 49/11, Norrköping, Sweden, 6 2016. Elsevier.

[26] H Tschoeke. 75 Jahre Großmotorenentwicklung im Spiegel der MTZ. *MTZ*, 76, 10 2015.

[27] Tutuianu, M. and Marotta, A. and Steven, H.and Ericsson, E. and Haniu,T. and Ichikawa, N. and Ishii, H. Development of a World-wide Worldwide harmonized Light duty driving Test Cycle (WLTC), UN/ECE/WP.29/GRPE/WLTP-IG.

[28] UNECE Transport Division. UN Vehicle Regulations - 1958 Agreement, Regulation No. 101 - Rev.3 - CO2 emission/fuel consumption.

[29] UNECE Transport Division. World Light duy Test Procedure development group (WLTP-DTP).

[30] I. Vibe. Brennverlauf und Kreisprozess von Verbrennungsmotoren. In *VEB Verlag Technik, Berlin, Germany*, 1970.

[31] G. Woschni. Beitrag zum Problem des Wärmeüberganges im Verbrennungsmotor. 26, 1965.

[32] Woschni, G. and Anisits, F. Eine Methode zur Vorausberechnung der Änderung des Brennverlaufs mittelschnellaufender Dieselmotoren bei geänderten Randbedingungen. *MTZ*, 34:106–115, 1973.

[33] J.C. Wurzenberger and T. Katrasnik. Development of future powertrains by simulation tools. In *TRA Transport Research Area Europe 2010*, Brussels, Belgium, 6 2010.

[34] Y.B. Zeldovich. The oxidation of nitrogen in combustion explosions. *Acta Physicochimica U.S.S.R.*, 21:577–628, 1946.

List of Figures

List of Tables

Appendix

Appendix A

Symbols

Symbol	Unit	Description
A	m^2	surface
c	J/kgK	specific heat capacity
c_p	kJ/kgK	specific heat constant at constant pressure
c_v	kJ/kgK	specific heat constant at constant volume
E_o	J	outer energy
e_o	J/kg	specific outer energy
f_{st}	$-$	stoichiometric air fuel coefficient
H_u	J/kg	lower heat value
h	J/kg	specific enthalpy
l	m	length
m	kg	mass
M	Nm	torque
N	rpm	engine speed
p	Pa	pressure
p_f	bar	friction mean effective pressure
p_i	bar	indicated mean effective pressure
P	W	power
q	J/kg	specific heat
Q	J	heat
R	J/kgK	specific gas constant
R	K/W	thermal resistance
R_m	$J/kmolK$	general gas constant

r	m	radius
S	J/K	entropy
T	$°C$	temperature
U	J	inner work
v	m^3/kg	specific volume
V	m^3	volume
V_c	m^3	compression volume
V_d	m^3	displacement volume
v	m/s	velocity
v_c	m/s	mean piston velocity
W	J	work
W_e	J	effective work
W_t	J	transported work
α_{gw}	W/m^2K	gas - wall heat transfer coefficient
β	$-$	shape factor of Vibe approximation
$\dot{m}_{air}$	mg/inj	air mass flow
$\dot{m}_{fuel}$	mg/inj	fuel mass
ϵ	$-$	compression ratio
η	$-$	efficiency
η_c	$-$	efficiency of Carnot process
η_{th}	$-$	thermodynamic efficiency
η_{ERR}	$-$	equivalent room ratio function
κ	$-$	isentropic exponent
λ	$-$	air fuel equivalence ratio
ω	sec^{-1}	rotational speed
ψ	$°$	conrod angle
φ	$°CA$	position in crank angle domain

Appendix B

Acronyms

AFR	air fuel ratio
BDC	bottom dead center
BMEP	brake mean effective pressure
CN	cetane number
ECU	engine control unit
EGR	exhaust gas recirculation
EOC	end of combustion
FMEP	friction mean effective pressure
HCU	hybrid control unit
ICE	internal combustion engine
IMEP	indicated mean effective pressure
MFB	mass fraction burned
MFB50	mass fraction burned 50%
MiL	Model-in-the-Loop
NEDC	New European Driving Cycle
ODE	ordinary differential equation
ROHR	rate of heat release
SOC	state of combustion
SOI	start of injection
TCE	Torque Combustion Engine
TCU	transmission control unit

TDC	top dead center
VGT	variable geometry turbine
WLTP	Worldwide harmonized Light-duty vehicle Test Procedure

Appendix C

Interfaces and labels

Label	Unit	Description
Eng_nrpm	rpm	engine speed
AFSCD_mfAir	mg/inj	actual air mass flow
AirCtl_mDesVal	mg/inj	demand air mass flow
INT_pb	bar	actual pressure in intake manifold
INT_pbDem	bar	demand pressure in intake manifold
INT_tc	°C	actual temperature in intake manifold
EXH_pb	bar	pressure in exhaust manifold
InjCrv_PhiMI1Des	°CA	position of main injection
InjCrv_phiPiI1Des	°CA	position of 1st pilot injection
InjCtl_qCurr	mg/inj	current injection mass flow
Inj_qPiI1Des	mg/inj	injection mass flow of 1st pilot injection
SMK_qLimSmk	mg/inj	maximum injection quantity for smoke limitation
APP_r	%	acceleration pedal position
ENG_tcCoolant	°C	temperature of coolant water

Table C.1: Input signals from ECU

Label	Value	Unit	Description
TRQC_Hu	43	J/mg	lower heat value
TRQC_LbdSt	14.5	-	Stoichiometric air fuel equivalence ratio
TRQC_Rs	8315.3	J/(mol K)	generic ideal gas constant

Table C.2: General Calibration Parameter

Label	Unit	Description
Lpiston	m	length of piston
D3	m	diameter to outer liner wall
D4w	m	diameter to outer cylinder block wall
D4o	m	diameter to outer coolant jacket wall
D4	m	diameter to inner coolant jacket wall
L2w	m	width piston shaft wall
L3f	m	width fire deck with valves
L4h	m	hight of coolant jacket
Loil	m	hight oil film between piston and liner
L3h	m	liner length
c_cb_i	J/(kg K)	spezific capacity coolant incoming
c_cb	J/(kg K)	spezific capacity coolant
c2	J/(kg K)	spezific capacity aluminum
c4	J/(kg K)	spezific capacity steel
koil	W/(m K)	heat conductivity oil
k_block	W/(m K)	heat conductivity cast iron
k_alu	W/(m K)	heat conductivity aluminium
rho_alu	kg/m^3	density aluminium
rho_block	kg/m^3	density cast iron
rho_water	kg/m^3	density water
mcb_dot	kg/s	coolant mass flow

Table C.3: Wall heat model specific parameter

Label	Unit	Description
TRQC_bore	m	Bore
TRQC_stroke	m	Stroke
TRQC_NrCyl	-	number of cylinders
TRQC_lConrod	m	length of conrod
TRQC_lCrankCase	m	length of crankcase
TRQC_rCompr	-	compression ratio epsilon
TRQC_Inertio	-	inertio of the engine

Table C.4: Engine specific parameter

Label	Unit	Description
TCE_tiFltWallTemp_P	s	filter time for cylinder wall temperature representing thermal interia
TCE_trqFMEP_MAP	Nm	engine friction torque
TCE_kTqGrad_MAP	Nm / s	torque gradient in soot limitation
TCE_tcWall_MAP	°C	calibration map for wall heat temperature
TCE_mVibe_MAP	-	reference map of Vibe shape parameter
TCE_IgnDelay_MAP	°CA	reference map for ignition delay
TCE_SOC_MAP	°CA	reference map for start of combustion
TCE_EOC_MAP	°CA	reference map for end of combustion
TCE_HTCoeffBas_MAP	-	reference map for heat transfer coefficient of simple wall heat transfer model
TCE_rEqR_MAP	-	reference map of equivalent room ratio function

Table C.5: Calibration parameter and reference values

Appendix D

Gas property tables

T	c_v	R	c_P	κ	c_v	R	c_p	κ	c_v	R	c_p	κ
	p	=	1 bar		p	=	10	bar	p	=	100	bar
298.15	0.774	287.6	1.062	1.372	0.774	287.6	1.062	1.372	0.774	287.6	1.062	1.372
300	0.7743	287.6	1.062	1.372	0.7743	287.6	1.062	1.372	0.7743	287.6	1.062	1.372
400	0.7982	287.6	1.086	1.361	0.7982	287.6	1.086	1.361	0.7982	287.6	1.086	1.361
500	0.8267	287.6	1.114	1.348	0.8267	287.6	1.114	1.348	0.8267	287.6	1.114	1.348
600	0.8575	287.6	1.145	1.335	0.8575	287.6	1.145	1.335	0.8575	287.6	1.145	1.335
700	0.889	287.6	1.177	1.324	0.889	287.6	1.177	1.324	0.889	287.6	1.177	1.324
800	0.9197	287.6	1.207	1.312	0.9197	287.6	1.207	1.312	0.9197	287.6	1.207	1.312
900	0.949	287.6	1.237	1.303	0.949	287.6	1.237	1.303	0.949	287.6	1.237	1.303
1000	0.976	287.6	1.264	1.295	0.976	287.6	1.264	1.295	0.976	287.6	1.264	1.295
1100	1.0007	287.6	1.288	1.287	1.0007	287.6	1.288	1.287	1.0007	287.6	1.288	1.287
1200	1.0228	287.6	1.31	1.281	1.0228	287.6	1.31	1.281	1.0228	287.6	1.31	1.281
1300	1.0425	287.6	1.33	1.276	1.0425	287.6	1.33	1.276	1.0425	287.6	1.33	1.276
1400	1.06	287.6	1.348	1.272	1.06	287.6	1.348	1.272	1.06	287.6	1.348	1.272
1500	1.0754	287.7	1.363	1.267	1.0755	287.6	1.363	1.267	1.0755	287.6	1.363	1.267
1600	1.089	287.7	1.377	1.264	1.0891	287.7	1.377	1.264	1.0891	287.6	1.377	1.264
1700	1.1012	287.7	1.389	1.261	1.1012	287.7	1.389	1.261	1.1013	287.7	1.389	1.261
1800	1.1118	287.9	1.4	1.259	1.1121	287.7	1.4	1.259	1.1122	287.7	1.4	1.259
1900	1.1213	288.1	1.409	1.257	1.1218	287.8	1.41	1.257	1.122	287.7	1.41	1.257
2000	1.1297	288.4	1.418	1.255	1.1304	288	1.418	1.254	1.1307	287.8	1.419	1.255
2100	1.1368	288.9	1.426	1.254	1.1381	288.2	1.426	1.253	1.1387	287.9	1.427	1.253
2200	1.1428	289.7	1.433	1.254	1.1448	288.6	1.433	1.252	1.1457	288.1	1.434	1.252
2300	1.1475	290.8	1.438	1.253	1.1505	289.1	1.44	1.252	1.1519	288.4	1.44	1.25
2400	1.151	292.3	1.443	1.254	1.1552	289.9	1.445	1.251	1.1575	288.7	1.446	1.249
2500	1.1532	294.3	1.448	1.256	1.1591	290.8	1.45	1.251	1.1621	289.2	1.451	1.249
2600	1.1541	296.9	1.451	1.257	1.1619	292.1	1.454	1.251	1.1661	289.8	1.456	1.249
2700	1.154	300	1.454	1.26	1.1637	293.7	1.457	1.252	1.1692	290.6	1.46	1.249
2800	1.1529	303.8	1.457	1.264	1.1648	295.6	1.46	1.253	1.1718	291.5	1.463	1.249
2900	1.1511	308.4	1.46	1.268	1.1651	297.8	1.463	1.256	1.1736	292.7	1.466	1.249
3000	1.1486	313.6	1.462	1.273	1.1647	300.4	1.465	1.258	1.1749	294	1.469	1.25
3100	1.1457	319.6	1.465	1.279	1.1638	303.4	1.467	1.261	1.1756	295.6	1.471	1.251
3200	1.1424	326.4	1.469	1.286	1.1625	306.8	1.469	1.264	1.1759	297.4	1.473	1.253
3300	1.1389	333.8	1.473	1.293	1.1608	310.6	1.471	1.267	1.1759	299.4	1.475	1.254
3400	1.1351	341.7	1.477	1.301	1.159	314.7	1.474	1.272	1.1755	301.5	1.477	1.256
3500	1.1314	349.8	1.481	1.309	1.1569	319.2	1.476	1.276	1.1748	303.9	1.479	1.259
3600	1.1278	357.6	1.485	1.317	1.1545	324.1	1.479	1.281	1.1738	306.4	1.48	1.261
3700	1.1244	365	1.489	1.324	1.1517	329.4	1.481	1.286	1.1724	309.2	1.482	1.264
3800	1.1216	371.5	1.493	1.331	1.1489	334.9	1.484	1.292	1.171	312.1	1.483	1.266
3900	1.1194	377.1	1.497	1.337	1.1462	340.5	1.487	1.297	1.1695	315.2	1.485	1.27
4000	1.1182	381.8	1.5	1.341	1.1439	346.3	1.49	1.303	1.1685	318.4	1.487	1.273

Table D.1: Gas properties for air fuel ratio $\lambda = 1.0$

		p	= 1 bar			p	= 10 bar			p	= 100 bar	
T	c_v	R	c_P	κ	c_v	R	c_p	κ	c_v	R	c_p	κ
298.15	0.7651	287.5	1.053	1.376	0.7651	287.5	1.053	1.376	0.7651	287.5	1.053	1.376
300	0.7654	287.5	1.053	1.376	0.7654	287.5	1.053	1.376	0.7654	287.5	1.053	1.376
400	0.7868	287.5	1.074	1.365	0.7868	287.5	1.074	1.365	0.7868	287.5	1.074	1.365
500	0.8134	287.5	1.101	1.354	0.8134	287.5	1.101	1.354	0.8134	287.5	1.101	1.354
600	0.8428	287.5	1.13	1.341	0.8428	287.5	1.13	1.341	0.8428	287.5	1.13	1.341
700	0.873	287.5	1.161	1.33	0.873	287.5	1.161	1.33	0.873	287.5	1.161	1.33
800	0.9027	287.5	1.19	1.318	0.9027	287.5	1.19	1.318	0.9027	287.5	1.19	1.318
900	0.9308	287.5	1.218	1.309	0.9308	287.5	1.218	1.309	0.9308	287.5	1.218	1.309
1000	0.9567	287.5	1.244	1.3	0.9567	287.5	1.244	1.3	0.9567	287.5	1.244	1.3
1100	0.9804	287.5	1.268	1.293	0.9804	287.5	1.268	1.293	0.9804	287.5	1.268	1.293
1200	1.0015	287.5	1.289	1.287	1.0015	287.5	1.289	1.287	1.0015	287.5	1.289	1.287
1300	1.0203	287.5	1.308	1.282	1.0203	287.5	1.308	1.282	1.0203	287.5	1.308	1.282
1400	1.0368	287.5	1.324	1.277	1.0369	287.5	1.324	1.277	1.0369	287.5	1.324	1.277
1500	1.0517	287.5	1.339	1.273	1.0517	287.5	1.339	1.273	1.0517	287.5	1.339	1.273
1600	1.0646	287.6	1.352	1.27	1.0647	287.5	1.352	1.27	1.0647	287.5	1.352	1.27
1700	1.0762	287.6	1.364	1.267	1.0762	287.6	1.364	1.267	1.0763	287.5	1.364	1.267
1800	1.0866	287.6	1.374	1.264	1.0866	287.6	1.374	1.264	1.0867	287.5	1.374	1.264
1900	1.0959	287.7	1.384	1.263	1.096	287.6	1.384	1.263	1.096	287.6	1.384	1.263
2000	1.1042	287.8	1.392	1.261	1.1044	287.6	1.392	1.26	1.1045	287.6	1.392	1.26
2100	1.1116	288	1.4	1.259	1.1121	287.7	1.4	1.259	1.1123	287.6	1.4	1.259
2200	1.1179	288.5	1.406	1.258	1.1189	287.9	1.407	1.257	1.1192	287.7	1.407	1.257
2300	1.1232	289.2	1.412	1.257	1.1249	288.2	1.413	1.256	1.1256	287.8	1.413	1.255
2400	1.1272	290.4	1.418	1.258	1.1301	288.6	1.419	1.256	1.1313	287.9	1.419	1.254
2500	1.1298	292	1.422	1.259	1.1344	289.2	1.424	1.255	1.1362	288.2	1.424	1.253
2600	1.1312	294.2	1.425	1.26	1.1377	290.1	1.428	1.255	1.1405	288.5	1.429	1.253
2700	1.1314	297	1.428	1.262	1.14	291.4	1.431	1.255	1.1441	289	1.433	1.253
2800	1.1306	300.5	1.431	1.266	1.1414	293	1.434	1.256	1.147	289.7	1.437	1.253
2900	1.129	304.7	1.434	1.27	1.142	295	1.437	1.258	1.1492	290.6	1.44	1.253
3000	1.1267	309.6	1.436	1.275	1.1418	297.4	1.439	1.26	1.1509	291.7	1.443	1.254
3100	1.124	315.3	1.439	1.28	1.1412	300.1	1.441	1.263	1.152	293	1.445	1.254
3200	1.1208	321.7	1.443	1.287	1.14	303.3	1.443	1.266	1.1526	294.5	1.447	1.255
3300	1.1176	328.6	1.446	1.294	1.1385	306.8	1.445	1.269	1.1527	296.3	1.449	1.257
3400	1.1141	336	1.45	1.301	1.1367	310.7	1.447	1.273	1.1525	298.3	1.451	1.259
3500	1.1106	343.6	1.454	1.309	1.1348	314.9	1.45	1.278	1.1519	300.5	1.452	1.261
3600	1.1072	351	1.458	1.317	1.1325	319.5	1.452	1.282	1.151	302.9	1.454	1.263
3700	1.1042	357.8	1.462	1.324	1.1301	324.4	1.455	1.287	1.1498	305.4	1.455	1.265
3800	1.1015	364	1.466	1.331	1.1274	329.6	1.457	1.292	1.1483	308.2	1.457	1.269
3900	1.0994	369.3	1.469	1.336	1.1248	334.9	1.46	1.298	1.1471	311	1.458	1.271
4000	1.0984	373.8	1.472	1.34	1.1228	340.3	1.463	1.303	1.1461	314.1	1.46	1.274

Table D.2: Gas properties for air fuel ratio $\lambda = 1.2$

T	p = 1 bar				p = 10 bar				p = 100 bar			
	c_v	R	c_P	κ	c_v	R	c_p	κ	c_v	R	c_p	κ
298.15	0.7586	287.5	1.046	1.379	0.7586	287.5	1.046	1.379	0.7586	287.5	1.046	1.379
300	0.7589	287.5	1.046	1.378	0.7589	287.5	1.046	1.378	0.7589	287.5	1.046	1.378
400	0.7784	287.5	1.066	1.369	0.7784	287.5	1.066	1.369	0.7784	287.5	1.066	1.369
500	0.8037	287.5	1.091	1.357	0.8037	287.5	1.091	1.357	0.8037	287.5	1.091	1.357
600	0.8321	287.5	1.12	1.346	0.8321	287.5	1.12	1.346	0.8321	287.5	1.12	1.346
700	0.8614	287.5	1.149	1.334	0.8614	287.5	1.149	1.334	0.8614	287.5	1.149	1.334
800	0.8902	287.5	1.178	1.323	0.8902	287.5	1.178	1.323	0.8902	287.5	1.178	1.323
900	0.9175	287.5	1.205	1.313	0.9175	287.5	1.205	1.313	0.9175	287.5	1.205	1.313
1000	0.9427	287.5	1.23	1.305	0.9427	287.5	1.23	1.305	0.9427	287.5	1.23	1.305
1100	0.9655	287.5	1.253	1.298	0.9655	287.5	1.253	1.298	0.9655	287.5	1.253	1.298
1200	0.9859	287.5	1.273	1.291	0.9859	287.5	1.273	1.291	0.9859	287.5	1.273	1.291
1300	1.0041	287.5	1.292	1.287	1.0041	287.5	1.292	1.287	1.0041	287.5	1.292	1.287
1400	1.0201	287.5	1.308	1.282	1.0201	287.5	1.308	1.282	1.0201	287.5	1.308	1.282
1500	1.0343	287.5	1.322	1.278	1.0343	287.5	1.322	1.278	1.0343	287.5	1.322	1.278
1600	1.0468	287.5	1.334	1.274	1.0468	287.5	1.334	1.274	1.0468	287.5	1.334	1.274
1700	1.058	287.5	1.346	1.272	1.058	287.5	1.346	1.272	1.058	287.5	1.346	1.272
1800	1.068	287.5	1.356	1.27	1.068	287.5	1.356	1.27	1.068	287.5	1.356	1.27
1900	1.077	287.6	1.365	1.267	1.0771	287.5	1.365	1.267	1.0771	287.5	1.365	1.267
2000	1.0851	287.7	1.373	1.265	1.0852	287.6	1.373	1.265	1.0853	287.5	1.373	1.265
2100	1.0923	287.9	1.38	1.263	1.0927	287.6	1.38	1.263	1.0928	287.5	1.38	1.263
2200	1.0986	288.3	1.387	1.263	1.0993	287.8	1.387	1.262	1.0996	287.6	1.387	1.261
2300	1.104	288.8	1.393	1.262	1.1053	288	1.393	1.26	1.1057	287.7	1.393	1.26
2400	1.1082	289.8	1.398	1.262	1.1105	288.3	1.399	1.26	1.1113	287.8	1.399	1.259
2500	1.1113	291.1	1.402	1.262	1.1149	288.8	1.404	1.259	1.1162	288	1.404	1.258
2600	1.1131	293	1.406	1.263	1.1184	289.6	1.408	1.259	1.1205	288.3	1.409	1.257
2700	1.1138	295.5	1.409	1.265	1.1211	290.6	1.412	1.259	1.1242	288.7	1.413	1.257
2800	1.1134	298.7	1.412	1.268	1.1228	292	1.415	1.26	1.1273	289.2	1.417	1.257
2900	1.1121	302.6	1.415	1.272	1.1238	293.7	1.418	1.262	1.1299	289.9	1.42	1.257
3000	1.1102	307.2	1.417	1.276	1.1241	295.8	1.42	1.263	1.1318	290.8	1.423	1.257
3100	1.1077	312.5	1.42	1.282	1.1238	298.3	1.422	1.265	1.1332	291.9	1.425	1.258
3200	1.1049	318.5	1.423	1.288	1.1229	301.2	1.424	1.268	1.1341	293.3	1.427	1.258
3300	1.102	325	1.427	1.295	1.1217	304.5	1.426	1.271	1.1346	294.8	1.429	1.259
3400	1.0987	332	1.431	1.302	1.1202	308.1	1.428	1.275	1.1347	296.6	1.431	1.261
3500	1.0954	339.2	1.435	1.31	1.1184	312.1	1.431	1.28	1.1343	298.6	1.433	1.263
3600	1.0923	346.1	1.438	1.316	1.1163	316.4	1.433	1.284	1.1336	300.8	1.434	1.265
3700	1.0894	352.7	1.442	1.324	1.1141	321	1.435	1.288	1.1326	303.2	1.436	1.268
3800	1.0869	358.5	1.445	1.329	1.1116	325.9	1.438	1.294	1.1314	305.7	1.437	1.27
3900	1.085	363.6	1.449	1.335	1.1092	330.9	1.44	1.298	1.1302	308.4	1.439	1.273
4000	1.084	367.9	1.452	1.339	1.1072	336	1.443	1.303	1.1294	311.3	1.441	1.276

Table D.3: Gas properties for air fuel ratio $\lambda = 1.4$

		p	$= 1$ bar			p	$= 10$ bar			p	$= 100$ bar	
T	c_v	R	c_P	κ	c_v	R	c_p	κ	c_v	R	c_p	κ
298.15	0.7538	287.4	1.041	1.381	0.7538	287.4	1.041	1.381	0.7538	287.4	1.041	1.381
300	0.754	287.4	1.041	1.381	0.754	287.4	1.041	1.381	0.754	287.4	1.041	1.381
400	0.7721	287.4	1.06	1.373	0.7721	287.4	1.06	1.373	0.7721	287.4	1.06	1.373
500	0.7964	287.4	1.084	1.361	0.7964	287.4	1.084	1.361	0.7964	287.4	1.084	1.361
600	0.824	287.4	1.111	1.348	0.824	287.4	1.111	1.348	0.824	287.4	1.111	1.348
700	0.8526	287.4	1.14	1.337	0.8526	287.4	1.14	1.337	0.8526	287.4	1.14	1.337
800	0.8808	287.4	1.168	1.326	0.8808	287.4	1.168	1.326	0.8808	287.4	1.168	1.326
900	0.9074	287.4	1.195	1.317	0.9074	287.4	1.195	1.317	0.9074	287.4	1.195	1.317
1000	0.932	287.4	1.219	1.308	0.932	287.4	1.219	1.308	0.932	287.4	1.219	1.308
1100	0.9543	287.4	1.242	1.301	0.9543	287.4	1.242	1.301	0.9543	287.4	1.242	1.301
1200	0.9742	287.4	1.262	1.295	0.9742	287.4	1.262	1.295	0.9742	287.4	1.262	1.295
1300	0.9918	287.4	1.279	1.29	0.9918	287.4	1.279	1.29	0.9918	287.4	1.279	1.29
1400	1.0074	287.4	1.295	1.285	1.0074	287.4	1.295	1.285	1.0074	287.4	1.295	1.285
1500	1.0211	287.4	1.309	1.282	1.0211	287.4	1.309	1.282	1.0211	287.4	1.309	1.282
1600	1.0333	287.4	1.321	1.278	1.0333	287.4	1.321	1.278	1.0333	287.4	1.321	1.278
1700	1.0441	287.5	1.332	1.276	1.0442	287.4	1.332	1.276	1.0442	287.4	1.332	1.276
1800	1.0538	287.5	1.341	1.273	1.0539	287.5	1.341	1.272	1.0539	287.4	1.341	1.272
1900	1.0626	287.5	1.35	1.27	1.0626	287.5	1.35	1.27	1.0627	287.4	1.35	1.27
2000	1.0705	287.6	1.358	1.269	1.0706	287.5	1.358	1.268	1.0707	287.5	1.358	1.268
2100	1.0776	287.8	1.365	1.267	1.0778	287.6	1.365	1.266	1.078	287.5	1.366	1.267
2200	1.0838	288.1	1.372	1.266	1.0844	287.7	1.372	1.265	1.0847	287.5	1.372	1.265
2300	1.0892	288.6	1.378	1.265	1.0902	287.9	1.378	1.264	1.0907	287.6	1.378	1.263
2400	1.0935	289.4	1.383	1.265	1.0954	288.2	1.384	1.263	1.0961	287.7	1.384	1.263
2500	1.0968	290.6	1.387	1.265	1.0998	288.6	1.388	1.262	1.101	287.9	1.389	1.262
2600	1.099	292.3	1.391	1.266	1.1034	289.3	1.393	1.262	1.1053	288.1	1.393	1.26
2700	1.1	294.6	1.395	1.268	1.1063	290.2	1.397	1.263	1.109	288.5	1.398	1.261
2800	1.1	297.5	1.398	1.271	1.1083	291.4	1.4	1.263	1.1122	288.9	1.401	1.26
2900	1.0991	301.1	1.4	1.274	1.1096	292.9	1.403	1.264	1.1149	289.5	1.404	1.259
3000	1.0974	305.5	1.403	1.278	1.1102	294.8	1.405	1.266	1.117	290.3	1.407	1.26
3100	1.0953	310.5	1.406	1.284	1.1102	297.1	1.407	1.267	1.1186	291.3	1.41	1.261
3200	1.0928	316.1	1.409	1.289	1.1096	299.8	1.409	1.27	1.1197	292.5	1.412	1.261
3300	1.0899	322.4	1.412	1.296	1.1086	302.9	1.412	1.274	1.1205	293.9	1.414	1.262
3400	1.087	329	1.416	1.303	1.1073	306.3	1.414	1.277	1.1208	295.5	1.416	1.263
3500	1.0839	335.9	1.42	1.31	1.1057	310.1	1.416	1.281	1.1206	297.4	1.418	1.265
3600	1.0809	342.5	1.423	1.316	1.1039	314.2	1.418	1.285	1.1201	299.4	1.42	1.268
3700	1.0781	348.8	1.427	1.324	1.1018	318.6	1.42	1.289	1.1194	301.6	1.421	1.269
3800	1.0758	354.4	1.43	1.329	1.0995	323.2	1.423	1.294	1.1183	304	1.422	1.272
3900	1.074	359.3	1.433	1.334	1.0973	328	1.425	1.299	1.1173	306.5	1.424	1.275
4000	1.073	363.5	1.437	1.339	1.0955	332.8	1.428	1.304	1.1166	309.2	1.426	1.277

Table D.4: Gas properties for air fuel ratio $\lambda = 1.6$

	p	= 1 bar			p	= 10 bar			p	= 100 bar		
T	c_v	R	c_P	κ	c_v	R	c_p	κ	c_v	R	c_p	κ
298.15	0.7468	287.4	1.034	1.385	0.7468	287.4	1.034	1.385	0.7468	287.4	1.034	1.385
300	0.7469	287.4	1.034	1.384	0.7469	287.4	1.034	1.384	0.7469	287.4	1.034	1.384
400	0.7631	287.4	1.051	1.377	0.7631	287.4	1.051	1.377	0.7631	287.4	1.051	1.377
500	0.786	287.4	1.073	1.365	0.786	287.4	1.073	1.365	0.786	287.4	1.073	1.365
600	0.8124	287.4	1.1	1.354	0.8124	287.4	1.1	1.354	0.8124	287.4	1.1	1.354
700	0.8401	287.4	1.128	1.343	0.8401	287.4	1.128	1.343	0.8401	287.4	1.128	1.343
800	0.8674	287.4	1.155	1.332	0.8674	287.4	1.155	1.332	0.8674	287.4	1.155	1.332
900	0.8932	287.4	1.181	1.322	0.8932	287.4	1.181	1.322	0.8932	287.4	1.181	1.322
1000	0.9169	287.4	1.204	1.313	0.9169	287.4	1.204	1.313	0.9169	287.4	1.204	1.313
1100	0.9384	287.4	1.226	1.306	0.9384	287.4	1.226	1.306	0.9384	287.4	1.226	1.306
1200	0.9574	287.4	1.245	1.3	0.9574	287.4	1.245	1.3	0.9574	287.4	1.245	1.3
1300	0.9744	287.4	1.262	1.295	0.9744	287.4	1.262	1.295	0.9744	287.4	1.262	1.295
1400	0.9893	287.4	1.277	1.291	0.9893	287.4	1.277	1.291	0.9893	287.4	1.277	1.291
1500	1.0024	287.4	1.29	1.287	1.0025	287.4	1.29	1.287	1.0025	287.4	1.29	1.287
1600	1.014	287.4	1.301	1.283	1.014	287.4	1.301	1.283	1.0141	287.4	1.302	1.284
1700	1.0244	287.4	1.312	1.281	1.0244	287.4	1.312	1.281	1.0245	287.4	1.312	1.281
1800	1.0338	287.4	1.321	1.278	1.0338	287.4	1.321	1.278	1.0338	287.4	1.321	1.278
1900	1.0422	287.5	1.33	1.276	1.0422	287.4	1.33	1.276	1.0422	287.4	1.33	1.276
2000	1.0498	287.5	1.337	1.274	1.0499	287.4	1.337	1.273	1.0499	287.4	1.337	1.273
2100	1.0566	287.7	1.344	1.272	1.0569	287.5	1.344	1.272	1.057	287.4	1.344	1.272
2200	1.0627	288	1.351	1.271	1.0632	287.6	1.351	1.271	1.0634	287.5	1.351	1.27
2300	1.068	288.4	1.356	1.27	1.0689	287.8	1.357	1.27	1.0693	287.5	1.357	1.269
2400	1.0726	289	1.362	1.27	1.074	288	1.362	1.268	1.0745	287.6	1.362	1.268
2500	1.076	290.1	1.366	1.27	1.0784	288.4	1.367	1.268	1.0792	287.8	1.367	1.267
2600	1.0785	291.5	1.37	1.27	1.0821	288.9	1.371	1.267	1.0835	288	1.372	1.266
2700	1.08	293.5	1.374	1.272	1.0851	289.7	1.375	1.267	1.0872	288.3	1.376	1.266
2800	1.0804	296.1	1.377	1.275	1.0875	290.7	1.378	1.267	1.0905	288.6	1.379	1.265
2900	1.0801	299.3	1.379	1.277	1.0891	292	1.381	1.268	1.0933	289.1	1.382	1.264
3000	1.079	303.2	1.382	1.281	1.09	293.7	1.384	1.27	1.0956	289.8	1.385	1.264
3100	1.0773	307.8	1.385	1.286	1.0904	295.7	1.386	1.271	1.0975	290.6	1.388	1.265
3200	1.0752	313	1.388	1.291	1.0903	298.1	1.388	1.273	1.0989	291.6	1.391	1.266
3300	1.0729	318.7	1.392	1.297	1.0898	300.8	1.391	1.276	1.1	292.8	1.393	1.266
3400	1.0702	324.9	1.395	1.303	1.0889	303.9	1.393	1.279	1.1005	294.3	1.395	1.268
3500	1.0675	331.2	1.399	1.311	1.0876	307.4	1.395	1.283	1.1007	295.9	1.397	1.269
3600	1.0648	337.4	1.402	1.317	1.0861	311.1	1.397	1.286	1.1007	297.6	1.398	1.27
3700	1.0623	343.2	1.406	1.324	1.0843	315.2	1.4	1.291	1.1002	299.6	1.4	1.272
3800	1.0601	348.5	1.409	1.329	1.0824	319.4	1.402	1.295	1.0994	301.8	1.401	1.274
3900	1.0584	353.2	1.412	1.334	1.0803	323.9	1.404	1.3	1.0986	304.1	1.403	1.277
4000	1.0576	357.1	1.415	1.338	1.0787	328.4	1.407	1.304	1.0982	306.5	1.405	1.279

Table D.5: Gas properties for air fuel ratio $\lambda = 2.0$

T	$p = 1$ bar				$p = 10$ bar				$p = 100$ bar			
	c_v	R	c_P	κ	c_v	R	c_p	κ	c_v	R	c_p	κ
298.15	0.7296	287.2	1.017	1.394	0.7296	287.2	1.017	1.394	0.7296	287.2	1.017	1.394
300	0.7297	287.2	1.017	1.394	0.7297	287.2	1.017	1.394	0.7297	287.2	1.017	1.394
400	0.7409	287.2	1.028	1.388	0.7409	287.2	1.028	1.388	0.7409	287.2	1.028	1.388
500	0.7603	287.2	1.048	1.378	0.7603	287.2	1.048	1.378	0.7603	287.2	1.048	1.378
600	0.7839	287.2	1.071	1.366	0.7839	287.2	1.071	1.366	0.7839	287.2	1.071	1.366
700	0.8092	287.2	1.096	1.354	0.8092	287.2	1.096	1.354	0.8092	287.2	1.096	1.354
800	0.8342	287.2	1.121	1.344	0.8342	287.2	1.121	1.344	0.8342	287.2	1.121	1.344
900	0.8578	287.2	1.145	1.335	0.8578	287.2	1.145	1.335	0.8578	287.2	1.145	1.335
1000	0.8795	287.2	1.167	1.327	0.8795	287.2	1.167	1.327	0.8795	287.2	1.167	1.327
1100	0.8989	287.2	1.186	1.319	0.8989	287.2	1.186	1.319	0.8989	287.2	1.186	1.319
1200	0.9161	287.2	1.203	1.313	0.9161	287.2	1.203	1.313	0.9161	287.2	1.203	1.313
1300	0.9313	287.2	1.219	1.309	0.9313	287.2	1.219	1.309	0.9313	287.2	1.219	1.309
1400	0.9445	287.2	1.232	1.304	0.9445	287.2	1.232	1.304	0.9445	287.2	1.232	1.304
1500	0.9562	287.2	1.243	1.3	0.9562	287.2	1.243	1.3	0.9562	287.2	1.243	1.3
1600	0.9666	287.2	1.254	1.297	0.9666	287.2	1.254	1.297	0.9666	287.2	1.254	1.297
1700	0.9758	287.2	1.263	1.294	0.9758	287.2	1.263	1.294	0.9758	287.2	1.263	1.294
1800	0.9842	287.2	1.271	1.291	0.9842	287.2	1.271	1.291	0.9842	287.2	1.271	1.291
1900	0.9918	287.2	1.279	1.29	0.9918	287.2	1.279	1.29	0.9918	287.2	1.279	1.29
2000	0.9986	287.3	1.286	1.288	0.9987	287.2	1.286	1.288	0.9987	287.2	1.286	1.288
2100	1.0049	287.4	1.292	1.286	1.005	287.3	1.292	1.286	1.0051	287.2	1.292	1.285
2200	1.0106	287.6	1.298	1.284	1.0109	287.3	1.298	1.284	1.011	287.2	1.298	1.284
2300	1.0157	287.9	1.304	1.284	1.0162	287.4	1.304	1.283	1.0163	287.3	1.304	1.283
2400	1.0202	288.3	1.309	1.283	1.021	287.6	1.309	1.282	1.0213	287.3	1.309	1.282
2500	1.024	289	1.313	1.282	1.0252	287.9	1.313	1.281	1.0258	287.4	1.313	1.28
2600	1.0272	289.9	1.317	1.282	1.0291	288.2	1.317	1.28	1.0298	287.6	1.317	1.279
2700	1.0297	291.2	1.321	1.283	1.0324	288.7	1.321	1.28	1.0335	287.8	1.321	1.278
2800	1.0313	293	1.324	1.284	1.0352	289.3	1.325	1.28	1.0368	288	1.325	1.278
2900	1.0324	295.2	1.328	1.286	1.0375	290.2	1.328	1.28	1.0397	288.3	1.328	1.277
3000	1.0327	298	1.331	1.289	1.0393	291.3	1.331	1.281	1.0423	288.7	1.331	1.277
3100	1.0325	301.4	1.334	1.292	1.0408	292.6	1.333	1.281	1.0447	289.2	1.334	1.277
3200	1.0317	305.3	1.337	1.296	1.0417	294.3	1.336	1.283	1.0466	289.9	1.337	1.277
3300	1.0306	309.7	1.34	1.3	1.0424	296.2	1.339	1.285	1.0484	290.6	1.339	1.277
3400	1.029	314.5	1.344	1.306	1.0426	298.4	1.341	1.286	1.0498	291.5	1.341	1.277
3500	1.0273	319.4	1.347	1.311	1.0424	301	1.343	1.288	1.0508	292.6	1.343	1.278
3600	1.0254	324.4	1.35	1.317	1.0419	303.8	1.346	1.292	1.0515	293.8	1.345	1.279
3700	1.0234	329.3	1.353	1.322	1.0411	306.9	1.348	1.295	1.0519	295.2	1.347	1.281
3800	1.0216	333.8	1.355	1.326	1.04	310.2	1.35	1.298	1.0521	296.7	1.349	1.282
3900	1.0201	337.9	1.358	1.331	1.0387	313.6	1.352	1.302	1.0521	298.4	1.351	1.284
4000	1.0195	341.4	1.361	1.335	1.0378	317.2	1.355	1.306	1.0522	300.2	1.352	1.285

Table D.6: Gas properties for air fuel ratio $\lambda = 5.0$